



5-2001

## Crystallization of polyethylenes at very high supercooling

John Edward Wagner  
*University of Tennessee*

Follow this and additional works at: [https://trace.tennessee.edu/utk\\_graddiss](https://trace.tennessee.edu/utk_graddiss)

---

### Recommended Citation

Wagner, John Edward, "Crystallization of polyethylenes at very high supercooling. " PhD diss., University of Tennessee, 2001.  
[https://trace.tennessee.edu/utk\\_graddiss/6404](https://trace.tennessee.edu/utk_graddiss/6404)

This Dissertation is brought to you for free and open access by the Graduate School at TRACE: Tennessee Research and Creative Exchange. It has been accepted for inclusion in Doctoral Dissertations by an authorized administrator of TRACE: Tennessee Research and Creative Exchange. For more information, please contact [trace@utk.edu](mailto:trace@utk.edu).

To the Graduate Council:

I am submitting herewith a dissertation written by John Edward Wagner entitled "Crystallization of polyethylenes at very high supercooling." I have examined the final electronic copy of this dissertation for form and content and recommend that it be accepted in partial fulfillment of the requirements for the degree of Doctor of Philosophy, with a major in Polymer Engineering.

Paul J. Phillips, Major Professor

We have read this dissertation and recommend its acceptance:

Roberto Benson, Kevin Kit, Jeffery Kovac

Accepted for the Council:

Carolyn R. Hodges

Vice Provost and Dean of the Graduate School

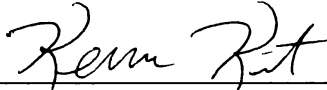
(Original signatures are on file with official student records.)

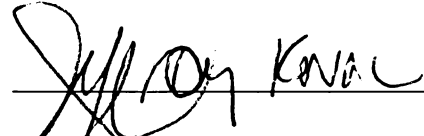
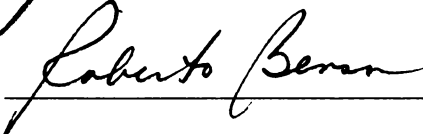
To the Graduate Council:

I am submitting herewith a dissertation written by John Edward Wagner entitled "Crystallization of Polyethylenes at Very High Supercooling". I have examined the final copy of this dissertation for form and content and recommend that it be accepted in partial fulfillment of the requirements for the degree of Doctor of Philosophy, with a major in Polymer Engineering.


  
\_\_\_\_\_  
Paul J. Phillips, Major Professor

We have read this dissertation  
and recommend its acceptance:

  
\_\_\_\_\_

  
\_\_\_\_\_  
  
\_\_\_\_\_

Accepted for the Council:

  
\_\_\_\_\_  
Interim Vice Provost and  
Dean of The Graduate School

# **CRYSTALLIZATION OF POLYETHYLENES AT VERY HIGH SUPERCOOLING**

A Dissertation  
Presented for the  
Doctor of Philosophy  
Degree  
The University of Tennessee, Knoxville

John Edward Wagner

May 2001

## **DEDICATION**

I would like to dedicate this work to my parents,  
Phyllis Jean Wagner and Robert Edward Wagner,  
whose constant help and encouragement  
empowered me to attain this degree.

Secondly, would like to also dedicate this work  
to my son, Alexander Ryan Wagner,  
who has served as my inspiration to  
complete the work for this degree.

## ACKNOWLEDGEMENTS

I would like to express my sincere appreciation to Professor Paul Phillips for his support, guidance, and encouragement that made this work possible, but also for the overall development of my scientific education. I would also like to thank Professors Roberto Benson, Kevin Kit, and Jeffery Kovac for serving as my committee members. I would especially like to thank Professor Joseph Spruiell, the head of the Materials Science and Engineering department, for allowing me the opportunity to study Polymer Engineering. The entire Materials Science and Engineering faculty has been a great aid to my studies, and I would not have reached this point without them. I owe a special thanks to Professors Edward Clark, Ben Oliver, and Charlie Brooks for many insightful discussions and advice. I am in great debt to the financial support of the Polymer Program of the National Science Foundation and to the University of Tennessee Center for Materials Excellence.

Much of the data presented in this dissertation was obtained using the Ding – Spruiell rapid cooling and crystallization facilities belonging to Dr. Joseph Spruiell. I am very grateful for being allowed to use these facilities. In addition, his graduate students Gary Holt, Eric Bond, and Pitt Supaphol were extremely cooperative in sharing instrumental time with me.

The coworkers in my laboratory provided a great deal of support in the completion of my degree. These include: Ken Monar, Stein Schreiber, Anita Dimeska,

Samir Abu-Iqyas, Ketan Panse, Mike Trapp, Justin Hwu, Bhushan Deshpande, Mrunalini Dhamdhere, Darnell Worley, Monica Schmidt, and Alexander Pal. Thank you Jeffrey DePriest, Claudia Chisamore, Marta Driesslein, Barbara Hegranes, and Thom Flak for helping to put many things into perspective.

To my brother Joseph, and my sisters Barbara and Jean and their families, thank you I could not have done it without you. Other important family members include niece Camille and nephews Nicholas, Bryan, and Cameron. Thank you Ruth Anne, Matt, and Mark for the much needed lift and a well-deserved break.

## ABSTRACT

The crystallization behavior of a series of ethylene-octene copolymers synthesized using metallocene catalysts has been studied using the Ding-Spruiell method of rapid cooling. In conventional crystallization experiments it was found, as expected, that the spherulite growth rates varied with octene content and molecular weight. When studied at rapid cooling rates the polymers generate their own pseudo-isothermal crystallization temperatures, in agreement with Ding – Spruiell’s studies on other systems, however, at the lowest temperatures of crystallization, the spherulite growth rates of all the copolymers studied merge. The WAXD results indicate at the faster crystallization rates that the size of the unit cell unit decreases with decreasing crystallization temperature. A resulting increase in the surface free energy plays a role in the behavior of the copolymers such that spherulitic growth rates of copolymers begin to surpass that of the linear polyethylene at very high supercooling. This is a change in the behavior of the copolymers that should be of considerable relevance to polymer processing conditions. Spinodal transformation could play a role in the leveling off of growth rates at high supercooling.

The crystallization and morphology of four LLDPE samples produced using metallocene catalysts through the copolymerization of ethylene and octene has been studied. The second part of the study is primarily concerned with the growth kinetics obtained through experimentally determined growth rates at different crystallization temperatures of low and high molecular weight samples. Using experimentally



determined equilibrium melting points secondary nucleation behavior is studied in detail. Three Regimes are seen for a molecular weight 101,000 with no branching and at 60,000 with branching at 4 octenes per 1000 carbons. Two Regimes have been obtained for a sample of similar molecular weight but with branching at 17 octenes per 1000 carbons. Lamellar thickness data in the rapid cooling region correlate well with previous studies of the equilibrium melting temperature of the linear polyethylene. Andrews plot data shows a three-stem nucleus in Regime III.

## TABLE OF CONTENTS

CHAPTERS	PAGE
1. INTRODUCTION	1
2. LITERATURE REVIEW	4
2.1 Molecular Conformation and Crystal Structure of PE	4
2.2 Catalysts for Polymerization of Olefins	6
2.2.1 Multi Site Heterogeneous or Zeigler-Natta Catalysts	6
2.2.2 Uniform Site Homogeneous or Metallocene Catalysts	7
2.3 Random Copolymers of Ethylene/ $\alpha$ -olefins	10
2.4 Polymer Crystallization	12
2.4.1 Crystallization Concepts	12
2.4.2 Single Crystals	12
2.4.3 Spherulites	14
2.4.4 Axialites	17
2.5 Crystallization Models For Random Copolymers	17
2.5.1 Exclusion Model	19
2.5.2 Mixing Entropy Term For Exclusion Model	23
2.5.3 Inclusion Model	27
2.5.4 Comparing Inclusion and Exclusion Models	29
2.6 Secondary Nucleation Theory	32

2.6.1	Model	33
2.6.2	Total Flux	35
2.6.3	Initial Lamellar Thickness	38
2.6.4	Free Energy of Fusion	38
2.6.5	Spinodal-assisted crystallization in polymer melts	40
2.6.5.1	Linear Theories	40
2.6.5.2	Crystallization in Polymer Melts	41
2.7	Regime Transition Analysis	49
2.7.1	Regime Analysis of Polyethylene Copolymers	50
2.7.2	Secondary Nucleation and Lateral Growth	53
2.7.3	Concept of Regime III Transitions	54
2.7.4	Crystallization Kinetics	57
2.7.5	Ozawa Equation	58
2.8	Melting of Polymer Crystals	61
2.8.1	Thermodynamic Considerations	61
2.8.2	Kinetic Considerations	62
2.8.3	Morphology of Polyethylene Spherulite	63
2.9	Small Angle X-Ray Scattering for Lamellar Thickness	64
2.9.1	Development of One Dimensional Correlation Function	64
2.9.2	Models for Determining Lamellar Thickness	67
3.	EXPERIMENTAL PROCEDURES	74
3.1	Materials	74

3.2	Differential Scanning Calorimetry (DSC)	74
3.3	Polarized Light Microscopy (PLM)	76
3.3.1	Linear Growth Kinetics	78
3.4	Non-isothermal Crystallization Under Rapid Cooling Rates	79
3.4.1	Introduction	79
3.4.2	Hot Stage System	81
3.5	Small Angle X-ray Scattering (SAXS)	87
3.6	Wide Angle X-ray Diffraction (WAXD)	89
3.6.1	Percent Crystallinity Measurement	89
4.	RESULTS	91
4.1	Linear Growth Kinetics	91
4.1.1	Copolymer Content	91
4.1.2	Measurement Dynamics	95
4.2	Morphology	97
4.2.1	Low Molecular Weight Series	97
4.2.2	Intermediate Molecular Weight Series	101
4.3	X-ray Analyses	104
4.3.1	Wide Angle X-ray Diffraction	104
4.3.2	Small Angle X-ray Scattering	110
4.4	Melting Behavior of Polyethylene Copolymers	110
4.5	Equilibrium Melting Temperature ( $T_m^\circ$ )	121
5.	DISCUSSION	124
5.1	Wide Angle X-ray Diffraction	124

5.2	Small Angle X-ray Scattering	125
5.3	Rapid Cooling Crystallization of Polyethylene	126
5.3.1	Measurement Dynamics	129
5.4	Alternative Mechanisms	133
5.4.1	Molecular Weight Effect	133
5.4.1.1	Chain Mobility	133
5.4.1.2	Cellulation in Polymers	136
5.4.2	Branch Effect	137
5.4.2.1	Friction Coefficient	137
5.4.2.2	Copolymer Equation	142
5.4.3	Growth and Nucleation Rate	144
5.4.4	Spinodal Transformation	146
5.4.5	Surface Free Energy of Copolymers	153
5.5	Morphology of Polyethylene	155
5.6	Thermal Analysis of Polyethylene Copolymers	157
5.7	Equilibrium Melting Temperature	159
5.8	Andrews Analysis of Polyethylene	160
5.9	Secondary Nuclei and Surface Spreading	170
5.10	Summary	172
6.	CONCLUSIONS	175
6.1	Conventional Crystallization Process	175
6.2	Rapid Cooling Crystallization	175

6.3 Spinodal Transformation or Alternative Intermediate States	177
7. FUTURE WORK	178
7.1 Rapid Cooling Effects	178
7.2 Lamellar Detail	178
7.3 Mechanical Properties	179
7.4 Pressure Effects	179
REFERENCES	180
VITA	189

## LIST OF TABLES

TABLE		PAGE
2.1	Uniform Site (Homogeneous) catalysts For Poly(olefins) Polymerization.	9
3.1.	Molecular Weight Characteristics and Equilibrium Melting Points.	75
3.2.	Copolymers Based On Linear Low-Density Polyethylene.	77
4.1	Summary Of Percent Crystallinity Results by WAXD.	107
4.2	Summary Of Unit Cell Parameters by WAXD.	108
4.3	Corrected SAXS Data for Linear Polyethylene.	114
4.4	Summary Of Percent Crystallinity Results by DSC.	115
5.1	Regime Transition Temperatures for Polyethylene and Copolymers.	141
5.2	Nucleus Shape Characteristics Calculated From Andrews' Analysis.	163
5.3	Regime Transition Analysis	171
5.4	Regime Analysis for II-III Transitions with Area Calculations	173

## LIST OF FIGURES

FIGURE		PAGE
Figure 2.1.	Unit cell: (a) PE chains inside the orthorhombic unit cell. (b) Plane projection of the unit cell	5
Figure 2.2.	A typical lamellar single crystal.	13
Figure 2.3.	The schematic of a growing spherulite.	15
Figure 2.4.	Growth forms leading to the spherical shape of mature spherulite.	16
Figure 2.5.	Exclusion and Inclusion Crystallization of Random Copolymers.	18
Figure 2.6.	Goldbeck-Wood Model.	24
Figure 2.7.	Random Copolymer Crystallization Models of Flory and Sanchez & Eby.	30
Figure 2.8.	The diagram of growth for one lamellar crystal	34
Figure 2.9.	Free-Energy of Formation of a Chain Folded Surface Nucleus.	36
Figure 2.10	Phase diagram for a polymer melt proposed for spinodal-assisted crystallization.	44
Figure 2.11.	Schematic representation of the late-stage spinodal texture for coexisting liquid phases with different conformations.	47
Figure 2.12.	Regime transition analysis from crystal growth rate data.	52
Figure 2.13.	Schematic diagrams of Regime I, II, and III crystal growth.	55
Figure 2.14.	Electron Density Distributions and Correlation Function $K(z)$	69
Figure 2.15	Self Correction Triangle	71



<b>FIGURE</b>	<b>PAGE</b>
Figure 3.1. Experimental System for rapid cooling.	80
Figure 3.2. Hot stage system for rapid cooling.	82
Figure 3.3. Sample assembly used in experiments.	84
Figure 3.4. Schematic diagram of the light-depolarizing microscope.	85
Figure 3.5. Relative crystallinity as a function of time and temperature.	86
Figure 3.6. The schematic diagram of the 10m small angle X-ray scattering spectrometer at ORNL.	88
Figure 4.1. Radius as a function of crystallization time for a specified crystallization temperature, $T_c$ .	92
Figure 4.2. Growth rate for ethylene copolymers. a) Plot of Growth rate (G) verse crystallization temperature ( $T_c$ ) for ethylene copolymers. b) Error bars for the growth rate (G) verse crystallization temperature ( $T_c$ ) for ethylene copolymers.	93
Figure 4.3. Linear polyethylene LPE-54/101 at 122°C (Regime II) with arrow pointing to the fringe of the spherulite.	96
Figure 4.4. Morphology of L4-M at 92.5°C (Regime III).	98
Figure 4.5. Morphology of L11-M at 83°C (Regime III).	99
Figure 4.6. Morphology of L4-M at 117°C (Regime II).	100
Figure 4.7. Morphology of LPE 54/101 at 97.5°C (Regime III).	102
Figure 4.8. Morphology of H7-M at 87.5°C (Regime III).	103
Figure 4.9. Morphology of LPE 54/101 at 122°C (Regime II).	105
Figure 4.10. Morphology of LPE 54/101 at 127°C (Regime I).	106
Figure 4.11. Wide Angle X-ray diffraction LPE 54/101 with $T_c = 116^\circ\text{C}$ .	109
Figure 4.12. SAXS intensity profile for the LPE 54/101 at different $T_c$ 's.	111

<b>FIGURE</b>		<b>PAGE</b>
Figure 4.13	Lorentz corrected SAXS intensity profile for LPE 54/101 at $T_c = 90.0^\circ\text{C}$ .	112
Figure 4.14	One-dimensional correlation function analysis of the data from LPE 54/101 at $T_c = 90.0^\circ\text{C}$ .	113
Figure 4.15	Melting behavior of LPE 54/101.	117
Figure 4.16	Melting behavior of L4-M.	118
Figure 4.17	Melting behavior of L11-M.	119
Figure 4.18	Melting behavior of H7-M.	120
Figure 4.19	Melting temperature ( $^\circ\text{C}$ ) against reciprocal lamellar thickness ( $^\circ\text{A}^{-1}$ ) for the linear polyethylene a comparison with Kim.	122
Figure 5.1.	Logarithm of radial growth rate versus crystallization temperature for the polymers, as indicated.	127
Figure 5.2.	Logarithm of radial growth rate versus supercooling, using established equilibrium melting points of each individual copolymer.	128
Figure 5.3.	Secondary nucleation plot for the copolymers indicated (filled symbols are isothermal crystallizations; open symbols are pseudo-isothermal crystallizations obtained from rapid cooling experiments).	130
Figure 5.4.	The linear polyethylene LPE 54/101 of only Regime II showing the effect of fringes in spherulite measurements.	132
Figure 5.5	Secondary nucleation plots of linear growth rates showing the effect of molecular weight.	134
Figure 5.6	Secondary nucleation plots of linear growth rates showing the effect of increasing branching.	139
Figure 5.7.	Alloy compositions between spinodal points.	148
Figure 5.8.	Schematic composition profiles.	149

<b>FIGURE</b>		<b>PAGE</b>
Figure 5.9.	Log of growth rate verse impurity content of the linear and ethylene copolymers.	161
Figure 5.10	Possible nucleation and growth mechanisms.	167

## CHAPTER 1. INTRODUCTION

The most widely used crystalline polymer today is polyethylene (PE), with applications including films, moldings, bottles, tubings, coatings, and electrical insulators. This wide range of applications has resulted in many studies; however, a great deal of work remains to be done. There are considerable questions remaining concerning the effect of the variables such as temperature, pressure, molecular weight, and chain microstructure on the crystallization process of PE. The path of the polymer crystallization process determines its detailed structure, and therefore its physical and mechanical properties. Considerable work has been performed to determine the effect of these variables on the crystallization process of polymers.

Low-density polyethylene (LDPE) is a commercial class of polyethylene, produced through the copolymerization of ethylene and comonomers such as hexene or octene, thereby producing butyl or hexyl branches, respectively. To separate the effects of copolymer content from molecular weight, a series of cross-fractionated copolymers has been investigated (Lambert, 1994). Not well known at the present time are the sequence length distributions of the octene and ethylene mers within each molecule. In this dissertation, studies of random copolymers produced using metallocene catalysts will show that the crystallization behavior is very different from that of the Zeigler-Natta (ZN) materials, a result which has to be a consequence of the ZN polymers being non-random within each molecule.

Quiescent crystallization is usually separated into its component stages of primary nucleation, linear spherulite (or lamellar) growth and secondary crystallization. The linear growth rates will be considered in this dissertation. Regime theory describes linear spherulite growth in flexible polymers and is composed of two separate processes. The first process is the deposition of secondary nuclei on the growth face, usually denoted as occurring at a rate  $i$ . The second process is the subsequent growth along the face at the niches formed by the secondary nuclei, often referred to as the rate of surface spreading, and denoted by the rate  $g$ . The relative rates of these two processes determine the regime at which the crystallization occurs. The concept of transitions was first introduced by Lauritzen and Hoffman (1960) and has since been evaluated by Phillips and others (Hoffman, 1983; Hoffman, 1997; Phillips, 1979; Phillips, 1990).

Crystallization behavior of a series of ethylene-octene copolymers synthesized using metallocene catalysts has been studied using isothermal crystallization conditions and also the Ding-Spruiell method (Ding, 1996) of rapid cooling. As in conventional crystallization experiments, the spherulite growth rate varies with octene content and molecular weight. At rapid cooling rates the polymers generate their own pseudo-isothermal crystallization temperatures. This finding is in agreement with Ding – Spruiell’s studies on other systems. However, at the lowest temperatures of crystallization, what is observed is that the spherulite growth rates of all of the copolymers studied merge and are virtually indistinguishable. This is an indication of a major change of crystallization mechanism under these conditions, which is of considerable relevance to polymer processing conditions.

Copolymers have now been produced using metallocene catalysts, which are believed to produce random copolymers because of the nature of the catalytic process. DOW Chemical Company synthesized for us metallocene copolymers with molecular characteristics, as identical as possible, to those of the cross-fractionated samples. Previous studies of the melting point-lamellar thickness relations have shown that the equilibrium melting points of the polyethylene copolymers in this study are depressed by a factor greater than that predicted by the Flory equation (Kim, 1996; Kim et al., 2000).

The aim of this study is to investigate the crystallization behavior of this series of copolymers and determine the regime I-regime II and regime II-regime III transition temperatures. It will also be demonstrated here that, under very high supercoolings characteristic of commercial processing operations, the polymer behavior changes dramatically and is neither dependent on comonomer content nor on molecular weight. With a combination of polarized optical microscopy, small angle X-ray scattering, wide angle X-ray diffraction, rapid cooling experiments on the model system, and Differential Scanning Calorimetry (DSC) it is intended to develop an understanding of the crystallization behavior of these random copolymers.

## CHAPTER 2. LITERATURE REVIEW

### 2.1 Molecular Conformation And Crystal Structure Of PE

PE is a highly crystalline polymer that belongs to the Class 1 polymers (Wunderlich, 1980) containing one chain atom-repeating unit. The lowest energy planar zigzag (all-trans) chain conformation exists in the crystals and the chain axis is a  $2_1$  screw axis. The bond angles are determined experimentally to be  $107^\circ$  for the H-C-H angle and  $111^\circ$  for the C-C-C angle (Wunderlich, 1980).

PE is known to exhibit polymorphism, the most stable crystal structure being orthorhombic (Bunn, 1939). This crystalline structure forms under normal crystallization conditions either from the melt or from the solution. Depicted in Figure 2.1 is the arrangement of PE chains inside the orthorhombic unit cell, as well as the a-b plane projection. The number of chains per unit cell is 2 and the space group of the PE crystal is  $Pnma$ . Depending on the crystallization condition, the unit cell parameters are commonly quoted as (Van Krevelen, 1976):  $a = 7.417 \text{ \AA}$ ,  $b = 4.945 \text{ \AA}$  and  $c = 2.547 \text{ \AA}$ .

The monoclinic form of PE crystals can be formed when the PE crystals are formed under severe stress such as rolling or biaxial stretching (Hsieh, 1968). It should be noted that this form is metastable and upon heating it transforms into the stable orthorhombic form below the melting temperature. The unit cell parameters have been determined to be (Hsieh, 1968):  $a = 8.09 \text{ \AA}$ ,  $b = 2.53 \text{ \AA}$ ,  $c = 4.78 \text{ \AA}$  and  $\beta = 107.9^\circ$ .

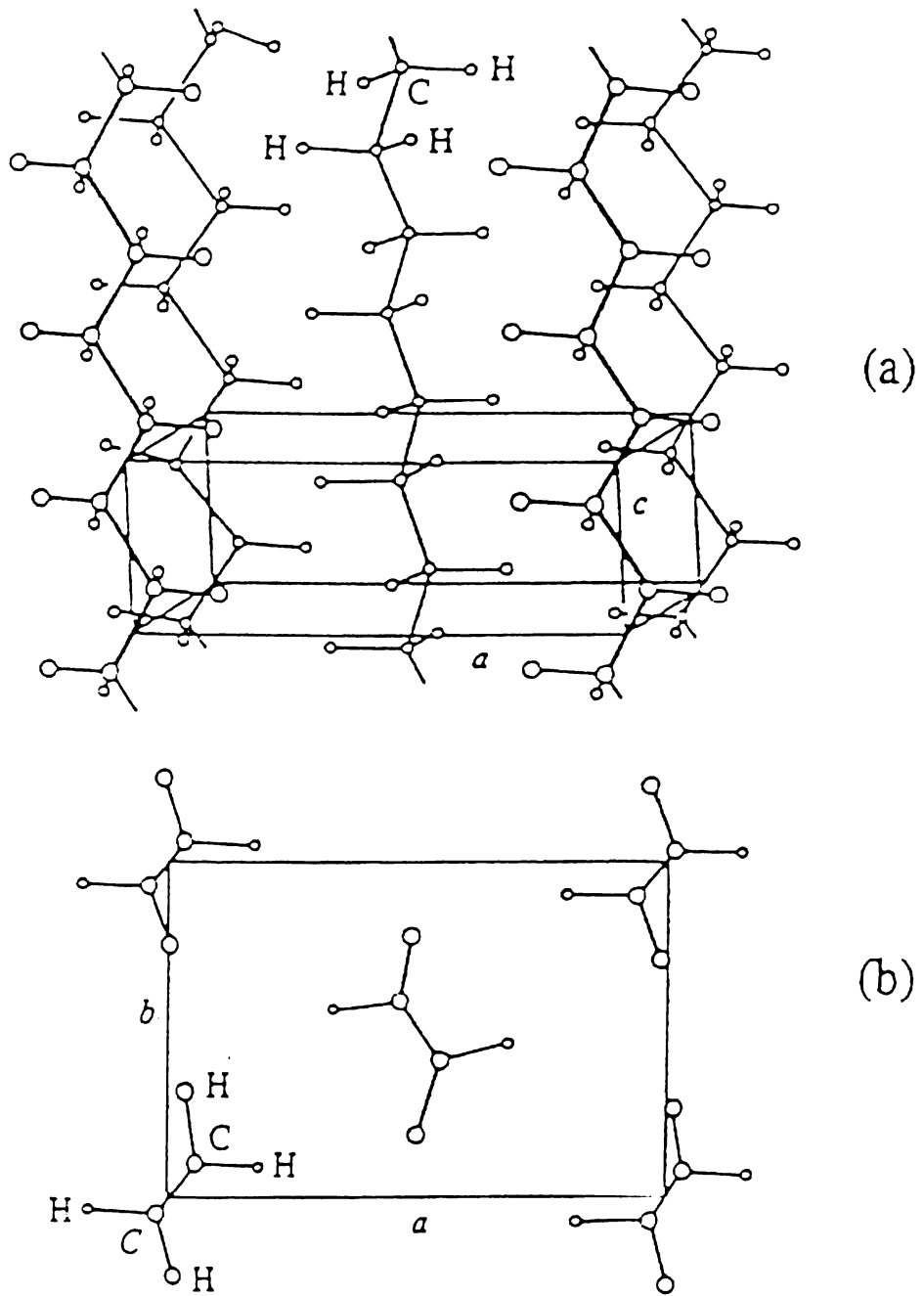


Figure 2.1: Unit cell: (a) PE chains inside the orthorhombic unit cell. (b) Plane projection of the unit cell (Bunn, 1939).



Here the number of chains per unit cell is still 2. Yet, another form of PE crystals can exist when PE is crystallized under high-pressure (i.e. 5000 kg/cm<sup>2</sup>) (Bassett, 1976).

## **2.2 Catalysts for Polymerization of Olefins**

### **2.2.1 Multi Site Heterogeneous or Zielger-Natta Catalysts**

Polyolefins originated with low-density polyethylene (LDPE) produced at high pressure (124Mpa, 18,000psi) and high temperature (100-300°C) in Imperial Chemical Industries, Ltd. (ICI) in 1933. Karl Zeigler et al. in Germany discovered that titanium tetrachloride (TiCl<sub>4</sub>) or vanadium tetrachloride (VCl<sub>4</sub>)/alkyl aluminum catalysts system can polymerize ethylene at room temperature and atmospheric pressure. Simultaneously G. Natta et al. in Italy found that the polymer from these catalysts shows crystalline properties. Various vinyl polymers such as high-density polyethylene (HDPE) or linear polyethylene (LPE), linear low-density polyethylene (LLDPE) and isotactic polypropylene have been produced commercially. These catalysts or initiator systems are referred to as Zeigler-Natta catalysts and are composed of an organometallic compound of a Group I-III metal with a halide of a Group IV-VII of the periodic table (O dian, 1981). Two main systems are titanium chloride with alkylaluminium (e.g., Et<sub>3</sub>Al/TiCl<sub>3</sub>) and chromium on silica. The catalyst systems are heterogeneous for some titanium-based systems and soluble for most vanadium-based catalysts. HDPE and LLDPE are produced

using both titanium- and chromium-based systems and isotactic polypropylene (iso-PP) is polymerized with titanium-based catalyst.

However, for the Ziegler-Natta catalysts molecular weight distribution control is difficult and the production of by-products of low molecular weight and low density due to their multi-site properties cannot be avoided. Multi-site terminology came from the fact that a heterogeneous (transition metal) catalyst species has various sites with different activity. Due to the different activity, the polymers produced with multi-site (or heterogeneous Zeigler-Natta catalyst) catalysts consist of various chain lengths resulting in different physical properties. In the case of the random copolymers of ethylene/ $\alpha$ -olefins (LLDPE), the narrow comonomer distribution as well as narrow molecular weight distribution is required. It is impossible to satisfy this requirement with heterogeneous catalysts since multiple active sites with different reactivity ratios for ethylene and comonomers cause polymers with broad MWD and broad short chain branches. New attempts to control polymer structure and properties have been concentrated on the preparation of catalysts with uniform activity.

### 2.2.2 Uniform Site Homogeneous or Metallocene Catalysts

The kinds of metallocene catalysts consisting of a Group IV transition metal complex with methylaluminoxane (MAO) have uniform activity and allow the production of polyolefins with controlled molecular weight, narrow molecular weight distribution

( $M_w/M_n \cong 2.0$ ) and stereoregular structures (Horton, 1994; Suhm, 1998). These uniform site catalysts are variously called (a) single site catalysts or homogeneous catalysts, due to their uniform activity compared to multi-site Ziegler-Natta catalysts with heterogeneous activity, (b) Kaminsky-type catalysts due to the contribution of Kaminsky et al. to improve activity of these catalysts, (c) metallocene catalysts and (d) constrained geometry catalysts (Dow Chemical Company). Although metallocene chemistry was started by Natta et al., the activity of the catalysts was too low to be useful (Wood, 1992). In 1980, Sinn and Kaminsky reported that the addition of a small amount of water increases the activity of these catalysts systems significantly (Sinn and Kaminsky, 1980).

The most popular single site catalyst systems (Horton, 1994; Gupta, 1994) are a combination of bent metallocenes, which are a Ti, Zr or Hf complex with two cyclopentadienyl ligands and two halides or alkyl ligands (1 in Table 2.1). Also, the cyclopentadienyl-amide catalysts (2 in Table 2.1), named Constrained Geometry catalysts by Dow Chemical, have only a single cyclopentadienyl ligand and seem to have been used in the production of LLDPE. In 1990, Dow filed for patents for these types of catalysts (European Patent Application 416 815) and 13 days later, Exxon did the same independently (European Patent Application 420 436).

The cyclopentadienyl-amide catalysts/excess MAO cocatalysts systems allow ethylene/1-octene copolymer of high molecular weight to be obtained. In these catalysts systems, molecular weight is controlled using hydrogen gas ( $H_2$ ).

Table 2.1. Uniform site (homogeneous) catalysts for poly(olefins) polymerization (Kim, 1996).

Code	Structures	Poly(olefins)	Expected Process	Expected Company
1		<p>HDPE LLDPE Atactic PP Ethylene/cycloalkene copolymer</p>	-	Exxon
2		<p>LLDPE(comonomer: 1-octene) Ethylene/styrene copolymer</p>	<p>High pressure, High temperature in solution</p>	Dow

M=Zr, Hf, Ti : X=Cl or Me

### 2.3 Random Copolymers of Ethylene/ $\alpha$ -olefins

To obtain narrow molecular weight distribution (MWD) from the poly(olefins) polymerized with heterogeneous catalysts, fractionation methods have been used such as temperature rising elution fractionation (TREF) for fractionation by crystallinity and composition of copolymer or solvent-gradient elution fractionation (SGEF) and successive reprecipitation fractionation for separation by the molecular weight. It is not easy to provide a large volume of resin with narrow molecular weight to the market. Recent catalysts developments allow the production of a new type of LLDPE by controlling its molecular weight distribution (MWD), comonomer incorporation, or homogeneous distribution of short chain branches, using single site homogeneous catalysts.

The first products using single site catalysts are copolymers of ethylene/ $\alpha$ -olefins of Exxon that has produced 15kt of LLDPE/year from the demonstration plant since 1991. Dow Chemical began producing 57kt of LLDPE/year using a titanium-based catalyst with a linked cyclopentadienyl-amide ligand in 1993.

Cyclopentadienyl-amide catalysts/excess MAO cocatalysts systems have  $\alpha$ -olefins (comonomers) that randomly incorporates to the propagating ethylene chain, which will cause uniform SCB distribution. MAO co catalysts have comonomer content that is independent of the chain length as well as significant comonomer incorporation into the polymer that is achieved without a large excess of comonomer. Very precise

control of molecular weight distribution ( $M_w/M_n \cong 2.0$ ) is possible. These controlled molecular parameters will produce uniform morphology. On the other hand, classical multi-site heterogeneous catalysts cause non-random copolymers with broad MWD and heterogeneous SCB distribution (i.e., shorter chains have a much higher  $\alpha$ -olefin content than the longer chains). LLDPE with narrow MWD shows sharper melting point, better hot tack and heat-seal properties, as well as higher clarity, better impact resistance and lower levels of alkan-soluble components (Horton, 1994, Schwank, 1993). Resins prepared with single site catalysts are being produced on a demonstration scale for niche markets and their costs remain high relative to competing resins.

Even with their unique advantages, there are practical processing problems with these new polymers. The narrow MWD makes the melt viscosity of polymers low shear sensitive. On the other hand, Dow overcame this problem by incorporating long chain branches into the linear short chain branched structure using cyclopentadienyl-amide catalysts. Final products show very high shear sensitivity and higher melt strength allowing facile processing. The technology is called in-site technology and is different from common single-site catalysts technology at the point that Constrained Geometry Homogeneous Catalyst is used (Schwank, 1993). It is known that Dow produces copolymers having from 2-12%(w/w) 1-octene to a thermoplastic elastomer with up to 20% (w/w) comonomer.

## 2.4 Polymer Crystallization

### 2.4.1 Crystallization Concepts

Many polymers can crystallize to some extent even though their chains are of considerable length. Several factors affect the ability of a polymer to crystallize. These factors include the structural regularity of the crystallizing chains, absence of bulky and irregularly spaced substituents on the polymer chain and the presence of vibrational and rotational motions in the chains so that the different conformations can be assumed. Polymers, which satisfy these conditions, may be able to crystallize, either from the melt or solution. Therefore structures may be formed in which the molecules tend to fold back and forth on themselves.

### 2.4.2 Single Crystals

Lamellar single crystals are formed upon the cooling of dilute solution of a flexible, crystallizable polymer. Keller (1957) demonstrated this technique by growing polyethylene single crystals from dilute solution. Single crystals are in the form of thin platelets, often hollow pyramids, approximately 100 Angstroms thick with molecular folds composing the top and bottom surfaces as depicted in Figure 2.2. Growth conditions such as solvent, temperature, concentration, and the rate of growth determine

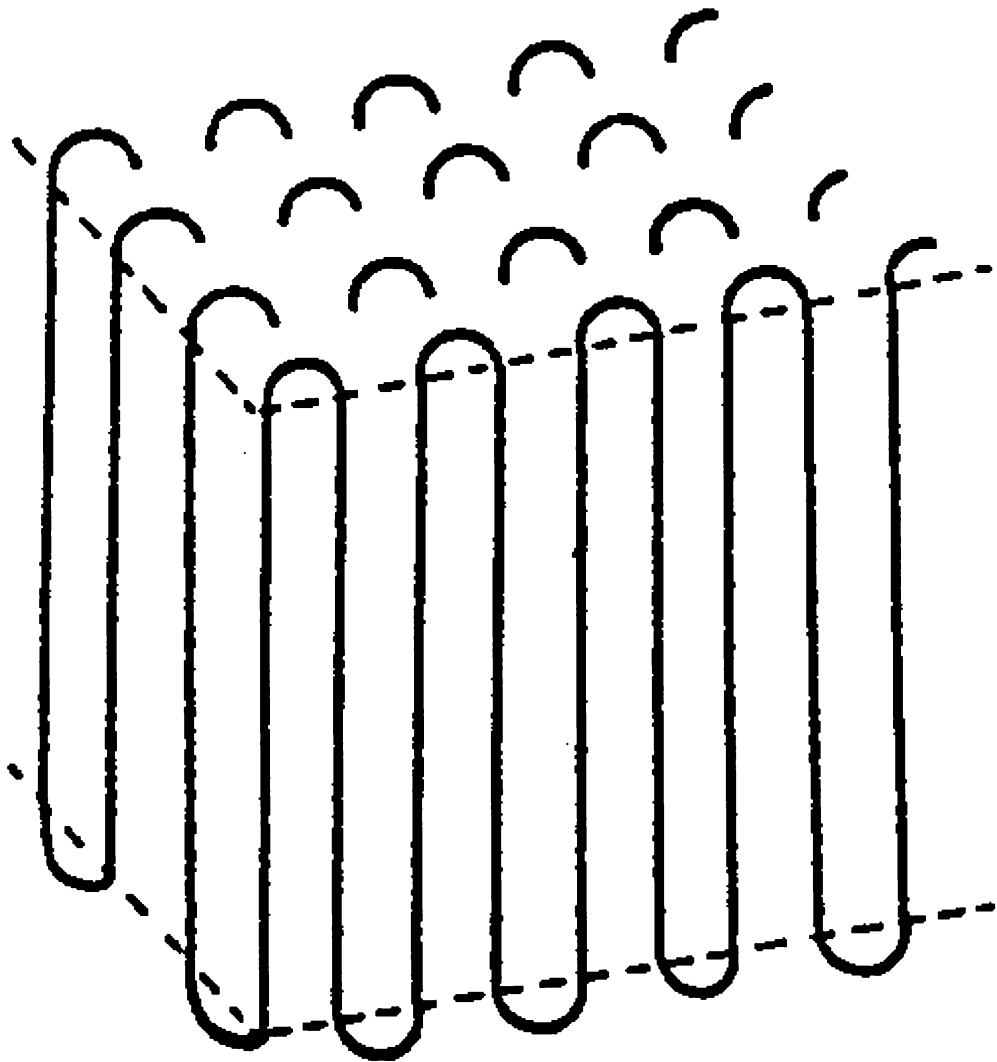


Figure 2.2: A typical lamellar single crystal (Lambert, 1991).



the size, shape, and regularity of the crystal. The thickness of the crystal depends upon the crystallization temperature as well as additional annealing time at the crystallization temperature.

Growth of the lamellae occurs primarily along the lateral faces of the single crystal. The growth consists of the folding of molecules along the lateral faces to form folded ribbons parallel to the prism faces, therefore leading to a subdivision of the crystal into sectors distinguished by the plane of folding. Distinctness of the sectors is the result of the formation of a hollow pyramidal morphology. However, these pyramids collapse upon sample collection resulting in crystals having wrinkles due to the flattening process.

#### 2.4.3. Spherulites

Polymers crystallized from the melt will often exhibit spherulite morphology. As shown in Figure 2.3, spherulites consist of chain folded lamellae radiating from a central point, and grow linearly with time until impingement occurs with other growing spherulites. The development of a spherulite depends upon its nucleation process. Primary crystallization begins with a single crystal, building up to a stack of single crystals, of an inhomogeneous entity, and evolves through sheaf-like morphologies ultimately obtaining its final spherical shape. Figure 2.4 shows a typical growth pattern. The spherical shape is maintained until neighboring spherulites impinge upon one

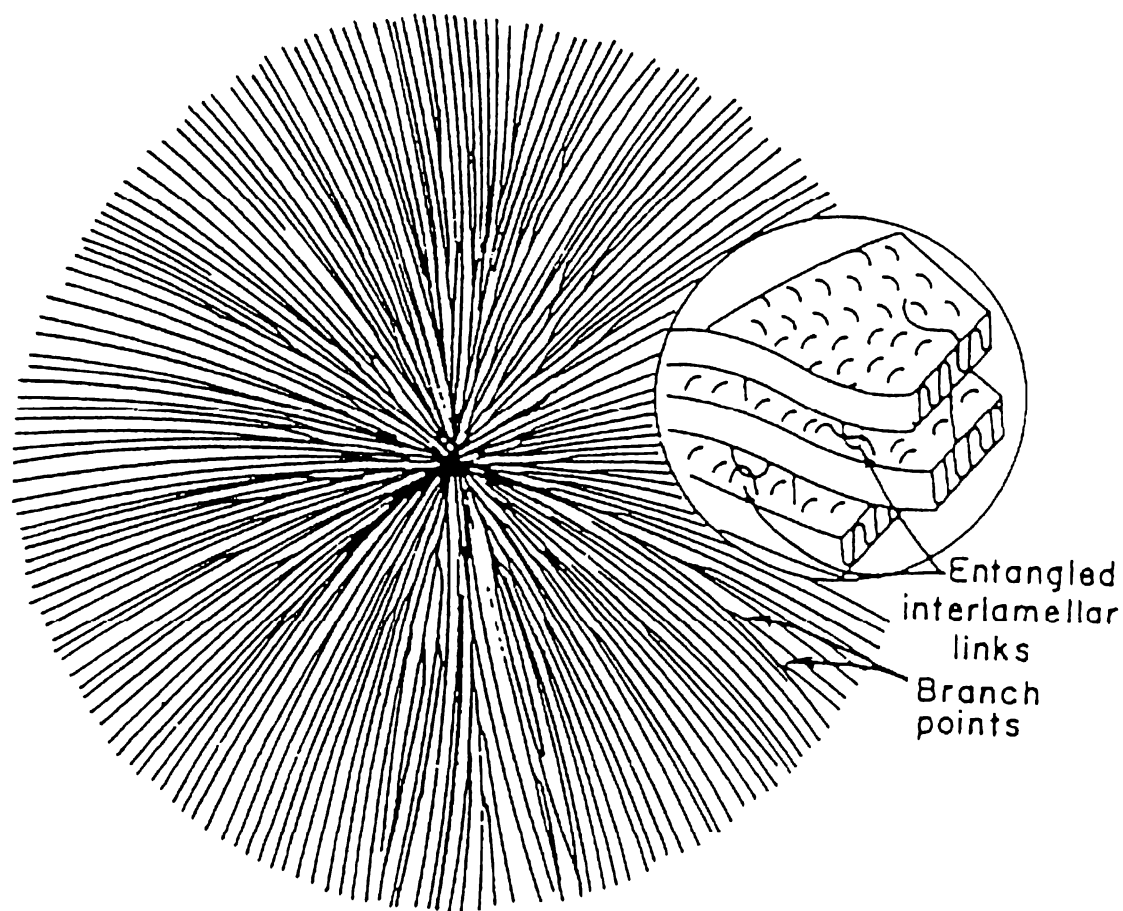


Figure 2.3: The schematic of a growing spherulite (Hoffman et al., 1975).

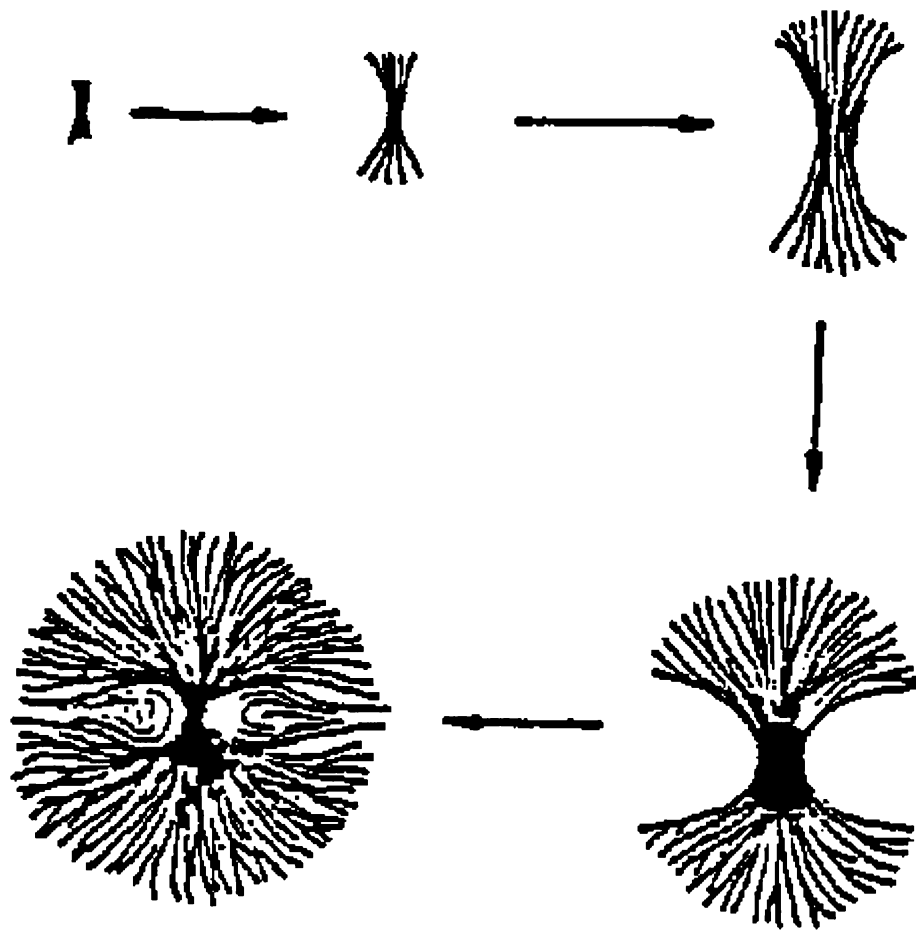


Figure 2.4: Growth forms leading to the spherical shape of a mature spherulite (Bassett, 1981).

another, resulting in a polyhedral shape. Secondary crystallization can take place within the spherulite, transforming a portion of the amorphous material between the lamellae into crystalline material.

#### 2.4.4 Axialites

Axialites are collections of crystal lamellae, which may exhibit the different characteristics of single crystals and spherulites depending upon the angle of view. Tie molecules or crystals between the lamellae may limit the extent of splaying in the axialite as suggested by Hearle (1982). Axialites are able to crystallize in a variety of supermolecular structures such as hedrites, ovoids, and spiral ovoids (Rabek, 1980).

### 2.5 Crystallization Models For Random Copolymers

There are two extreme methods for which a random copolymer can crystallize into one set of crystals. Flory (1955) describes one theory that is known as the exclusion model. In this model the copolymer crystals are composed only of the rich component, A. The dilute component, B, is excluded from the crystalline region. Sanchez and Eby (1973) argued another theory that the other extreme may be thermodynamically feasible, that is, component B exists as inclusions in crystals of component A. These components are shown in Figure 2.5. It is beneficial to determine the equilibrium melting temperature

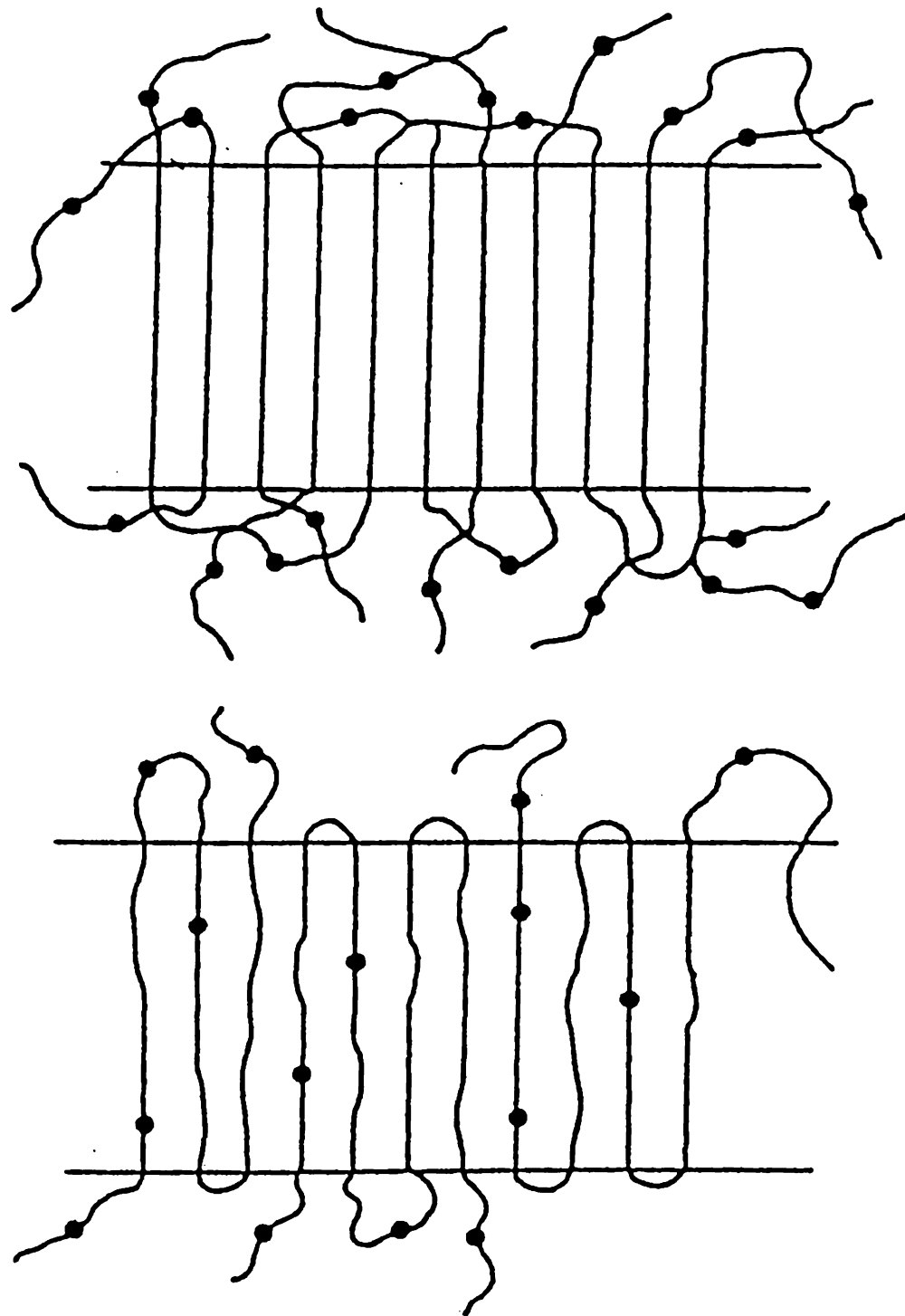


Figure 2.5: Exclusion and Inclusion Crystallization of Random Copolymers (Schreiber, 1998).

and lamellar thickness based on these two models, since many experiments in the literature determine how these quantities change with comonomer content.

### 2.5.1 Exclusion model

In the exclusion model developed by Flory (1955) the probability that a given unit in a polymer chain is the A component followed by an uninterrupted sequence  $\zeta - 1$  units long of A is given by  $P$ . The probability that sequences  $\zeta$  long of A in the amorphous polymer will be in equilibrium with crystallites  $\zeta$  long is related to the free energy by the following equation:

$$P_{\zeta}^e = \exp(-\Delta G_{\zeta} / RT) \quad (2.5.1)$$

A random copolymer that has not begun to crystallize the probability,  $P^0$ , can be related to the mole fraction of A by the following equation.

$$P_{\zeta}^0 = X_A p^{\zeta-1} \quad (2.5.2)$$

Here lower case  $p$  is known as the sequence propagation probability which is the probability that a given A group is followed by another A group regardless of what preceded the given A unit (Flory, 1955). For a truly random copolymer  $p = X_A$ , for block

copolymers  $p > X_A$ , and for alternating copolymers  $p < X_A$ . For a copolymer to crystallize  $P^0 > P^e$  is required for one or more values of  $\zeta$ . Making the assumption that the copolymer is perfectly random, and setting  $P^0 = P^e$  for a condition of equilibrium the following equation is developed:

$$(X_A)^\zeta = \exp(-\Delta G_\zeta / RT) \quad (2.5.3)$$

To fully evaluate this equation one must define the free energy term. Flory (1955) gives the following equation:

$$\Delta G_\zeta = \zeta \Delta G_u - 2\sigma_e \quad (2.5.4)$$

Where:

$$\Delta G_u = \Delta H_u - T\Delta S_u \quad (2.5.5)$$

$$T_m^\circ = \frac{\Delta H_u}{\Delta S_u} \quad (2.5.6)$$

$$\Delta G_u = \Delta H_u \left[ 1 - \left( T / T_m^\circ \right) \right] \quad (2.5.7)$$

The fold surface free energy,  $\sigma_e$ , is discussed in detail in sections 2.6.1 and 2.7.1. The surface free energy is at the area at the fold of the lamellae. This site provides a site for nucleation to occur. Subscript  $u$  corresponds to per unit component A.  $T_m^\circ$  is the melting temperature of the homopolymer of component A. The lamella thickness,  $l$ , can be related to the crystallite length,  $\zeta$ , by knowing the length of the crystallizing unit, component A. Inserting the free energy term into equation 2.5.3 and then taking the natural log of both sides.

$$\zeta \ln(X_A) = \frac{2\sigma_e}{RT} - \zeta \frac{\Delta H_u}{R} \left[ \frac{1}{T} - \frac{1}{T_m^\circ} \right] \quad (2.5.8)$$

$$T_m(\zeta) = \frac{T_m^\circ \left[ 1 - \frac{2\sigma_e}{\Delta H_u} \frac{1}{\zeta} \right]}{1 + \frac{RT_m^\circ}{\Delta H_u} \ln \left( \frac{1}{X_A} \right)} \quad (2.5.9)$$

$$T_m(\zeta \rightarrow \infty) = T_m^\circ(X_A) = \frac{T_m^\circ}{1 + \frac{RT_m^\circ}{\Delta H_u} \ln \left( \frac{1}{X_A} \right)} \quad (2.5.10)$$

Equation 2.5.9 is the melting temperature for a crystal of length  $\zeta$ . Equation 2.5.10 applies to an infinitely thick crystal or the equilibrium melting temperature for the copolymer. Observe that as the mole fraction of the rich component is reduced the



melting temperature decreases. The critical lamella length can also be determined by rearranging equation 2.5.9. This result is shown in equation 2.5.11:

$$\zeta_c = \frac{2\sigma_e T_m^\circ}{\Delta H \left[ T_m^\circ - T \left( 1 + \frac{RT_m^\circ}{\Delta H_u} \ln \left( \frac{1}{X_A} \right) \right) \right]} \quad (2.5.11)$$

#### 2.5.1.1 Revised Flory Equations of Fusion

Hoel (1998) considered extended-chain (EC) crystalline polymer systems that are composed of linear polyethylene as well as discussing more thermodynamic information on their melting and crystallization (Wunderlich, 1980; Mandelkern, 1989). To analyze extended-chain crystalline systems composed of linear polyethylene, Flory's conventional theory of fusion was reconsidered by introducing a new concept of crystallinity. This new treatment was applied to melting of a low molecular weight polyethylene fraction ( $M_n = 5600$ ) isothermal bulk crystallized. It was found that a very large lamellar thickness was caused by a very small increase in crystallization temperature that can satisfactorily be explained by a significant change in interfacial free energy of the crystallite end. It was concluded that the  $\sigma_{ec}$  (interfacial free energy) 14-17 kJ/mol might be the most appropriate for EC composed of a linear polyethylene of  $x \leq 400$  units.

## 2.5.2 Mixing Entropy Term For Exclusion Model

The exclusion model has been adjusted by Goldbeck-Wood to account for mixing entropy contributions in forming the lamellar crystals (Goldbeck-Wood, 1992). The adjustment was developed from an extension of the Sadler-Gilmer model for polymer crystallization (Sadler and Gilmer, 1986). The assumption is made that each stem in the lamellar crystal is built up through a process of attachment and detachment of small segments at the growth face. Segments can only be added and removed from the outermost stem as depicted in Figure 2.6 (Armistead and Goldbeck-Wood, 1992).

The first segment will have a probability of 1 of being component A, and it will contribute a free energy similar to equation 2.6.7. The second segment will also contribute this amount of free energy, however Goldbeck-Wood considers that there is also a mixing entropy term,  $S_2 = -k \ln p$ . Therefore the  $i$ th segment would have the following mixing entropy contribution:

$$S_i = -k \ln p^{(i-1)} \quad (2.5.12)$$

This gives the free energy of a lamellar crystal due to fusion with average thickness  $\zeta$  equal to the following when summing over the normalized thickness distribution  $C(i)$ .

$$S_i = -k \ln p^{(i-1)} \quad (2.5.12)$$

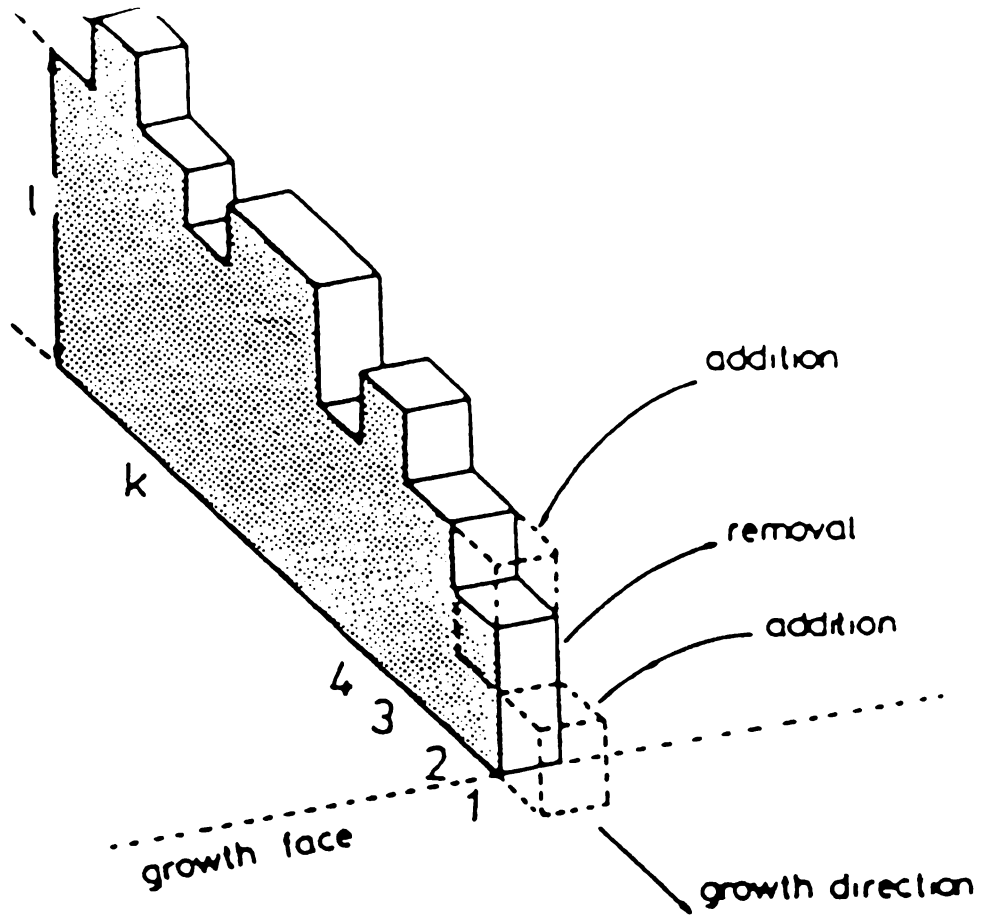


Figure 2.6. Goldbeck-Wood Model (Armistead and Goldbeck-Wood, 1992).

This gives the free energy of a lamellar crystal due to fusion with average thickness  $\zeta$  equal to the following when summing over the normalized thickness distribution  $C(i)$ .

$$\zeta \Delta G_u = \Delta H \left( 1 - \frac{T}{T_m^\circ} \right) \left[ \sum_{i=1}^N i C(i) \right] + kT \left[ \sum_{i=1}^N C(i) \sum_{j=1}^i (j-1) \ln p \right] \quad (2.5.13)$$

Simplifying where:

$$\zeta = \sum_{i=1}^N i C(i)$$

$$\sum_{j=1}^i (j-1) = \frac{i^2 - 1}{2}$$

The following equation is obtained for the free energy of fusion per segment:

$$\Delta G_u = \Delta H \left( 1 - \frac{T}{T_m^\circ} \right) + \frac{kT}{2\zeta} \left( \sum_{i=1}^N i^2 C(i) - \zeta \right) \ln p \quad (2.5.14)$$

When a Gaussian distribution is assumed to describe the stem lengths, where,

$$\sum_{i=1}^N i^2 C(i) = \zeta_{\min}^2$$

then 2.5.14 reduces to the following when we assume  $\zeta = \zeta_{\min}$ . Where  $\zeta_{\min}$  is the minimum lamellar thickness required to have the melt in equilibrium with the crystal at a given temperature, T.

$$\Delta G_u = \Delta H \left( 1 - \frac{T}{T_m^\circ} \right) + kT \frac{\zeta - 1}{2} \ln p \quad (2.5.15)$$

At equilibrium the total free energy will be zero. Equation 2.5.4 can then be rearranged to an expression for  $\Delta G_u$  and set equal to equation 2.5.15.

$$\Delta G_u = \frac{2\sigma_e}{\zeta_{\min}} = \Delta H \left( 1 - \frac{T}{T_m^\circ} \right) + kT_m \frac{\zeta_{\min} - 1}{2} \ln p \quad (2.5.16)$$

Here T is now equal to  $T_m$ , which is the melting point of the lamellar crystal with thickness  $\zeta_{\min}$ . Solving for  $T_m$  the following equation is obtained, which can be compared to equation 2.6.9 above that Flory developed.

$$T_m(\zeta_{\min}) = T_m^\circ \frac{\left[ 1 - \frac{2\sigma_e}{\zeta_{\min}} \right]}{1 - \left( \frac{\zeta_{\min} - 1}{2} \right) \frac{kT_m^\circ}{\Delta H} \ln p} \quad (2.5.17)$$

The term  $(\zeta_{\min}-1)/2$  is due to the mixing entropy according to Goldbeck-Wood's formulation. Without this term it is essentially identical is Flory's equation 2.5.9 above.

### 2.5.3 Inclusion Model

For the inclusion model Sanchez and Eby considered there to be an excess enthalpy involved in forming the inclusion or defect (Sanchez and Eby, 1973). Heat of fusion is modeled as a simple linear relationship with mole fraction of the dilute component B. As in the exclusion model the heat of fusion and entropy are considered to be independent of temperature. In addition, the entropy is considered to be independent of composition. The heat of fusion is given by:

$$\Delta H(T, X) = \Delta H(T_m^\circ) - X_B \cdot \Delta H_d \quad (2.5.18)$$

Here  $\Delta H_d$  is the excess enthalpy due to the formation of a crystal defect (Sanchez and Eby, 1973). Note that the mole fraction of the dilute component,  $X_B$  is used instead of the rich component as in the exclusion model. The equilibrium melting temperature is obtained by the following method.

$$T_m^\circ(X_B) = \frac{\Delta H(T_m^\circ(X_B))}{\Delta S(T_m^\circ(X_B))} \quad (2.5.19)$$

$$T_m^\circ(X_B) = \frac{\Delta H(T_m^\circ(X_B))}{\Delta H(T_m^\circ)} T_m^\circ \quad (2.5.20)$$

$$T_m^\circ(X_B) = \left(1 - \frac{\Delta H_d}{\Delta H(T_m^\circ)} X_B\right) T_m^\circ \quad (2.5.21)$$

Equation 2.5.21 indicates that the equilibrium melting temperature will decrease with increasing amount of the dilute component.

It is also possible to determine the melting temperature as a function of lamellar thickness for the inclusion model. This is similar to the number of units in a sequence,  $\zeta$ , used in the exclusion model. For this case the units of  $l$  are not specified, and they do not necessarily have to be the same as  $\zeta$ . As a result the lamellar thickness is going to be much smaller than the other two dimensions of the crystal and the bulk free energy,  $\Delta G$ , of the crystal will be zero at equilibrium. The bulk free energy of fusion of the crystal can be related to the lamella thickness.

$$\Delta G_f = \frac{2\sigma_e}{l} \quad (2.5.22)$$

$$\Delta G_f = \Delta H(T, X_B) - T\Delta S(T, X_B) \quad (2.5.23)$$

By substituting equations 2.5.18 and 2.5.21 into equation 2.5.23 and rearranging produces the following two equations for the melting temperature as a function of lamella thickness and the critical lamella thickness using equation 2.5.22.

$$T_m^\circ(l) = \left(1 - \frac{2\sigma_e}{\Delta H(T_m^\circ)} \frac{1}{l} - \frac{\Delta H_d}{\Delta H(T_m^\circ)} X_B\right) T_m^\circ \quad (2.5.24)$$

$$l_c = \frac{2\sigma_e T_m^\circ}{\Delta H(T_m^\circ) \left(T_m^\circ - T - \frac{\Delta H_d T_m^\circ}{\Delta H(T_m^\circ)} X_B\right)} \quad (2.5.25)$$

#### 2.5.4 Comparing Inclusion and Exclusion Models.

As seen in Figure 2.7  $T_m^\circ(X_B)$  is plotted as a function of  $X_B$  for both the Flory exclusion and the Sanchez and Eby models. The values for the equations are the following,  $T_m^\circ$  was 461 K for the homopolymer,  $\Delta H_v = \Delta H(T_m^\circ)$  was 1370 cal/mole of monomer,  $\sigma_e$  was 2.45 kcal/mole (Sanchez and Eby, 1975). Both of these show a nearly linear decrease in  $T_m^\circ$  with increasing  $X_B$ . However, by changing the parameters one can change which model has the steepest slope. Unless one can independently determine these values, it is difficult to decide which model appears to be occurring in a given copolymer system.

By comparing 2.5.11 with 2.5.25 it is possible to see that both models predict an increase in thickness with an increase in mole fraction of B. This appears to be counterintuitive for the exclusion model. Even as  $X_B$  increases, there will be sequences long enough for crystallization at the higher-level critical lamellar thickness, even though



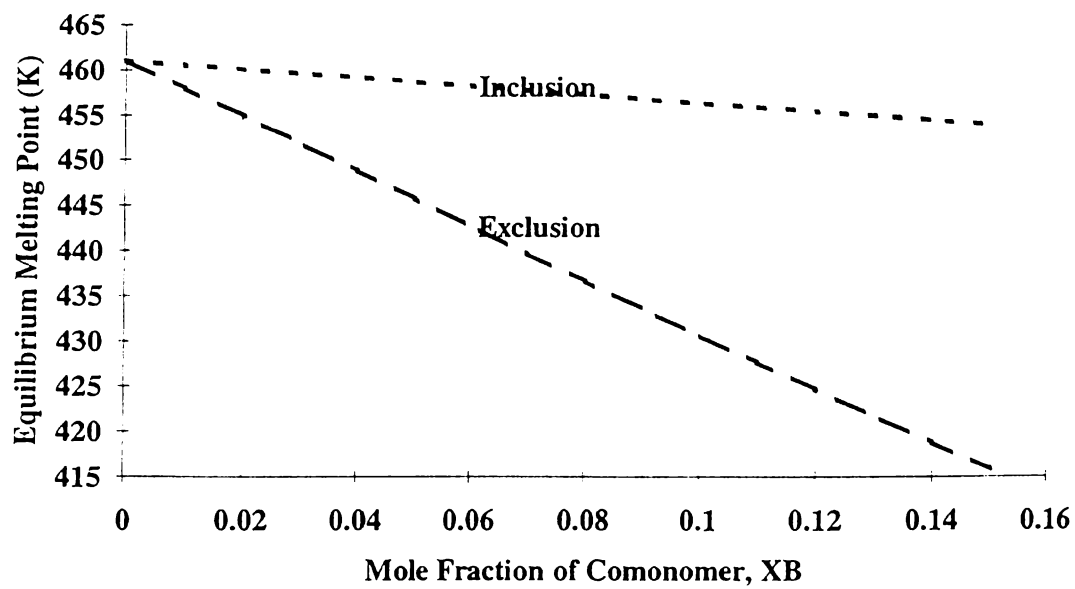


Figure 2.7. Random Copolymer Crystallization Models of Flory and Sanchez & Eby (Schreiber, 1998).

the average sequence length has decreased. This means that the lamella thickness can increase due to the random nature of the copolymer, but there will be a decrease in the crystallinity because less sequence long enough are available. In a block copolymer this obviously does not occur because there is only one sequence length available, and the lamella thickness and crystallinity will both decrease as  $X_B$  increases. Without knowledge of the specifics both models show similar responses in the melting temperature and lamella thickness. It is therefore difficult for one to make a decision on what type of model occurs based on measurements of these two quantities. In addition, the actual thickness will be a function of temperature as well as composition. In theory if one assumes that the enthalpies are additive then one can determine that the observed enthalpies of the two models will differ by the same amount. Sanchez and Eby give the equations for the enthalpy of both models (Sanchez and Eby, 1975).

### **Inclusion Model**

$$\frac{\Delta H^\circ}{\chi} = \Delta H - \chi_B \Delta H_d - 2\Delta H_e / l \quad (2.5.26)$$

### **Exclusion Model**

$$\frac{\Delta H^\circ}{\chi} = \Delta H - 2\Delta H_e / l \quad (2.5.27)$$

$\Delta H_e$  is the excess enthalpy required in forming the basal surfaces of the copolymer crystal.  $\chi$  is the crystallinity, and  $\Delta H^*$  is the observed heat of fusion. For the inclusion model  $X_B$  affects the observed enthalpy whereas the exclusion model is unaffected once the enthalpy is normalized with the degree of crystallinity.

Sanchez and Eby have also considered the copolymer crystallization between the two extremes discussed above (Sanchez and Eby, 1975). In this model, the mole fraction of inclusions in the crystal may be less than the mole fraction in the amorphous phase. This model fit experimental data for L- and DL- Lactides (Fischer et. al., 1973 and Sterzel, 1973). Furthermore the model predicts increases in lamella thickness with increasing mole fraction of the non-crystallizing unit. It should be noted that all three models assume that the amount of component B is small, less than 10 or 20%.

## **2.6 Secondary Nucleation Theory**

The Lauritzen-Hoffman theory (Hoffman, 1997) will be used to analyze the kinetic data, as it has a wide range of applicability, giving good correlation with experimental data. The theory of Hoffman et al. (1976) will be reviewed here, as well as some recent advances in the theories of crystallization.

### 2.6.1 Model

In describing polymer lamellar crystal growth the model seen in Figure 2.8 can be used.  $a$ ,  $b$ , and  $l$  are the width, thickness, and height of the surface nucleus, respectively, with  $l$  being fixed at any specified under cooling.  $L$  is the crystal width, and  $\sigma$  and  $\sigma_e$  are the lateral and fold surface free energies, respectively. Surface nucleus grows in the “g” direction, with the measured growth in the “G” direction. However, when  $v_f = v - 1$  folds have been formed, the free energy of formation of the crystal is, ignoring chain effects:

$$\Delta\Phi_v = 2bl\sigma + 2v_f ab\sigma_e - vabl\Delta f \quad (2.6.1)$$

Where for large  $v$ ,  $\Delta\Phi_v$  becomes,

$$\Delta\Phi_v = 2bl\sigma + vab(2\sigma_e - l\Delta f) \quad (2.6.2)$$

The surface nucleus starts when a polymer segment or set of segments from the undercooled melt attaches itself to the crystal surface and comes into crystallographic register with the substrate, forming the first stem at the cost of  $2bl\sigma$ . The molecule then folds back on itself and crystallizes adjacent to the first stem. The adjacent stem is the most probable site for reentry after folding, as attachment on a non-adjacent position will add an extra term of  $2bl\sigma$  to equation 2.6.1. As adjacent reentry folding is repeated, a surface nucleus will approach a region of stability as it grows in the “g” direction. The

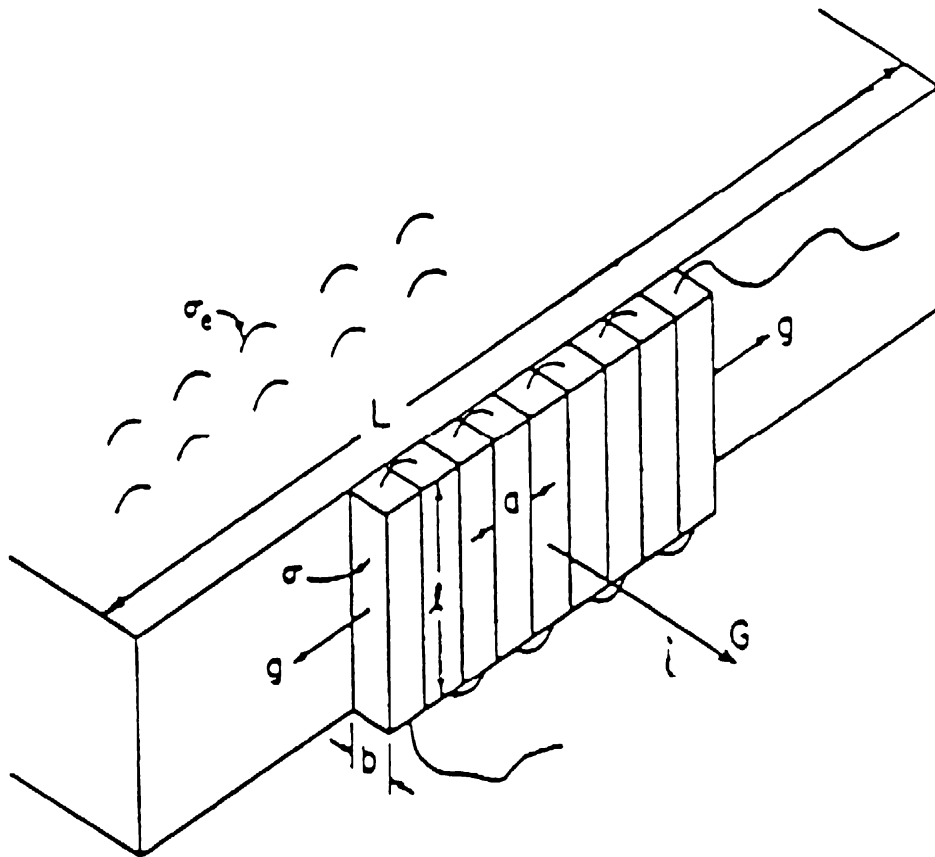


Figure 2.8: The diagram of growth for one lamellar crystal (Phillips, 1990).

surface nucleus goes through a maximum in its free energy of formation at or near the first stem ( $v=1$ ), and then gradually approaches the region of stability as the number of stems increases as shown in Figure 2.9. Figure 2.9 shows that the nucleation process is a set of connected rate processes, where between states  $V = 0$  and  $V = 1$ ,  $A_0$  and  $B_1$  are the forward and backward reactions, respectively. Growth is a nucleation-controlled process in which the large barrier due to the creation of new surfaces must first be overcome to initiate the nucleus, with subsequent steps leading to the stable region.

## 2.6.2 Total Flux

A general steady state expression for the flux  $S$  over the barrier to nucleation may be given as:

$$S = N_0A_0 - N_1A_1 \quad (2.6.3)$$

Where  $N_0$  and  $N_1$  are the occupational numbers for  $v = 0$  and  $1$  respectively, and  $A_0$  and  $A_1$  are the rates of the forward and reverse reactions between states  $v = 0$  and  $1$ , respectively. The net rate of reaction of nuclei of length “ $l$ ” is:

$$S(l) = \beta N_0 \exp\{-2bl\sigma + \psi abl(\Delta G)/kT\} \\ \times [1 - \exp\{-abl(\Delta G) + 2ab\sigma_e/kT\}] \quad (2.6.4)$$

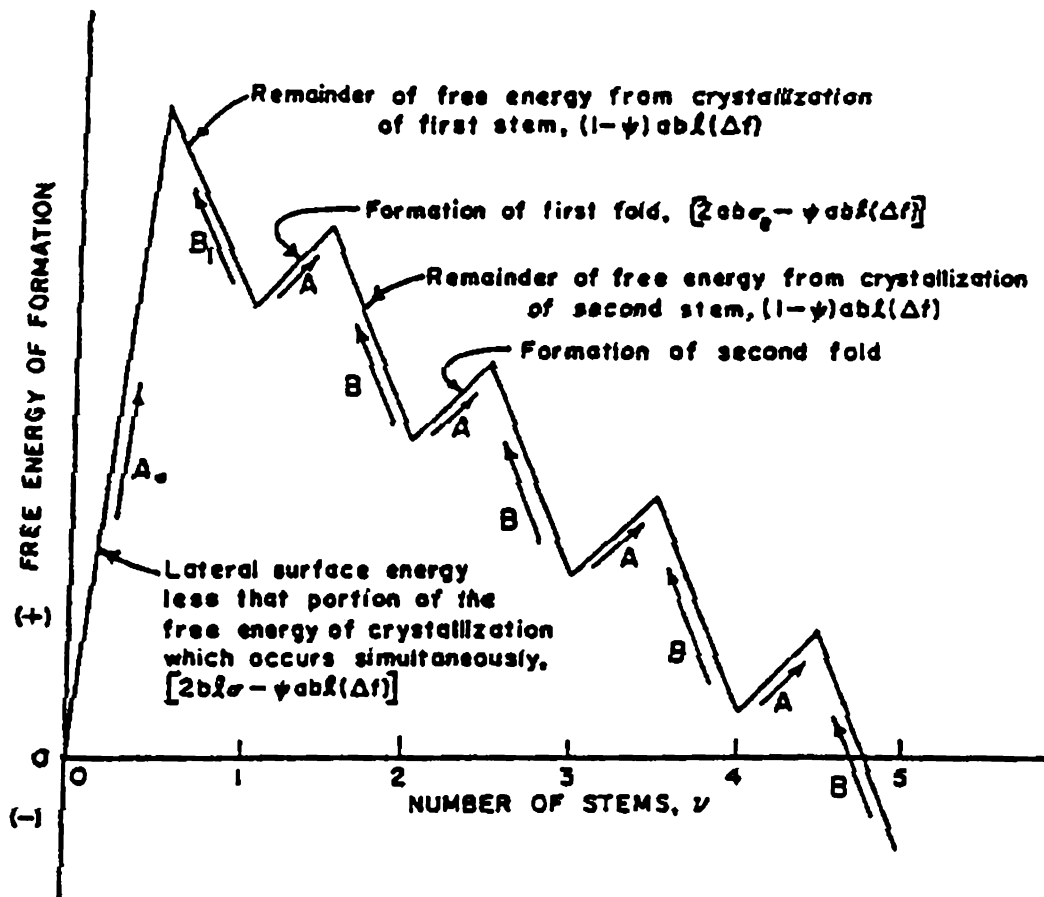


Figure 2.9: Free Energy of Formation of a chain folded surface nucleus (Hoffman et al., 1975).

Where  $\beta$  is the retardation factor accounting for retardations to molecular motion resulting from the fact that the polymer molecules must be transferred from the site of crystallization  $\Delta G$  is the bulk free energy of fusion,  $T$  is the crystallization temperature, and  $\Psi$  is the fraction of the free energy apportioned to the activation energy of the forward reaction (Hoffman et al., 1975).

The term  $\psi$  is related to whether or not the polymer molecule is physically adsorbed on the surface prior to crystallographic attachment onto the substrate. When the polymer molecule moves directly from the melt onto the growth face so that each segment simultaneously acquires its lateral and surface free energy of fusion, the value of  $\psi$  will be unity. The polymer molecule is physically adsorbed onto the growth face before crystallographic attachment. The crystallographic attachment results in the free energy of fusion occurring after a localized migration, producing  $\psi$  values less than unity. The case of  $\psi$  equal to 0 is due to a weak adsorption from the sub cooled liquid of a set of segments with a total length that is half that of a fold period. This is followed by surface migration and crystallographic attachment to the growth face, with simultaneous deposition of the other units in the chain to complete the stem. Here  $\psi = 0$  and  $\psi = 1$  are considered to be extremes, and the case  $1 > \psi > 0$  is expected in real polymer systems.



### 2.6.3 Initial Lamellar Thickness

The initial lamellar thickness,  $l_g^*$ , prior to isothermal thickening, is the average value of  $l$  calculated from the flux  $S_T$ :

$$l_g = (l/l_n) \int_{2\sigma_e/\Delta G}^{\infty} lS(l)dl / (l/l_n) \int_{2\sigma_e/\Delta G}^{\infty} S(l)dl \quad (2.6.5)$$

This will give:

$$l_g^* = \frac{2\sigma_e}{\Delta G} + \frac{kT}{2b\sigma} \times \frac{[2 + (1 - 2\psi)a\Delta G]/2\sigma}{(1 - a\Delta G\varphi/2\sigma)[1 + a\Delta G(1 - \varphi)/2\sigma]} \quad (2.6.6)$$

The last term in equation 2.6.6 is  $\delta l$ , the additional thickness required for the crystal to grow at a finite rate.  $\delta l$  is only a weak function of undercooling, but a strong function of  $\psi$ .

### 2.6.4 Free Energy of Fusion

The free energy of fusion ( $\Delta G$ ) can be approximated near the melting temperature by assuming the heat of fusion to be independent of temperature, so that:

$$\begin{aligned}\Delta G &= \Delta H_f^\circ - T\Delta S_f = \frac{\Delta G_f^\circ - T(\Delta G_f^\circ)}{T_m^\circ} \\ &= \Delta G_f^\circ \left(1 - \frac{T}{T_m^\circ}\right)\end{aligned}\quad (2.6.7)$$

Here  $\Delta G_f^\circ$  is the heat of fusion per unit volume of crystal at the equilibrium melting temperature  $T_m^\circ$ , and  $\Delta T$ , equal to  $T_m^\circ - T$ , is the undercooling. It is not good to assume that  $\Delta G_f^\circ$  does not vary with temperature at high undercooling since it decreases as the temperature is lowered. This causes equation 2.6.7 to overestimate  $\Delta G$  at high undercoolings. Hoffman and Weeks (1962) introduced a correction factor to compensate for the error in  $\Delta G_f^\circ$  at high undercoolings:

$$f = \left(\frac{2T}{T_m^\circ + T}\right)\quad (2.6.8)$$

Where  $T$  is the crystallization temperature. Then  $\Delta G$  is modified in equation 2.2.7 to give:

$$\Delta G = \left(\frac{\Delta G_f^\circ}{T_m^\circ}\right) f\quad (2.6.9)$$

The factor is approximately unity at lower undercoolings, but results in a decrease in  $\Delta G$  at higher undercoolings in its reduction of the heat of fusion with decreasing temperature.

### 2.6.5 Spinodal-Assisted Crystallization In Polymer Melts

A major unsolved problem is the dynamics of first order phase transitions is the dynamical behavior of a system following a quench into the unstable region of the phase diagram. In this section several attempts to understand the early stages of this instability, which is often, termed spinodal transformation. These include linear theories due primarily to Hillert (1961), Cahn (1968), and Cook (1970), and the most successful non-linear theory so far developed, due to Langer, Bar-on, and Miller (1975). In this section most of the details are omitted, because there is at the moment no completely satisfactory theory.

#### 2.6.5.1 Linear Theories

The first qualitative theoretical understanding of the long-wavelength instability, which characterizes spinodal transformation, is due to Cahn (Gunton, 1983). Cahn noted that immediately following a quench into the unstable region of the phase diagram the initial fluctuation in concentration should be small. The validity of Cahn's linearized theory is now considered by many authors to be at best limited to very short times

following the quench. The early stages of this instability are often termed spinodal transformation.

#### 2.6.5.2 Crystallization in polymer melts

Recent experiments have shown that in some polymer melts quenched below the melting temperature, spinodal kinetics are observed in small-angle X ray scattering before the emergence of Bragg peaks at wide angles. Olmsted (1998) proposed that the coupling between density and secondary order parameters chiefly chain conformation, but also orientation gives rise to a liquid-liquid binodal buried within the equilibrium liquid-crystalline solid coexistence region. Shear is shown to enhance the kinetic role of this hidden bimodal.

Upon cooling a polymer melt sufficiently far below its equilibrium melting temperature  $T_m^\circ$ , a hierarchy of ordered structures emerges (Strobel, 1996). First, there are crystalline 'lamellae', comprising regularly packed polymer chains, each of which is ordered into a specific helical conformation. These lamellae interleave with amorphous layers to form 'sheaves', which in turn organize to form superstructures (i.e. spherulites). This hierarchy of structures may be probed by various techniques: i.e. wide-angle X-ray diffraction (WAXD) is sensitive to atomic order within lamellae ('Bragg peaks'), while small-angle X-ray scattering (SAXS) probes lamellae and their stacking. Olmsted for the earliest stages of ordering in a supercooling polymer melt proposed a model, 1998. In a

supercooled simple liquid, the following description (Frenkel, 1946) is widely accepted. Nuclei of the lower free energy crystal phase are constantly formed by thermal fluctuations. But the cost of creating an interface means that only large enough nuclei grow, therefore, the melt is metastable. An induction time,  $\tau_i$ , elapses before the probability of forming such ‘critical nuclei’ becomes significant. This picture is usually deemed appropriate for melts; instead effort is focused on explaining the anisotropic shape and growth rate of crystal nuclei (Goldbeck-Wood, 1995).

In the ‘classical’ picture of polymer melt crystallization we expect, and indeed observe, Bragg peaks in WAXD after an induction period,  $\tau_i$ . SAXS accompanies the WAXD, corresponding to interleaved crystal lamellae and amorphous regions (Strobel, 1996). No SAXS is expected during  $\tau_i$ . However, recent experiments have reported SAXS peaks during the induction period and before the emergence of Bragg peaks. Initially, the SAXS peak intensity grows exponentially while its position remains constant, the behavior predicted by Cahn-Hilliard (CH) theory for spinodal transformation – the spontaneous growth of fluctuations indicative of thermodynamic instability (Gunton, 1983). Later the peak moves to smaller angles, stopping suddenly when Bragg peaks emerge. By fitting to CH theory, an extrapolated spinodal temperature (at which the melt first becomes unstable towards local density fluctuations)  $T_s < T_m^\circ$  can be obtained (Olmsted, 1998).

A plausible explanation for the observation of spinodal dynamics in polymer melts is the presence of a metastable liquid-liquid (LL) phase coexistence curve (or

binodal') buried inside the equilibrium liquid-crystal coexistence region as shown in Figure 2.10. Quenching sufficiently below the equilibrium melting point  $T_m^\circ$ , we may cross the spinodal associated with the buried LL binodal at temperature  $T_s < T_m^\circ$ .

In Figure 2.10,  $T_m$  and  $T_s$  are the melting and spinodal temperatures encountered along the constant density quench path (dotted line). Parameters used are  $R_{Mb} = 0.8$ ,  $kBT^* = 0.29E_0$ ,  $v = 1.4E_0\omega$ ,  $\lambda = 0.1 a_{vo}$ ,  $b = -0.4 (v_{oa3}/E_0)^{1/2}$ ,  $c = 0.5a_2v_0/E_0$ , and  $\alpha = 0.8 / \omega$ . Inset shows the measured induction time as a function of temperature for isotactic polypropylene (Olmsted, 1998).

In order to crystallize, polymer chains must adopt the correct conformation. For example, the chains in crystalline polyethylene have the all-trans (or 'zig-zag') conformation, while in the melt the conformation is randomly trans or gauche. Generally, the preferred conformation is some form of helix. Furthermore, the radius of gyration of a very long chain changes very little during crystallization. This suggests that neighboring segments adopt the correct conformation and crystallize 'in situ' (Dettenmaier, 1980). It is commonly assumed that conformational and crystalline (intrachain and interchain) ordering occurs simultaneously. Olmsted (1998) suggests that processes can occur sequentially.

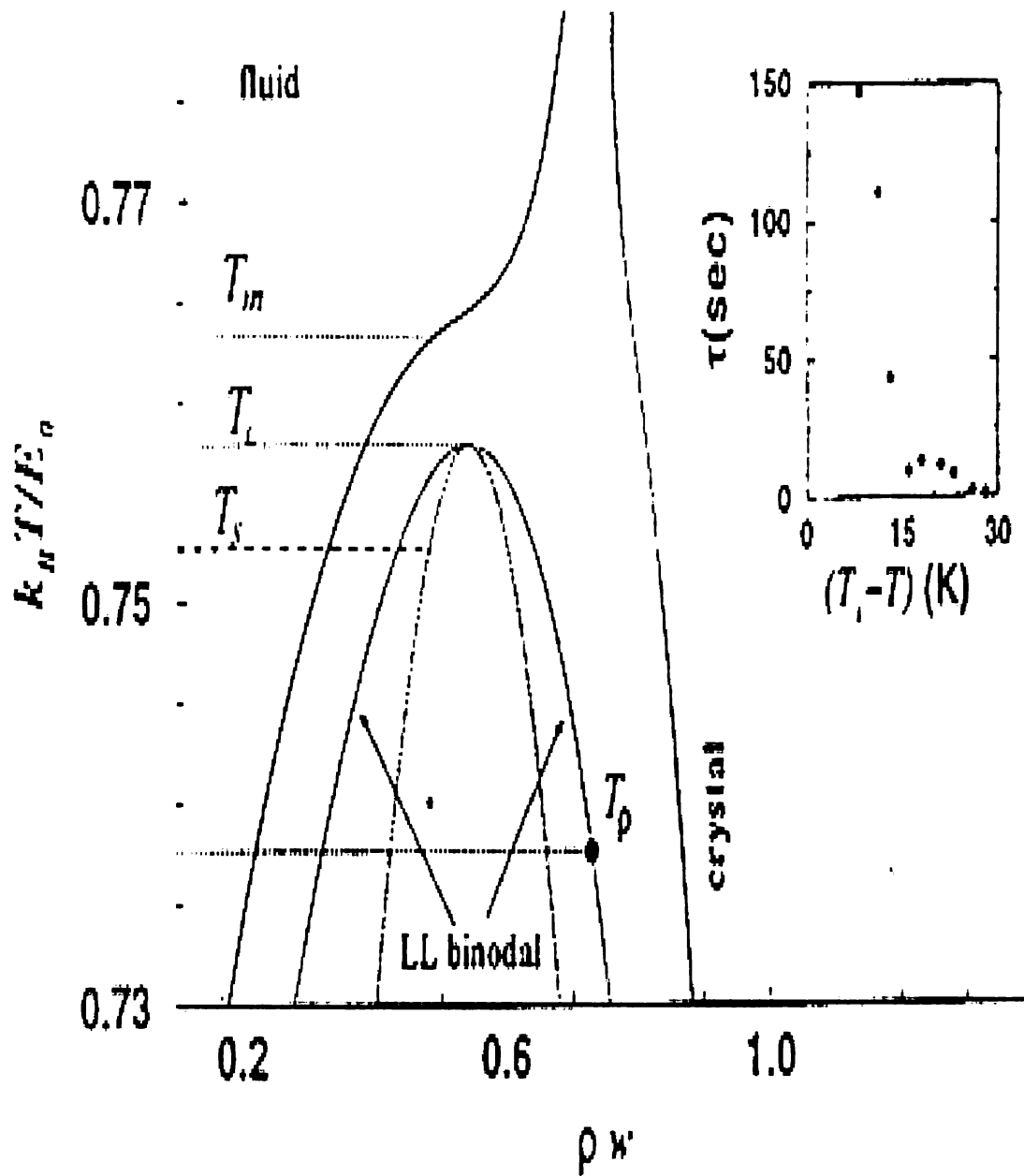


Figure 2.10 Phase diagram for a polymer melt proposed for spinodal-assisted crystallization (Olmsted, 1998).

In a melt, it is believed that chain conformation alone cannot drive a phase transition. However, conformation is coupled to density. Chains with the ‘correct’ (helical) conformation typically pack more densely than those with more or less random conformations. Moreover, the energy barriers between different rotational isomeric states (RIS) are density-dependent (Pratt, 1978). Conformational-density coupling can induce a LL phase transition. A phenomenological free energy which incorporates these effects is a function of the following order parameters: the average mass density  $\bar{\rho}$ ; the coefficients  $\{\rho_q\}$  in the Fourier expansion of the crystal density in terms of the appropriate stars of reciprocal lattice vectors  $\{q\}$  which essentially the intensities of Bragg peaks (Landau, 1980); and the occupancies  $\{\eta_i\}$  of various RIS and therefore chain conformation.

If it is assumed that a single  $\rho_q \equiv \rho^*$  and a single  $\eta$  suffice, corresponding to a fictitious polymer with body-centered cubic crystal structure (Alexander, 1975) and two RIS. The Gibbs free energy per unit volume has three components:

$$f = f_0(\bar{\rho}) + f^*(\bar{\rho}, \rho^*) + f(\eta, \bar{\rho}, \rho^*) \quad (2.9.10)$$

The first term,  $f_0$  is the free energy of a melt with random chain conformations. Equation-of-state fits to polymer liquids suggests the following form:

$$f_0(\bar{\rho}) = Rk_B T \bar{\rho} \ln \left[ \left( \frac{1}{\bar{\rho}} \right) - \varpi \right] \quad (2.9.11)$$



where  $R$  and  $\omega$  are tabulated for many polymers (Brandrup, 1989). The bare Landau free energy if crystallization is taken to be (Landau, 1980; Alexander, 1978):

$$f_*(\bar{\rho}, \rho_*) = \bar{\rho} \left[ \frac{1}{2} a(\bar{\rho}, T) \rho^2 + \frac{1}{3} b \rho_*^3 + \frac{1}{4} c \rho_*^4 \right] \quad (2.9.12)$$

$f_n$  describes how the distribution of chain conformations varies smoothly from random ( $\eta=0$ ) to totally ordered (helix,  $\eta=1$ ) as the temperature is lowered to zero (Flory, 1989).

The characteristic length scale associated with the developing spinodal texture gives rise to a SAXS peak, which evolves initially according to Cahn-Hilliard theory (Kawasaki, 1976). The coarsening of this texture is observed to be arrested at the end of the induction period (typical scale  $\xi_m$ ), when Bragg peaks appear in WAXD. It is at present unclear how the spinodal texture at the end of the induction period evolves into spherulites. However, the final spinodal texture length scale  $\xi_m$  evidently controls the thickness of the first crystal lamellae. Moreover, large stress will develop once one of the two liquids in a bicontinuous texture, Figure 2.11 crystallizes. It is expected that such a texture to fragment into individual crystalline lamellae.

Figure 2.11 shows a schematic representation of the late-stage spinodal texture for coexisting liquid phases with different conformations, showing a single chain; thin line =

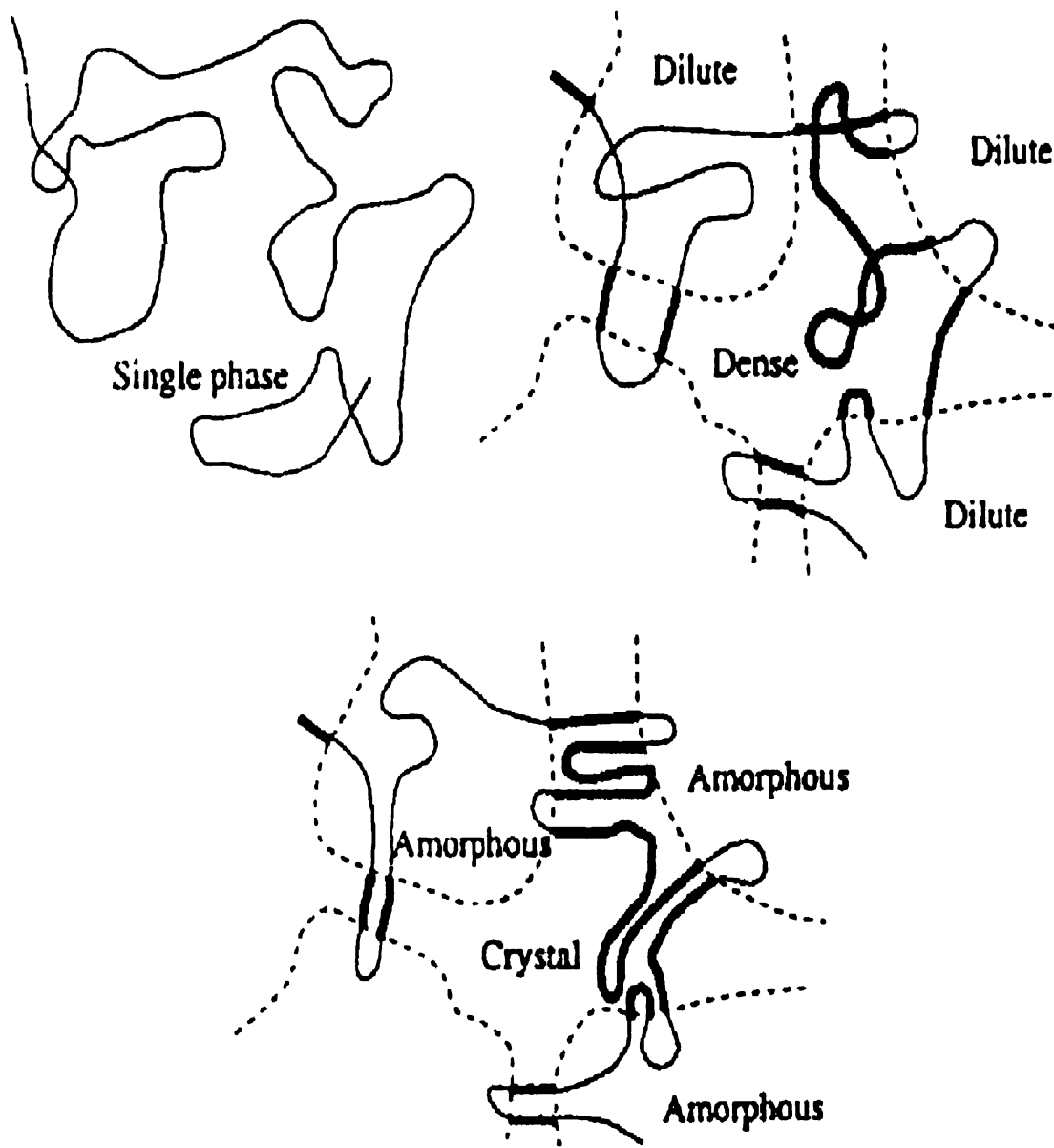


Figure 2.11. Schematic representation of the late-stage spinodal texture for coexisting liquid phases with different conformations (Olmsted, 1998).

disordered conformation, thick line = correct (helical) conformation for crystallization. Each chain is a 'conformational copolymer'.

The arguments developed so far have been based on conformational-density coupling. Once a polymer segment has adopted the correct helical conformation its persistence length should increase, which couples to the orientation order of chains. Indeed, depolarized light scattering by Imai and coworkers has suggested the existence of orientation fluctuations during the spinodal phase of a crystallizing PET melt (Imai, 1995). Provided that orientation ordering is not strong enough to induce a separate transition, then the inclusion of a nematic order parameter in equation 2.6.10 only renormalizes the coefficients in  $\eta$ -dependent terms. In some cases, the increasing chain stiffness accompanying conformational order may be sufficient to drive an isotropic→nematic transition, resulting in a three-step process: melt → (isotropic) liquid(1) + liquid (2), followed by liquid (2) → nematic → crystal.

Until recently, spinodal scattering was mainly observed in polymer melts crystallizing under shear (Strobl, 1996; Miller, 1979). This may be understood in a natural way within the present framework. Shear and extensional flow couples principally to the orientation of polymer segments, hence straightening chains and enhancing  $\eta$ , thereby biasing the tendency towards LL separation. A simple way to incorporate this is to renormalize the activation energy  $E$  as  $e - v_0\sigma$  where  $\sigma$  is the stress. It is highly suggestive that, for appropriate values of stress under strong flow (the plateau modulus  $G_0$ ) and volume ( $v_0$  above), the LL bimodal of Figure 2.10 is shifted upward

significantly (by  $\delta T_s \sim 0.01E_o/kB$ ). Flow will shift the liquid-solid coexistence curve much less because the regions with crystalline order will resist deformation.

## 2.7 Regime Transition Analysis

The crystal growth rate of polyethylene has been found to be constant with time before any retardation caused by the impingement of neighboring spherulites that were formed at the beginning of the nucleation process. This linear crystal growth rate is also dependent on the crystallization temperature from experimental observations. Lauritzen and Hoffman first introduced the concept of regime transitions into the crystallization of polymers after an investigation on linear polyethylene fractions (Hoffman et al., 1961, 1976). This included experimental verification of the regime I-II transition shown in polyethylene fractions. Existence of crystal growth regimes is based on the secondary nucleation theory and may be anticipated as a function of molecular weight and chemical structure of the polymers (Alamo, 1982). Phillips (1979) predicted the existence of a third regime. Hoffman (1983) derived the mathematical relationships of regime III crystallization. For linear PE fractions others have identified three crystallization regimes (Martinez et al., 1984, Barham, 1982).

### 2.7.1 Regime Analysis of Polyethylene Copolymers.

The theory of crystallization regimes (Alamo, 1982) describes the relationship between the growth rate of spherulites and the crystallization temperature. The growth of the spherulite is represented schematically in Figure 2.3, the enlarged section of the figure depicting the branches of the spherulite that are made of lamellar crystals. In Figure 2.8 the growth rate of the spherulite is equivalent to the growth of a single lamellar crystal. There are two rates to be considered which are  $i$  and  $g$ . These contribute to the growth rate of the lamellar crystal, which in turn relates to the growth rate of the spherulite,  $G$ . The rate of deposition of secondary nuclei onto the growing lamellar surface is labeled  $i$ . Lateral surface spreading across the growing lamellar surface is represented by  $g$ . The ratio of  $i$  to  $g$  with crystallization temperature produces three different regimes.

The secondary nucleation theory rate equation takes the form of:

$$G = G_0 \exp \left[ -\frac{U^*}{R(T - T_\infty)} \right] \exp \left[ \frac{K_g}{f(T_m^\circ - T)T} \right] \quad (2.7.1)$$

Where  $G$  is the linear growth rate,  $U^*$  is the activation energy for transport of the segments to the crystallization site,  $R$  is the gas constant,  $T$  is the crystallization temperature, and  $T_\infty$  is the temperature at which all motions associated with viscous flow cease and is defined as  $T_\infty = T_g - 30^\circ\text{C} = -85^\circ\text{C}$ . The  $T_g$  of polyethylene is  $-55^\circ\text{C}$ . For

polyethylene, the molecular motions that cause the glass transition are associated with a rearrangement of molecules by local motions such as kink motions (Uedono, 1997).  $T_m^\circ$  is the equilibrium melting point.

The nucleation constant  $K_g$  is defined as:

$$K_g = \frac{nb\sigma\sigma_e T_m^\circ}{k\Delta H_f} \quad (2.7.2)$$

Where  $n$  is 4 for regimes I and III and 2 is for regime II. By analyzing the slope in Figure 2.12, the nucleation constant  $K_g$  can be determined and then the product of surface energy ( $\sigma\sigma_e$ ) can be calculated using the following values,

where:

$\sigma$  is the lateral surface free energy,  $11.8 \text{ erg cm}^{-2}$

$\sigma_e$  is the fold surface free energy,  $90 \text{ erg cm}^{-2}$

$k$  is the Boltzman constant,  $1.3806 \times 10^{-16} \text{ erg molecule}^{-1} \text{ deg}^{-1}$

$\Delta H_f$  is heat of fusion,  $2.80 \times 10^9 \text{ erg cm}^{-3}$

$b_o$  is layer thickness,  $41.5 \times 10^{-8} \text{ cm}$

$f$  is the temperature dependence of  $\Delta H_f$  the heat of fusion, and usually  $f = 2T/(T_m^\circ + T)$

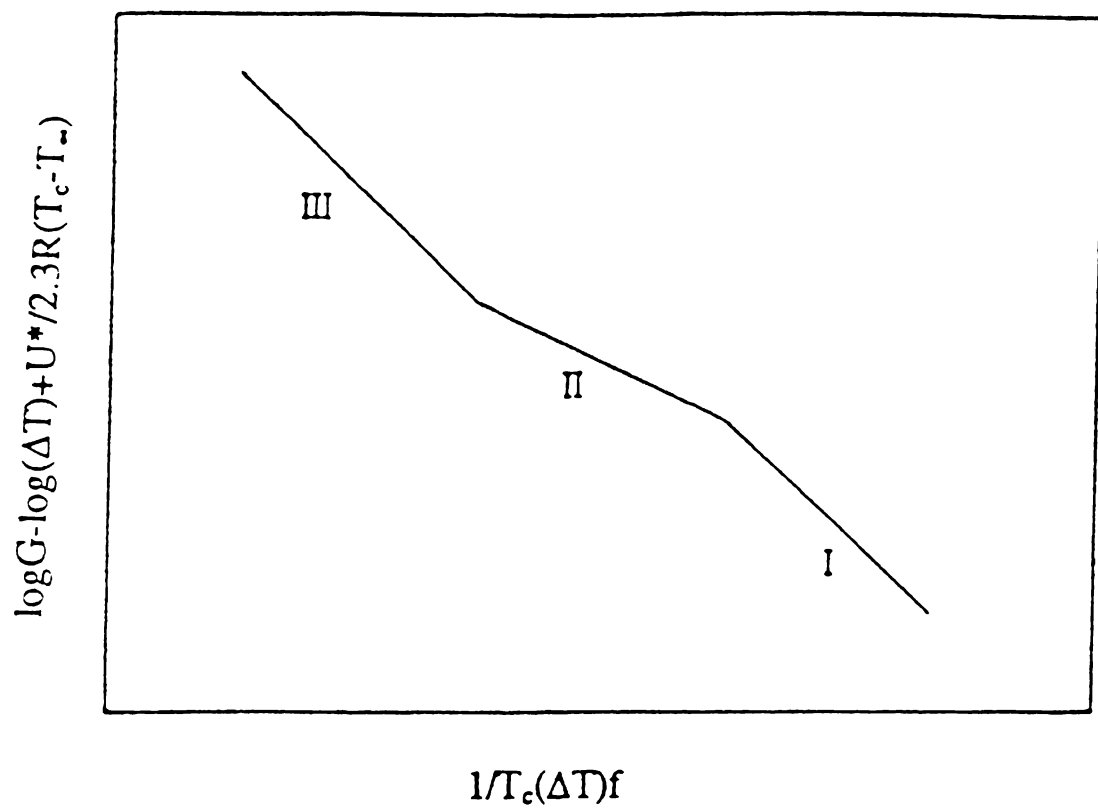


Figure 2.12. Regime transition analysis from crystal growth data (Allen, 1972).

## 2.7.2 Secondary Nucleation and Lateral Growth

Regimes are generally envisioned as resulting from the relative rates of the two competing processes of secondary nucleation and surface spreading. The rate of secondary nucleation is denoted as  $i$ . The rate of surface spreading is denoted as  $g$ . When expressed as units of area covered by unit time, the regimes correspond to the following conditions:

regime I       $i \ll g$

regime II      $i \sim g$

regime III     $i \gg g$

Regimes in polymer crystallization are distinguished by the relative rates of nucleation,  $i$ , of polymer stems onto the substrate surface and of lateral spreading,  $g$ , of polymers across the layer of the substrate.

For crystal growth in Regime I, the lateral spreading rate proceeds rapidly after surface nucleation is completed ( $i \ll g$ ). The entire substrate surface is covered before another successive surface nucleates. The crystal growth that occurs at high temperatures can be considered as a process of single nucleus growing on a mono-crystal-layer. The linear crystal growth rate  $G$  is observed to be proportional to the surface nucleation rate,  $i$ . Growth rate,  $G$ , which is normal to the substrate, is given by:



$$G_I (\text{cms}^{-1}) \equiv ib_oL \quad (2.7.3)$$

Where  $b_o$  is the layer thickness and  $L$  is the substrate length. Figure 2.13 shows a schematic diagram of regime I crystal growth.

As the crystallization temperature is decreased Regime II is approached. Where numerous nuclei are put down on the substrate of length  $L$ , the observable growth rate is defined for Regime II as:

$$G_{II} \equiv b_o(2ig)^{1/2} \quad (2.7.4)$$

At the intermediate crystallization temperatures the surface nucleation rate  $i$  is approximately equal to the lateral spreading rate  $g$  ( $i = g$ ). Numerous nuclei are put down on the mono-crystal layer.

### 2.7.3 Development of the Concept of Regime III Transitions

As the crystallization temperature is further decreased Regime III is obtained. The rate of deposition of secondary nuclei (Hoffman, 1983),  $i$ , is very large, being greater than the rate of lateral surface spreading,  $g$ , ( $i \gg g$ ). Since  $g$  is small, the growth rate is controlled by  $i$  with  $G \propto i$ . Overall, the number of surface nuclei per unit length

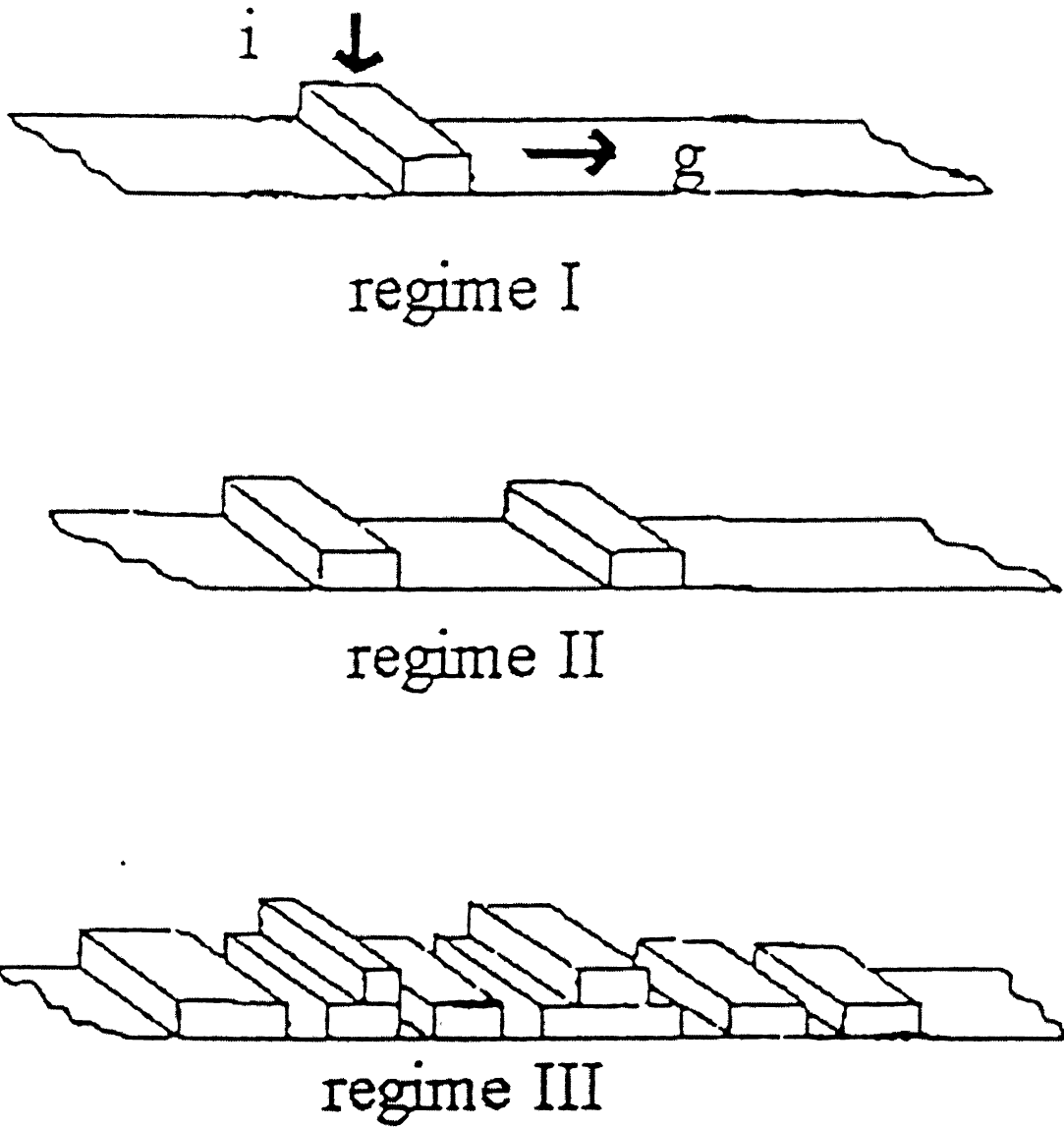


Figure 2.13: Schematic diagrams of Regime I, II, and III crystal growth (Hoffman, 1997).

increases as shown in Figure 2.13. The overall relationship between the regimes is shown in schematic plots of  $\log G$  vs.  $T_c$  and of  $\ln G + Q^*D/RT$  vs.  $1/T(\Delta T)$  that are representative of the experimental results.

There are some special features of Regime III crystallization that are worth noting. Crystallization in this regime has both technical and scientific importance. In processing, PE is frequently in effect “quench-crystallized” which definitely invites crystallization in Regime III. From a scientific standpoint, the importance of Regime III stems partly from neutron scattering and IR spectroscopy studies aimed at uncovering chain morphology or molecular trajectory of melt-crystallized PE. Neutron scattering studies clearly show that the molecular morphology characteristic of Regime III (Hoffman, 1997), is clearly more disorganized than that of regimes II or I. The kinetic data (Hoffman et al., 1975) imply the presence of a relatively high degree of adjacency in PE fractions of moderate molecular weight crystallized from the melt in Regime I, whereas the neutron scattering and IR studies (Hoffman et al., 1975) for comparable molecular weights suggest considerably poorer adjacency for PE specimens crystallized in Regime III.

The growth rate in regime III is defined (Hoffman, 1997) according to:

$$G_{III} \text{ (cm s}^{-1}\text{)} \equiv b_0 i(n_{III} a_0) \quad (2.7.5)$$

where  $n_{III}$  is between 2.0 – 2.5. For the case of single stems with no folds, a simulation by Guttman and DiMarzio (1983) gave  $n_{III}$  as  $\sim 1.5$  at the onset of regime III. For PE, where a substantial fraction of ‘tight’ folds must occur even in regime III because of the Gambler’s Ruin topological requirements,  $n_{III}$  can be estimated to be  $\sim 2.0-2.5$ .

#### 2.7.4 Crystallization Kinetics

To understand the molecular weight effect on the crystallization kinetics at fixed branch content, consider classical reptation behavior of a polymer chain. The rate of reptation of a single of a single chain, so-called reeling-in rate,  $r(cm/sec)$ , from the molten state to the substrate decreases with chain length as well as the rate of surface spreading  $g(cm/sec)$ . With the comparison of  $g$  with  $r$  it is easier to understand the reptation behavior of a single chain than with the net nucleation rate,  $i(nuclei/sec-cm)$ , because of the consistency of the units. Both rate  $r$  and  $g$  have known molecular weight dependence. The reeling-in rate  $r$  is faster by as much as about 36 times the surface spreading rate  $g$  (Hoffman, 1988). The fact of  $r > g$  seems to be reasonable due to the niche on the substrate, which will reduce the thermodynamic barrier. This may make the multiple nucleation possible leading to the physical phenomena of regime II. However, this depends on the substrate length ( $L$ ). We can consider two extreme cases, depending on the relative quantity of the distance,  $l_{reptation}$ , from an arbitrary place at which a single chain starts to move to the substrate and the substrate length,  $L$  : case (i)  $l_{reptation} \geq cL$  and case (ii)  $l_{reptation} \leq cL$ . The case (i) can cause the surface spreading domination, since

the faster  $r$  can not interrupt a polymer chain to spread on the substrate due to the long traveling distance to substrate and the system will have the same result with the regime I of the secondary nucleation theory. The case (ii) may lead to multiple nucleations on the substrate with same manner probably leading regime III. Faster  $r$  will allow a single polymer chain to deposit on the thermodynamically favorable location of substrate and shorter  $l_{reptation}$ . A faster  $r$  than  $L$  will make a reeling-in polymer chain interrupt the surface spreading of the already-deposited polymer chain. As  $l_{reptation}/L$  is reduced at constant  $L$ , the more polymer chains tend to be on the substrate, which creates more niches. As more thermodynamically favorable niches are created the rate of deposition and growth rate will be accelerated.

### **2.7.5 Ozawa Equation**

A novel approach was developed to study the non-isothermal crystallization kinetics of polymers based on the Ozawa equation (Chuah, 1998). The method determines the Avrami exponent,  $n$ , using exclusively the data confined to the primary crystallization regime. It was applied to a selection of eleven semi crystalline polymers including some biodegradable polymers.

Bulk crystallization of a polymer would lead to various degrees of crystallinity, which might have profound effects on, among others, its thermal, mechanical and optical properties. A number of theories were proposed to rationalize the kinetics of this

important transformation phenomenon (Wunderlich, 1976), providing insight into the underlying molecular processes and the resulting morphology. For example, Avrami has derived an equation for the isothermal crystallization kinetics expressed in terms of the time dependence of the volume fraction of crystalline material,  $X_v$ , by considering the rates of nucleation and volume increase in lamellar crystals as the major kinetic events (Avrami, 1941). This particular model is characterized by two parameters including the Avrami exponent,  $n$ , which is susceptible to the crystallization mechanism.

Although the Avrami equation is applied extensively in studying the polymer crystallization behavior under isothermal conditions, it is rather irrelevant to most polymer processing operations, such as injection-molding process, which usually involves rapid quenching of molten polymers. This situation was envisaged by Ozawa, who extended the Avrami model to non-isothermal crystallization conditions (Ozawa, 1971) depicted by:

$$X_v = 1 - \exp(-f_c l q^n) \quad (2.7.6)$$

Where  $f_c$  is the cooling crystallization function and  $q$  is the cooling rate. Equation (2.7.6) is applied to determine the exponent  $n$ , which is assumed to be temperature-independent, for some semi crystalline polymers (Ozawa, 1971; Eder, M., 1983; Lopez, 1989) by taking  $f_c$  as a constant at a designated temperature,  $T$ . Apparently, only a limited number of  $X_v$  data are available for the foregoing analysis as the onset of crystallization varies considerably with the cooling rate. In addition, the equation is valid exclusively for

primary crystallization before crystal growth impingement takes place at high transformation.

Recently, Caze (1997) has assumed an exponential increase of  $f_c$  with  $T$  upon cooling. On this basis, the temperatures at the peak and the two inflection points of the exothermic with skew Gaussian shape are linearly related to  $\ln(q)$  in order to estimate the exponent  $n$ . However, this treatment seems to hold only for  $q < 10 \text{ Kmin}^{-1}$  for unfilled and filled polypropylene (PP), because of the superposition of crystallization regimes 1 and 2 at higher  $q$ .

Findings by Chuah (1998) suggest that non-isothermal crystallizations of HDPE, LDPE, PP, PIP, POM, and PHBA seem to proceed via heterogeneous nucleation and 3-dimensional spherulitic growth. Chuah obtained an  $n$  value of  $2.97 \pm 0.04$  by using cooling rates varying from  $0.5$  to  $10 \text{ K min}^{-1}$ . However, Phillips and Lambert (Phillips, 1990) have concluded that  $n = 2.93 \pm 0.12$  by monitoring the changes in the transmitted light intensity during the isothermal crystallization of the particular polyolefin. It is noted that some workers tend to ignore the importance of volume change on crystallization, which could introduce significant errors in the determination of  $n$  (Wunderlich, 1976).

Any discrepancies between the results from the Ozawa equation and the Avrami equation can be primarily attributed to the differences in the thermal history, crystallization conditions, and sample impurity. However, precise interpretation of the exponent  $n$  is not possible with the complementary information on the morphology and

crystallization mechanism. Despite this, the Ozawa equation is a useful tool for depicting the dynamic crystallization behavior of polymers. More importantly, it provides a practical means of assessing the Avrami exponent reliably over a wide range of supercoolings.

## 2.8 Melting of Polymer Crystals

The melting of a polymer is considered to be a reversible process in which its ordered crystalline regions are converted into a disordered amorphous phase. Melting of a polymer crystal is controlled by such factors as lamellar thickness, surface free energies, lattice imperfections, and internal stress fields, primary of which is the lamellar thickness.

### 2.8.1 Thermodynamic Considerations

For a single lamellar polymer crystal, the free energy of formation may be written as:

$$\Delta\phi = 2(a+b)l\sigma + 2ab\sigma_e - abl\Delta G \quad (2.8.1)$$



Where  $a$ ,  $b$ , are the lateral dimensions,  $l$  is the crystal thickness,  $\Delta f$  is the bulk free energy of fusion, and  $\sigma$  and  $\sigma_e$  are the lateral and fold surface free energies, respectively. Since  $a \gg l$  and  $b \gg l$ , the first term in equation 2.8.1 may be neglected.

When the polymer crystal melts,  $\Delta\phi = 0$ . Using this condition and equation 2.6.7 one obtains:

$$T_m = T_m^\circ \left[ 1 - \frac{2\sigma_e}{\Delta h_f^\circ l} \right] \quad (2.8.2)$$

Where  $T_m^\circ$  is the equilibrium melting point and  $\Delta h_f^\circ$  is the heat of fusion per unit volume of the crystal. This equation forms the basis of the Thompson-Gibbs plot. Therefore a plot of  $T_m$  versus  $1/l$  must be linear with an intercept of  $T_m^\circ$  the value of  $\sigma_e$  can be determined from the slope.

### 2.8.2 Kinetic Considerations

In many polymers, the lamellar thickness is found to be larger than the initial lamellar thickness:

$$l = \lambda g^* \quad (2.8.3)$$

Combining this equation with equation 2.6.6 and substituting for  $\Delta G$  from equation 2.6.7 yields:

$$l = \frac{2\sigma_e T_m^\circ \gamma}{\Delta h_f^\circ \Delta T} + l\gamma\delta \quad (2.8.4)$$

$(2\sigma_e/\Delta G) \gg \delta l$  is a simplifying assumption, which is reasonable for crystals formed at low supercoolings. Upon combination with equation 2.8.2:

$$T_m = T_m^\circ - \left(\frac{\Delta T}{\gamma}\right) \quad (2.8.5)$$

This suggests that the melting point of a crystal thickened by a factor  $\gamma$  is approximately a linear function of its crystallization temperature, since  $T_c = T_m^\circ - \Delta T$ .

### 2.8.3 Morphology of Polyethylene Spherulite

The formation of spherulites in polymers is a feature of crystal growth that is still not well understood. That is reflected in the varying views as to what constitutes the essential nature of a spherulite (Hoffman, 1976; Keith, 1987). It is quite certain that spherulites develop through the initial formation of a framework of lamellae, termed dominant, and later formation of lamellae termed subsidiary, which are crystallized

between the established dominant lamellae (Bassett, 1984). Al-Raheil (1999) performed morphology studies using transmission electron microscopy which showed that the largest proportion of the early objects was monolayers associated with a giant screw dislocation, and the remaining objects were multilayers. Al-Raheil found that the lamella always extends along the *b*-axis. A screw dislocation usually forms either when two lamella touch each other or from defects inside the crystal itself. The lamellar habit at high-crystallization temperatures is elliptic, which is in agreement with the result obtained by Organ and Keller (1985) at high temperature from poor solvents. The traces of the {1 1 0} were identified, and the angle between the different planes is 67°30'.

## 2.9 Small Angle X-ray Scattering for Lamellar Thickness

### 2.9.1 Development of One Dimensional Correlation Function

If a model is assumed in which the lamellar crystals are essentially flat and parallel, then from diffraction theory the Lorentz corrected intensity,  $I_{LC}(q)$  would follow equation 2.9.1 below (Vons and Cortège, 1967).

$$I_{LC}(q) = 2V \int_0^{\infty} K(z) \cos(qz) dz \quad (2.9.1)$$

Where  $V$  is the scattering volume,  $z$  is the coordinated perpendicular to the layers, and  $K(z)$  is the one-dimensional correlation function, which is described by equation 2.9.2 as shown.

$$K(z) = \int_0^{\infty} \eta(\xi - z) \eta(\xi) d\xi \quad (2.9.2)$$

The local fluctuations in the electron density, the difference between the average and the local electron density, are designated  $\eta(\xi)$ . Since  $I_{LC}(q)$  and  $K(z)$  are Fourier transforms of one another the following equation applies:

$$K(z) = \frac{1}{2V} \int_0^{\infty} I_{LC}(q) \cos(qz) dq \quad (2.9.3)$$

So far this development assumes that the intensity is measured in absolute units. However this is not necessary if the one dimensional correlation function is normalized. For  $z = 0$  the  $K(z = 0)$  will be equal to the average of the square of the local electron density fluctuations from equation 2.9.2. Looking at equation 2.9.3, it can be seen that the cosine function will become 1 when  $z = 0$ . Therefore the correlation function  $K(z)$  can be normalized by dividing by the correlation function at  $z = 0$ ,  $K(0)$ . Therefore using equation 2.9.3 and the above result, along with the definition for the Lorentz corrected intensity produces a formula for the normalized one-dimensional correlation function,

$$K_I(z) = \frac{\int_0^{\infty} q^2 I(q) \cos(qz) dq}{\int_0^{\infty} q^2 I(q) dq} \quad (2.9.4)$$

The measured intensity,  $I(q)$ , does not need to be in absolute units for equation 2.9.4 to hold. In order to obtain  $K_I(z)$ , the Lorentz corrected curve must be integrated from zero to infinity. The data will not go to zero because of the beam stop, or infinity because of the physical limits of the two dimensional position-sensitive detector. A line connecting the two points can approximate the intensity function between zero and the lowest  $q$  value. For extrapolating to infinity, the data is assumed to follow Porod's law for a two-phase system. Therefore the intensity,  $I(q)$  will be directly proportional to  $q^{-4}$  as  $q$  goes to infinity. A plot of  $I(q)$  versus  $1/q^4$  will provide the proportionality constant. This will then allow an equation for calculating the intensity function as it approaches infinity. It should be noted that this method assumes that there are sharp boundaries between the layers. This can be checked by plotting  $I(q)$  versus  $q$  on a log-log plot. The slope of the plot should be  $-4$ . If this slope is not obtained then another method for extrapolating the curve will be necessary. This would most likely involve using the slope obtained in a plot of  $I(q)$  versus  $q$  on a log-log plot as well as the intercept. Also data points at high  $q$  may need to be disregarded due to diffraction from the unit cell.

## 2.9.2 Models for Determining Lamellar Thickness

One method, which is often used to obtain the lamellae thickness from SAXS data, involves determining the long period (Vonk, 1988). It is assumed that the lamellae system can be modeled by a set of alternating layers of amorphous and crystalline sections. The long period is equal to the thickness of one crystalline layer and one amorphous layer. The lamellae thickness or crystal thickness,  $d$ , is therefore simply the long period,  $L$ , multiplied by the fraction of the polymer which is crystalline,  $w_c$ , as shown in equation 2.9.5.

$$\bar{d} = d = w_c L \quad (2.9.5)$$

The weighted average of the long period can be obtained from the maximum in the Lorentz corrected intensity curve,  $I_{LC}(q)$  using Bragg's law. Therefore the lamellar thickness calculating using this method would correspond to a weighted average (Vonk, 1988). However, this method assumes that the lamellae are separated by the same amount of amorphous material, and that the crystallinity is constant in each long period layer. These two assumptions do not have a physical basis to support them. It is very possible that there is variation in the thickness of the amorphous layers, even if the crystal layers are of the same thickness. This would cause there to be a distribution of the crystallinity throughout the sample, which would cause equation 2.9.5 to be invalid.

The long period in this study is measured from the one-dimensional correlation function. Figure 2.14 reproduced from Strobl and Schneider (1980b) shows the case in which the lamellae and amorphous layers are of constant thickness (a). The long period is obtained from the point at which the one-dimensional correlation function goes through the first maximum after zero. Parts (b)-(d) of Figure 2.14 show somewhat more physically realistic systems. Notice that in all the  $K(z)$  curves there is a section between  $z = 0$  and  $z = d$  where  $dK(z)/dz$  is a constant. This slope can be related to the specific inner surface by the following equation:

$$\frac{dK(z)}{dz} = -\frac{O_s}{2}(\eta_c - \eta_a)^2 \quad (2.9.6)$$

As stated earlier at  $z = 0$  the one dimensional correlation function will be equal to the square of the local electron density fluctuations. This value can be related to the electron density difference of the crystalline and amorphous phases with the following equation:

$$Q = K(0) = w_c(1-w_c)(\eta_c - \eta_a)^2 \quad (2.9.7)$$

Therefore extrapolating the section of the  $K(z)$  curve which is straight to  $z = 0$  will result in the value  $Q$  as shown in equation 2.9.7. If the value of the specific inner surface,  $O_s$ , can be determined then the equation for the extrapolated line can be calculated since the slope and intercept are known. The specific inner surface is simply the surface area

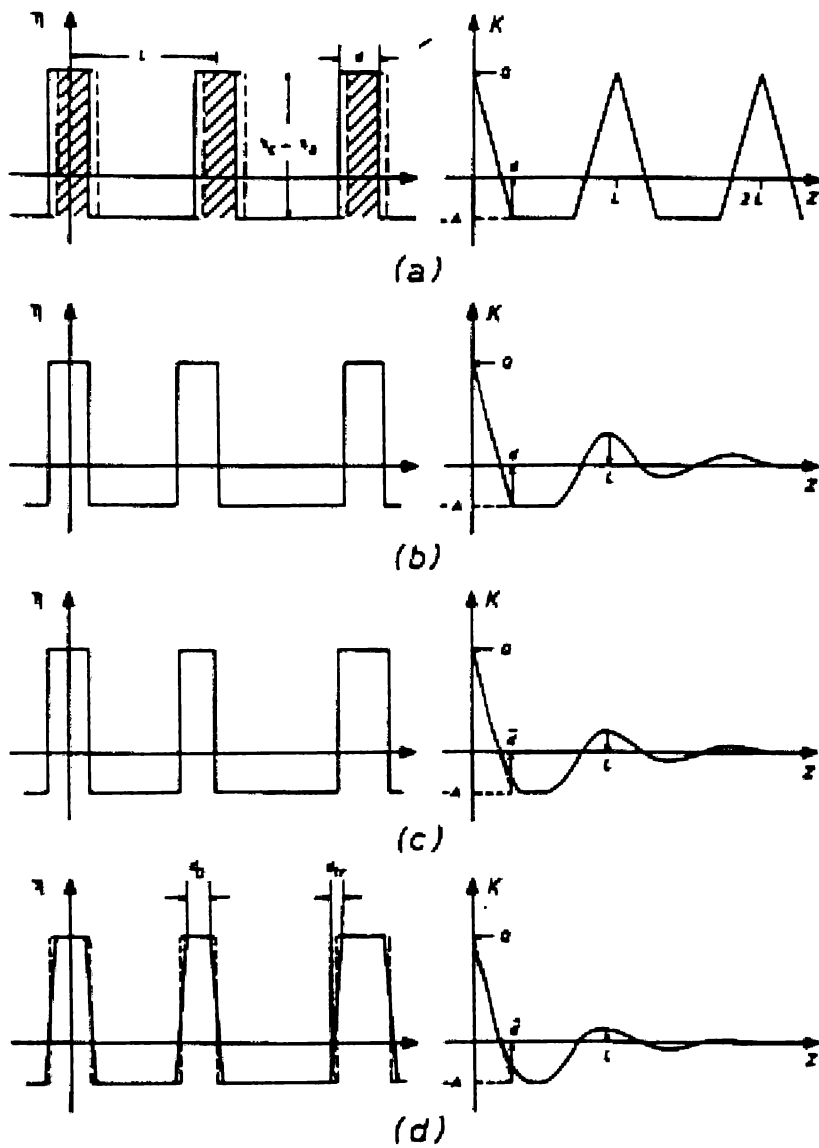


Figure 2.14. Electron Density Distributions and Correlation Function  $K(z)$  (Strobl, 1980b).



divided by the volume. The area will be twice the area of the one surface of the crystal, and crystal and an amorphous layer are equal to one long period. Therefore the specific inner surface is  $2/L$  or in terms of the lamellae thickness  $2w_c/d$ . The equation:

$$K(z) = -\frac{w_c}{d}(\eta_c - \eta_a)^2 z + w_c(1 - w_c)(\eta_c - \eta_a)^2 \quad (2.9.8)$$

This line forms the hypotenuse of what is known as the “self correction triangle”. Figure 2.15 reproduced from Strobl et al. (1980b) shows this triangle. If the  $K(z)$  curve has a flat section that is not disturbed by the first maxima, then this can be used as the base of the “self correction triangle”. The value of  $K(z)$  at this point,  $-A$ , would be the square of the difference between the average electron density and the amorphous phase electron density. Using equation 2.9.8 and setting  $z = d$ , the lamellae thickness, it can be shown to be the number average of the lamellar thickness (Vonk and Kortleve, 1967, Strobl and Schneider, 1980 a and b, Vonk, 1988).

The above method is based on absolute intensities, which would require calibration using a sample of known scattering power. However, Vonk et al (1967 and 1988) has developed a very similar method using relative intensities and using the normalized one dimensional correlation function,  $K_l(z)$ . In this case  $-A$  will be equal to  $-w_c/(1-w_c)$ . The value of  $z$  at  $K_l(z) = -A$  will still remain to be the number average lamellae thickness,  $d$ .

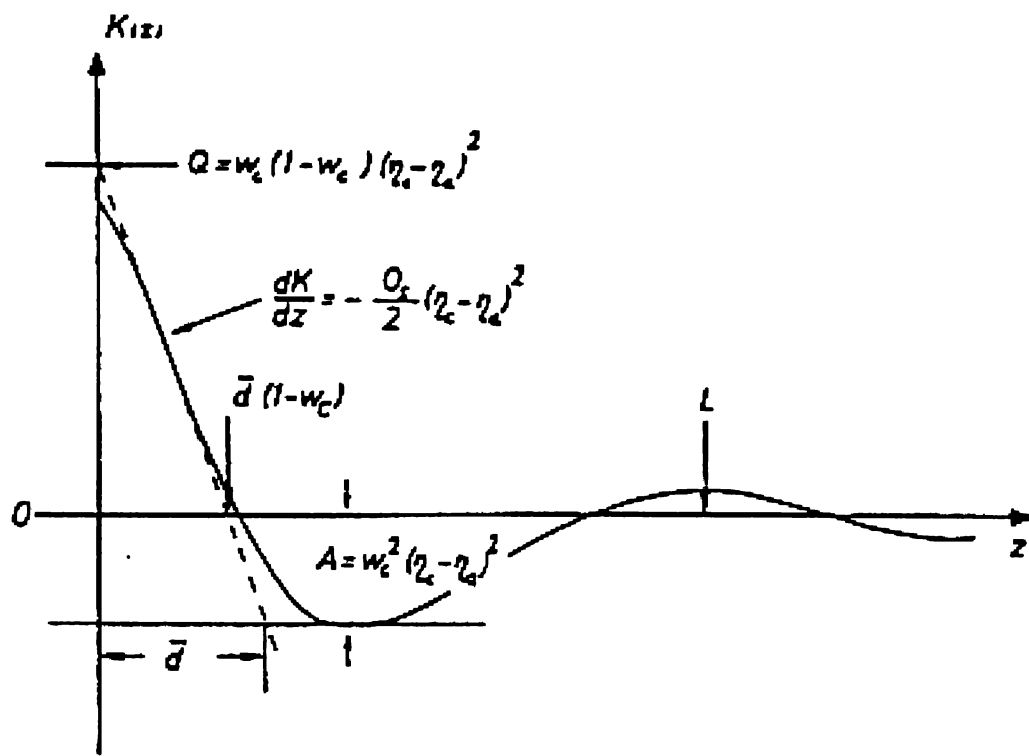


Figure 2.15. Self Correction Triangle (Strobl, 1980b).

Both these methods are based on the crystallinity being less than 50%,  $w_c < 0.5$  (46-49). The equations can easily be adjusted for crystallinities above 0.5 by switching  $w_c$  to  $w_a = (1-w_c)$  and  $\eta_a$  and  $\eta_c$ . However, for there to be a flat section before the first maxima the crystallinity should be either less than 30% or more than 70%. If at first the maxima does interfere with this baseline of the “self correction triangle” adjustments can be made with additional measurements. For the absolute intensity method, by determining the average density of the sample and knowing the density of the amorphous material the value of  $A$  can be calculated by the following equation:

$$A = (\langle \eta \rangle - \eta_a)^2 = \left[ (\langle \rho \rangle - \rho_a) \frac{\Sigma_i}{M_o} \right]^2 \quad (2.9.9)$$

Where  $\rho$  is the mass density,  $M_o$  is the formula weight of the repeat unit, and the  $\Sigma Z_i$  is the sum of the atomic numbers of the atoms in the repeat unit (the number of electrons). For the relative intensity method, the calculation of the value of  $A$  is more involved. First the fraction crystalline must be measured by wide angle X-ray diffraction to obtain  $w_{cw}$ . From this the crystallinity, which would correspond to SAXS,  $w_{cs}$ , can be calculated from the following quadratic equation:

$$w_{cs}^2 + (B-1)w_{cs} - Bw_{cw} = 0 \quad (2.9.10)$$

Where

$$B = \frac{1}{3} + \frac{1}{E \left( \frac{dK_l(z)}{dz} \right)_{z=E}}$$

$$E = -\frac{4}{R} \left( \frac{dK_l(z)}{dz} \right)$$

$$R = \frac{\langle |\text{grad}\eta|^2 \rangle}{\langle \eta^2 \rangle} = \frac{\int_0^\infty q^4 I(q) dq}{\int_0^\infty q^2 I(q) dq}$$

The value, which would normally correspond to  $d$ , the lamellae thickness at  $A$  is actually equal to  $\Delta+d$ . Where  $\Delta$  is a correction for the width of the transition layer as seen in Figure 2.14 and is equal to the following for  $w_{cs} < 0.5$  (Vonk and Kortleve, 1967, Vonk, 1988):

$$\Delta = \frac{2E \left( \frac{2}{3} - w_{cs} \right)}{(1 - w_{cs})} \quad (2.9.11)$$

Knowing  $w_{cs}$  and then calculating  $\Delta$  the lamellar thickness could then be determined. Once the lamellar thickness is determined, the equilibrium melting point is easily obtained. It is simply the intercept of a plot of melting peak temperature versus inverse lamellar thickness.

## CHAPTER 3. EXPERIMENTAL PROCEDURES

### 3.1 Materials

Ethylene-octene random copolymers with branch content, molecular weight and polydispersity ( $M_w/M_n$ ) controlled by homogeneous catalysts of metallocene type and a linear polyethylene were supplied and characterized by the Dow Chemical Company. Details of as-received samples are listed in Table 3.1. Here the code H, L, number and ZN and M stand for the high molecular weight, low molecular weight, methyl groups per 1000 carbon (i.e. branch content), Zeigler-Natta catalysts, and metallocene catalysts, respectively. The linear growth rate data of LPE-ZN-13/18 was taken from the work of Hoffman et al. (1975). Linear growth data of L4-ZN was taken from Lambert (1994). Isothermal linear growth rates work for L11-M and H17-M was done by Abu-Iqyas (paper to be submitted). To calculate the mole fraction of branching points in this study, we used the  $CH_3/1000C$ , assuming a branch as a point defect.

### 3.2 Differential Scanning Calorimetry (DSC)

Thermal analysis was performed under a nitrogen atmosphere using a Perkin-Elmer Series 7 differential scanning calorimeter (DSC) with a cooling accessory. The calibration of the DSC was carried out with indium ( $T_{onset} = 156.6^\circ C$ ,  $\Delta H_f = 28.45 J/g$ ) several times until the known onset temperature ( $T_{onset}$ ) was within  $\pm 0.1^\circ C$ . After

Table 3.1: Molecular Weight Characteristics and Equilibrium Melting Points

Sample	$M_n$	$M_w$	$M_w/M_n$	Branches/ 1000 $\text{CH}_3$	$T_m$ ° (°C) <sup>a</sup>
LPE-13/18 <sup>(b)</sup>	13,040	18,100	1.39	0	142.4
LPE-54/101	53,900	101,300	1.88	0	142.7
L4-ZN <sup>(c)</sup>	13,400	23,600	1.76	4.22	142.3
L4-M	27,300	59,900	2.19	3.98	139.3
H7-M	43,600	94,000	2.16	6.84	140.4
L11-M	21,200	43,700	2.06	10.86	134.9
H-17	48,700	102,700	2.11	16.92	134.1

a)  $T_m$ ° calculated from equilibrium melting point studies by Kim (1996).

b) Hoffman et al. (1975) sample.

c) Lambert et al. (1994) sample.

completing the study, the  $T_{\text{onset}}$  was re-measured and the deviation from the known  $T_{\text{onset}}$  of indium was always within  $\pm 0.15^\circ\text{C}$ . In all melting experiments, the DSC heating rate was  $10^\circ\text{C}/\text{min}$ . In the DSC thermogram the peak temperature was chosen as the melting temperature.

### **3.3 Polarized Light Microscopy (PLM)**

Polarized light microscopy (PLM) was used for the measurements of the linear growth rate of the linear PE fraction and the branched PE fractions. An Olympus polarizing microscope with an attached 35 mm camera was used in conjunction with a Mettler FP-82 hot stage. The hot stage with an iron constantan thermocouple was calibrated in a hot water bath and the precision of the temperature control was  $\pm 0.1^\circ\text{C}$ . For all the fractions, thin films were prepared by melt-pressing a small amount of the samples between the cover glass and glass slide at a temperature of  $150^\circ\text{C}$ . Specimens were first melted at  $10^\circ\text{C}$  above their melting temperatures for 2 minutes in a customized hot stage. The samples were then inserted into the Mettler hot stage at a pre-set temperature for isothermal crystallization. During crystallization, linear crystal growth rates were measured through the eyepiece of the microscope. The morphology was studied by taking the photographs with ASA 100 or 200 films at each crystallization temperature. For faster crystallization rates the images were recorded on a camera attached to a VCR and TV monitor. Table 3.2 shows the series of copolymers used and

Table 3.2: Copolymers Based On Linear Low-Density Polyethylene

Sample	$M_w/M_n$	Mole Percent of Copolymer	Experiments performed	
			Isothermal Crystallization	Pseudo-Isothermal Crystallization
LPE-54/101	1.88	0.00 <sup>a</sup>	X	X
L4-M	2.19	3.98	X	X
H7-M	2.2	6.84	X	X
L11-M	2.06	10.86		X
H-17	2.11	16.92		X

a) Trans/1000C = 0.003, vinyls/1000C = 0.135, vinylidenes/1000C = 0.013



their specific mole percents of copolymer as well as the experiments performed.

In the study of kinetics of both isothermal and nonisothermal crystallization PLM has been used to obtain the crystallization temperature,  $T_c$ . In previous uses of PLM in nonisothermal crystallization, the highest cooling rate obtained was less than 100 °C/min (Kim et al., 1991). This upper limit of cooling rate was a result of the hot stage not being able to create a constant cooling rate higher than that value.

The temperature measured in PLM is that of air surrounding the heating element. In PLM the temperature description is usually much worse than in DSC. This is because the heating element is much larger in PLM and there is a greater air layer and cover glasses between sample and heating elements. The situation will be much worse if the hot stage is saturated by the flowing  $N_2$ . There is little chance for the heat of crystallization to affect the measured temperature as a result of the huge difference between sample and heating elements and complicated layers of air or glass. It has to be concluded that the constant cooling rate in PLM can only refer to the one of the hot stage.

### 3.3.1 Linear Growth Kinetics

Linear growth measurements were obtained by following the growth of the crystallizing entities as a function of time using an Olympus BH2 optical microscope

with attached Olympus 35 mm camera. The change in dimension of the growing entity was measured as a function of time from a projection of slides shot during the growing process, and the growth rate calculated as the slope from a plot of radius versus time. Typically measurements were made on at least five entities for statistical purposes. In the isothermal experiments the temperature of the samples were controlled as mentioned above using a Mettler FP5 hot stage and temperature controller. The temperature measurements for the rapid cooling non-isothermal experiments will be discussed in a section to follow.

### **3.4 Non-Isothermal Crystallization Under Rapid Cooling Rates**

#### **3.4.1 Introduction**

This rapid cooling non-isothermal crystallization technique is based on Polarized Light Microscopy (PLM) to study the nonisothermal crystallization of polymers at average cooling rates of up to 3500 °C per minute. The non-isothermal crystallization experiment is shown in Figure 3.1. The experimental quantities that can be measured include temperature, light intensity, and spherulite diameter. For this purpose, a sample chamber, heating and cooling system, and data collection systems were developed. With this experimental technique the polymer temperature, light intensity with analyzer, the light intensity without analyzer, diameter of spherulites (recorded on VHS video tape by a VCR using a Sony color video camera) can be measured simultaneously. Due to the

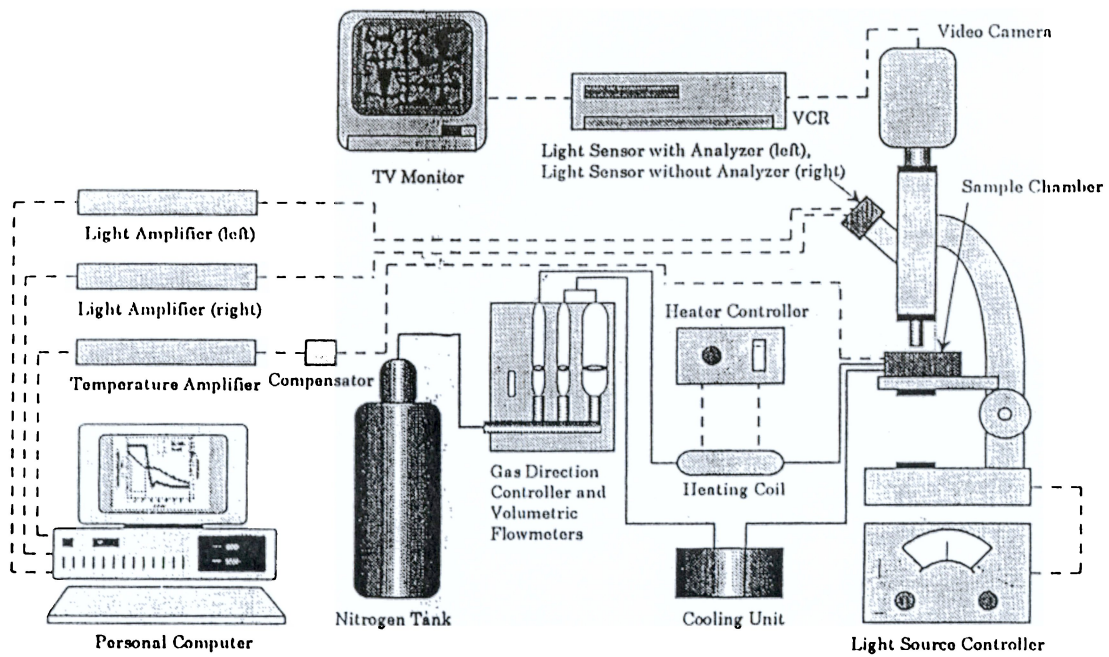


Figure 3.1: Experimental System for rapid cooling (Spruiell, private communication)

light scattering effect caused by numerous nuclei under the fast cooling condition the two light intensities are measured. The entire experimental system is made up of a light depolarizing microscope, hot stage system, light intensity measurement, temperature measurement unit, and spherulite diameter measurement system.

### 3.4.2 Hot Stage System

The configuration of the hot stage system is set up to hold, heat and cool the sample. The schematic of the hot stage system is shown in Figure 3.2. The sample chamber is composed of six inlets: two for heating, two for cooling, and two for exhausting the nitrogen gas. Double inlets are designed to improve the uniformity of heating and cooling. It is in this way that the sample is heated and cooled.

Nitrogen gas is introduced from a tank and goes through the first solenoid valve, which is used to cut the nitrogen to stop heating, but without cooling. A second solenoid valve allows nitrogen to go to either the cooling or heating line. On the heating line there is a heat exchanger to heat the air to the desired temperature. The valve has the capability of switching the nitrogen from heating to cooling without a time interval. When the sample is heated up and stabilization is completed (typically 1 to 2 seconds at 160°C) cooling air is turned on, and the system is designed to start collecting the data automatically from a given temperature (150°C for PE). The entire time from the start

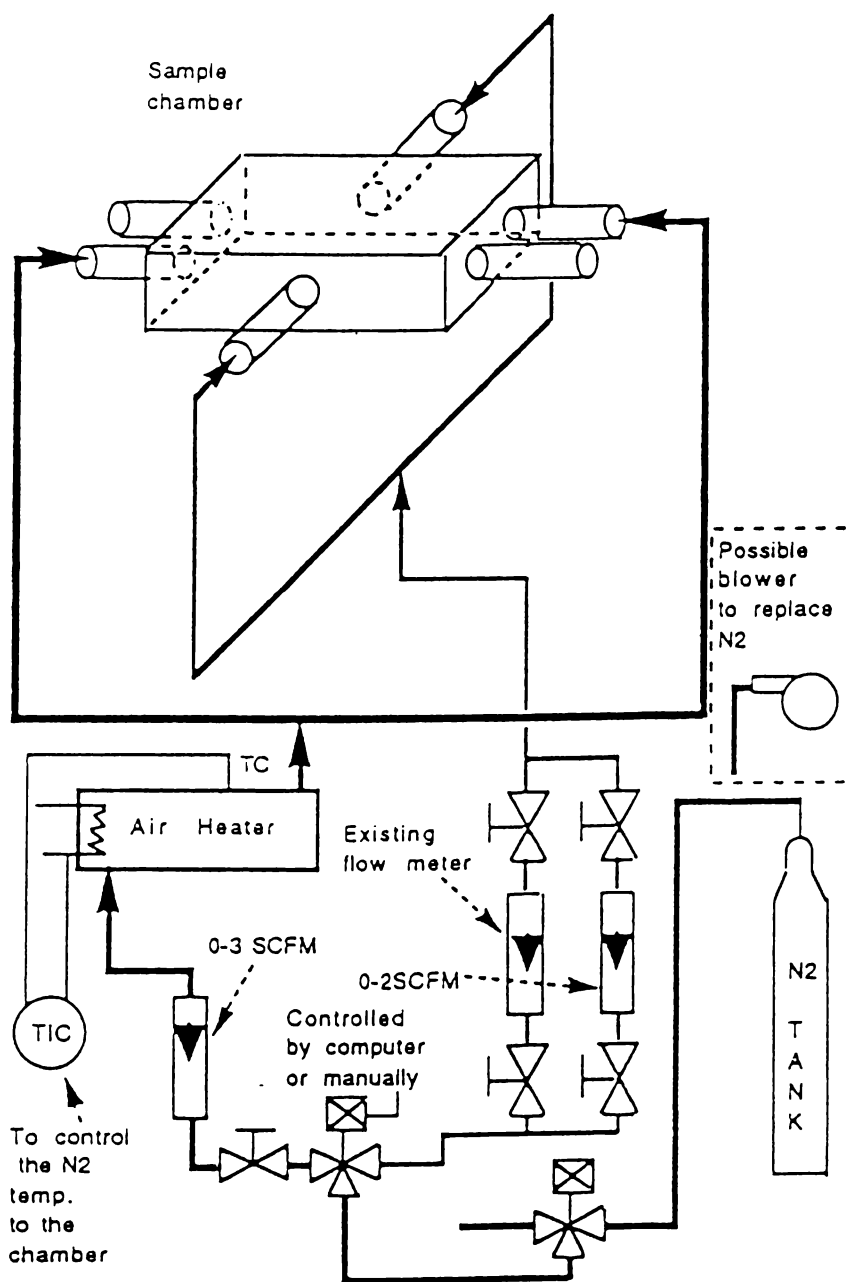


Figure 3.2: Hot stage system for rapid cooling (Ding, 1996).

temperature of 150°C to end of crystallization experiment at room temperature is typically 3 seconds. The flow meter sets up the heating rate in the heating line. Two flow meters in the cooling line control and measure the cooling rate, which makes the cooling condition repeatable. Two flow meters with different ranges allow for a large variation of the cooling rate. A temperature controller regulates the nitrogen temperature. Tubing before the heater is flexible since the temperature is low there. The flexible tubing is used to separate the vibration caused by the nitrogen source and allow the hard Teflon tubing to contract and expand. The nitrogen flow rate controls the cooling rate.

The polymer is in the shape of a film and has a thickness of 40  $\mu\text{m}$ . As shown in Figure 3.3, samples are placed between two glass cover slips and have a thickness of 152  $\mu\text{m}$ . The entire sample assembly is fixed in the sample chamber.

Light intensities with and without analyzer are simultaneously measured as shown in Figure 3.4. Two photodiodes are placed at the two eyepieces of the microscope. The analyzer was placed just before one of the two photodiodes. Each of the signals from the photodiodes is sent to the IBM PC after they are modified by custom made electronic signal suppressors.

The way the system was originally designed was to give data that when plotted will overlap as shown in Figure 3.5. Relative crystallinity is going to be zero at the melt temperature. The pseudo-crystallization temperature is the in the diagram, shown as

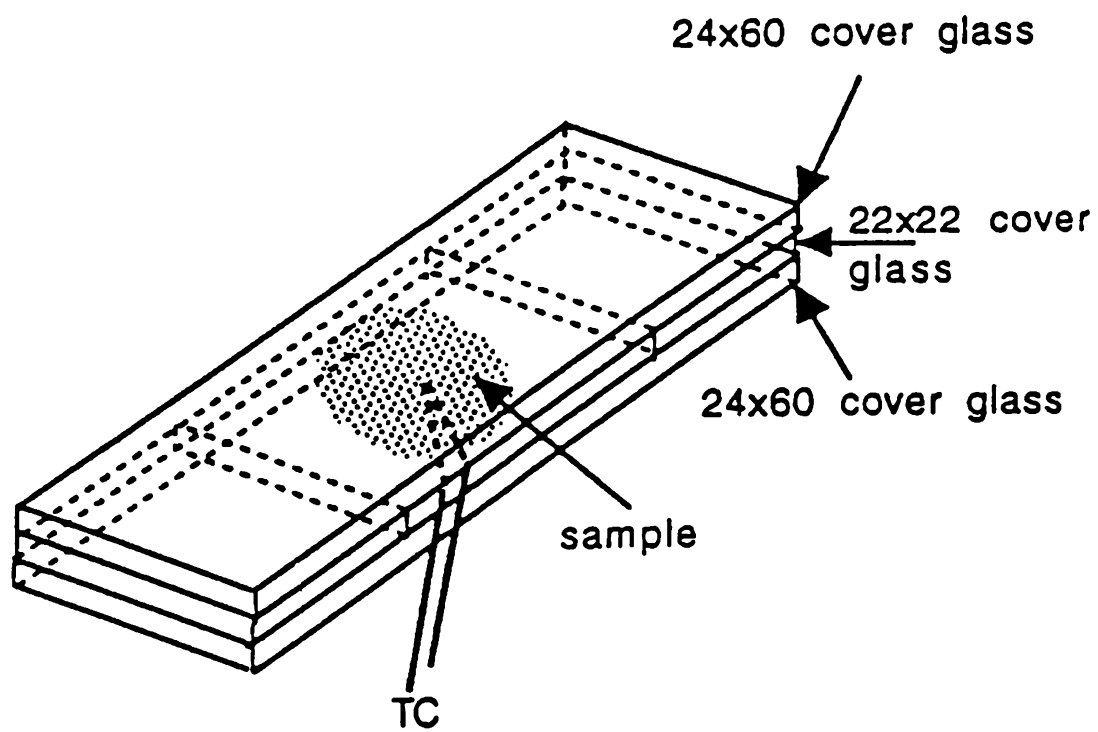


Figure 3.3: Sample assembly used in experiments (Ding, 1996).

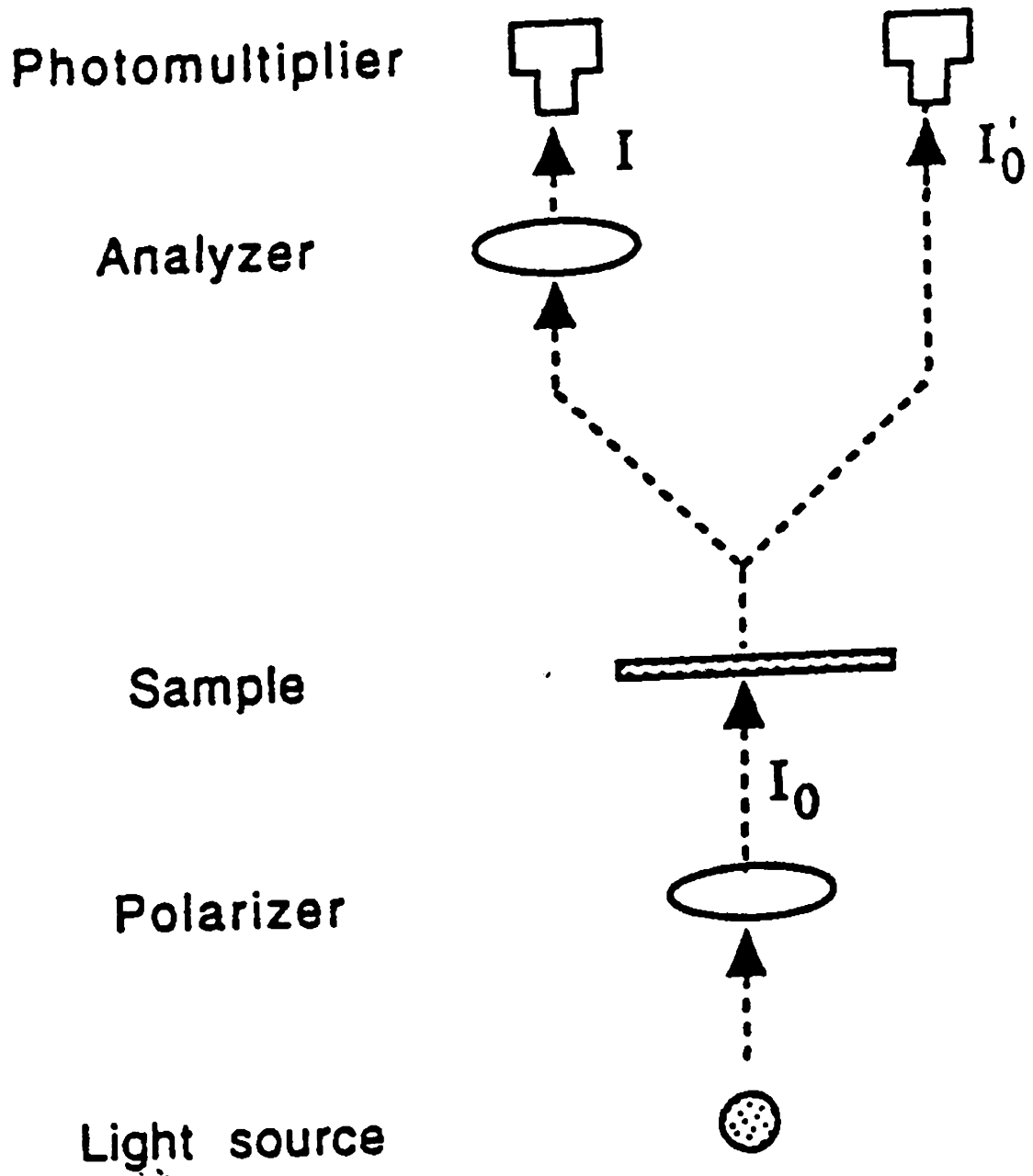


Figure 3.4: Schematic diagram of the light-depolarizing microscope (Ding, 1996)



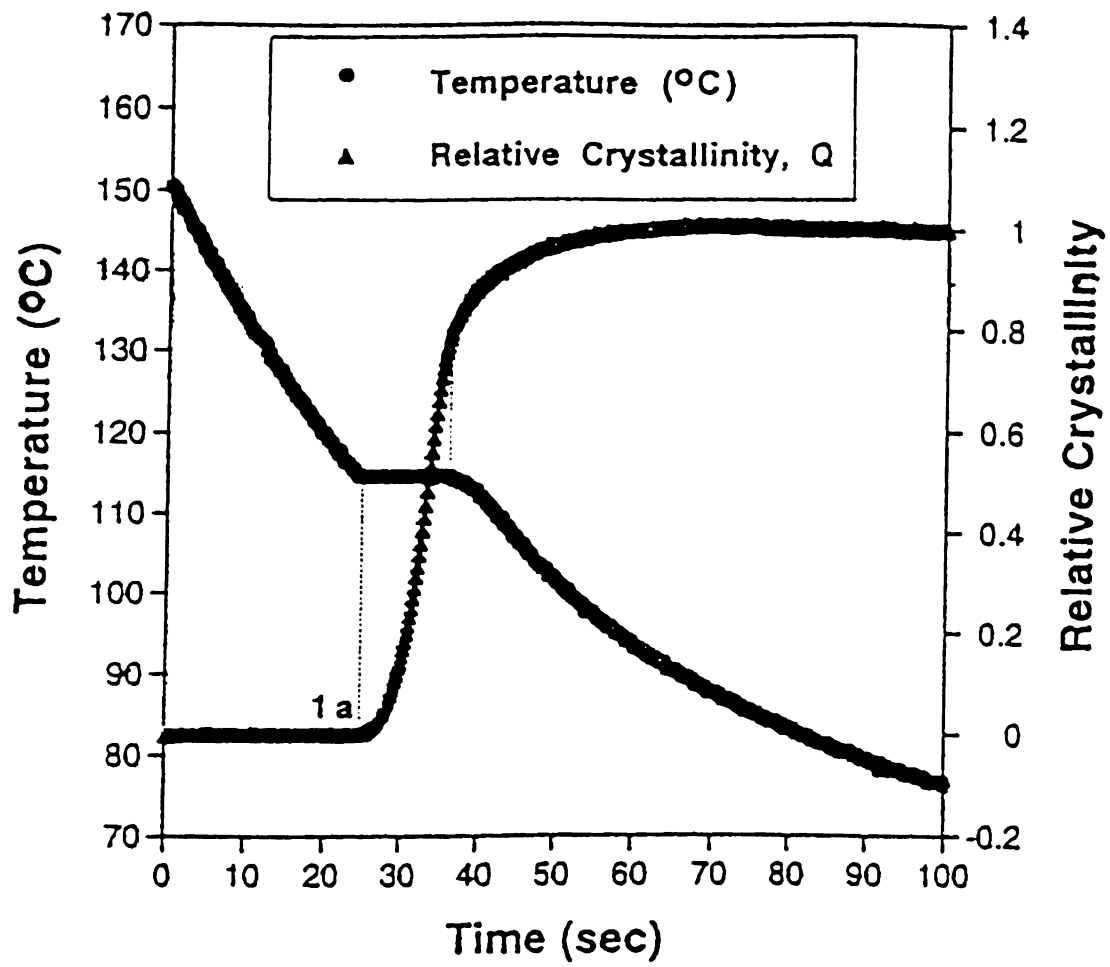


Figure 3.5. This figure shows the relative crystallinity of polypropylene as a function of time and temperature (Spruiell, private communication).

position  $I_a$ , at which the temperature stays constant for a period of time (sec). The percent crystallinity however will rapidly increase to its ultimate value at the end of constant temperature period. As the temperature drops, maximum crystallinity is reached.

The video camera is mounted on the microscope, VCR and TV is used to record the process of spherulite growth, 30 frames per second are currently obtained by the system. The spherulite diameter is measured on the TV screen.

### **3.5 Small Angle X-Ray Scattering (SAXS)**

In order to study the morphological parameters of the polymers, the 10m Small Angle X-Ray Scattering Spectrometer (SAXS) of Oak Ridge National Laboratory (ORNL) was used. A schematic diagram is shown in Figure 3.6 (Hendricks, 1978). The ORNL-SAXS allows the measurement of a true scattering pattern, which is free from the procedures of collimation (desmearing) correction (Wignall, 1990). The X-ray generator was a 12 kW Rigaku-Denki rotating anode and only  $CuK\alpha$  radiation ( $\lambda=1.54\text{\AA}$ ) was used at an accelerating voltage 40 kV and a current of 100 mA. The monochromator a pyrolytic graphite crystal. The detector a 2-dimensional position-sensitive proportional counter with resistance wire mesh of a dimensional 20 cm x 20 cm. The X-ray source-to-sample was 3.5 m and sample-to-detector (SDD) was 5.115 m that provides the

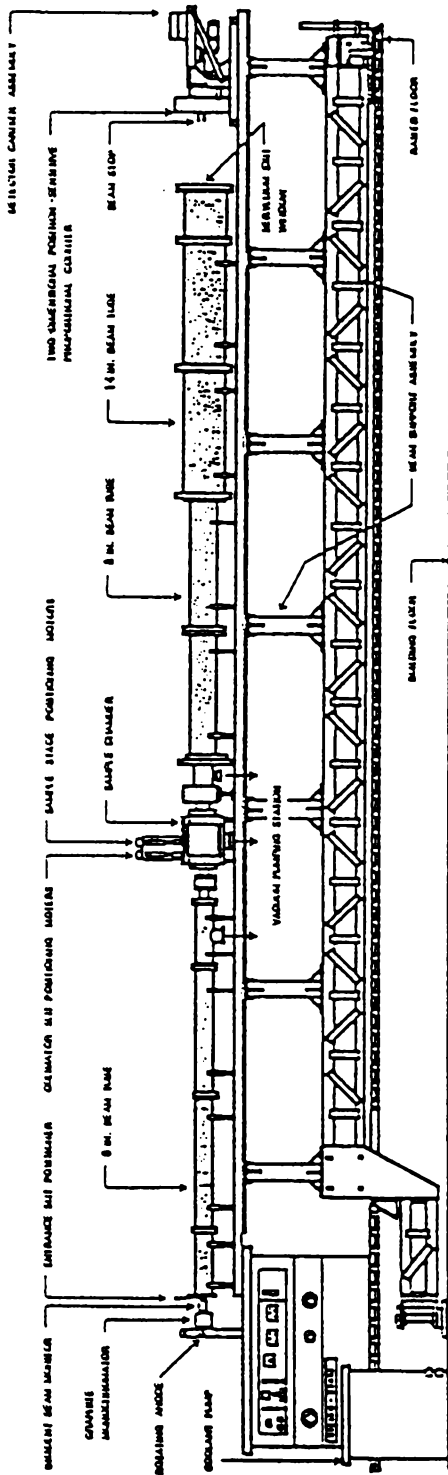


Figure 3.6: The schematic diagram of the 10m small angle X-ray scattering spectrometer at ORNL (Wignall, 1990).

highest resolution at room temperature (RT) and was 5.065 m for measurement at crystallization temperature ( $T_c$ ). The reason for using different geometry between RT and  $T_c$  is that different sample holders for  $T_c$  experiments were used at fixed geometry, SDD = 5.115 m. Both geometries will be described as 5 m geometry for simplicity.

### 3.6 Wide Angle X-Ray Diffraction (WAXD)

Wide-angle X-ray diffraction studies are carried out using the Rigaku diffractometer at reflection mode, which connected to the Digital pdp-11/34 computer and Rigaku Geigerflex<sup>TM</sup> system with JADE 3.1 analysis software. WAXD is calibrated using the silicon standard ( $2\theta = 24.465^\circ$ ). Unit cell parameters are calculated using the digitized data, the  $d$  spacing values for the 110, 200, and 011 crystalline peaks.  $\text{CuK}\alpha$  radiation ( $\lambda=1.51\text{\AA}$ ) is used at 35kV and 30mA. The scan range of  $2\theta$  is  $10^\circ \sim 50^\circ$  and the step size was  $0.05^\circ$ , and normally the run time was 45 min.

#### 3.6.1 Percent Crystallinity Measurement

To determine the fraction, which was crystalline in the polyethylene copolymers, the amorphous phase was centered at  $2\theta$  equal to  $20^\circ$ . For polyethylene, the 110 and 200 crystalline peaks that occur around  $2\theta=21.3^\circ$  and  $2\theta=23.5^\circ$  respectively were used for the calculation of the degree of crystallinity. The data was digitized to obtain the raw data.

Using the commercial software program Peak Fit, the relative areas of the amorphous and two major crystalline peaks were determined in a method previously outlined by Ruland (1961) and Wunderlich (1980). The crystalline diffraction peaks were separated from the amorphous region by drawing a line connecting the minima between the crystalline peaks. The diffraction pattern was then separated into three areas corresponding to the amorphous area, (110), and (200) peak areas. The measured areas after correction represent the relative intensities  $I_A$ ,  $I_{110}$ ,  $I_{200}$  since the relative areas of the crystalline and amorphous peaks are proportional to the number of electrons, and therefore the mass in the crystalline and amorphous regions. Crystallinities were determined using the method of Nichols (1954). The three peaks were corrected for atomic scattering factors, absorption, temperature, and diffraction. The combined correction factors for the amorphous, (110), and (200) peaks are 0.69, 1.00, and 1.43, respectively. The crystallinity is then expressed by the relation:

$$w_c = 100 \times \frac{I_{110} + 1.43I_{200}}{I_{100} + 1.43I_{200} + 0.69I_A} \quad (3.4.1)$$

The term  $w_{cw}$  is the weight fraction of the polymer sample, which is crystalline as determined by WAXD. The fitting program also determined the peak positions.

## CHAPTER 4. RESULTS

### 4.1 Linear Growth Kinetics

Linear growth rates were calculated from the slopes of the plots of the radius of the growing entity versus time for the crystallization entity, as discussed previously. An example of this procedure is given in Figure 4.1 for LPE 54/101, for crystallization temperatures ranging from 94.4°C to 105.6°C. The nonlinear portion of the lines in Figure 4.1 is due to impingement of the growing entities during crystallization, resulting in a leveling off of the measured radius.

#### 4.1.1 Copolymer Content

Figure 4.2.a and 4.2.b show that increased copolymer content reduces the rate of crystallization for LPE 54/101, L4-M, L11-M, and H7-M respectively. In Figure 4.2.a it can be seen that branching reduces the rate of crystallization by a factor of 4 at 105°C from LPE 54/101 to L4-M. The crystallization temperature at 1000 ( $\mu\text{m}/\text{sec} \times 100$ ) is reduced by 9°C from LPE 54/101 to L4-M. Similar results can again be seen in Figure 4.2.a where copolymer content reduces the crystallization rate by a factor of 100 at 96°C from L4-M to L11-M, and the crystallization temperature at 500 ( $\mu\text{m}/\text{sec} \times 100$ ) is reduced by 24°C. The change in crystallization rate from L11-M to H7-M is very small,

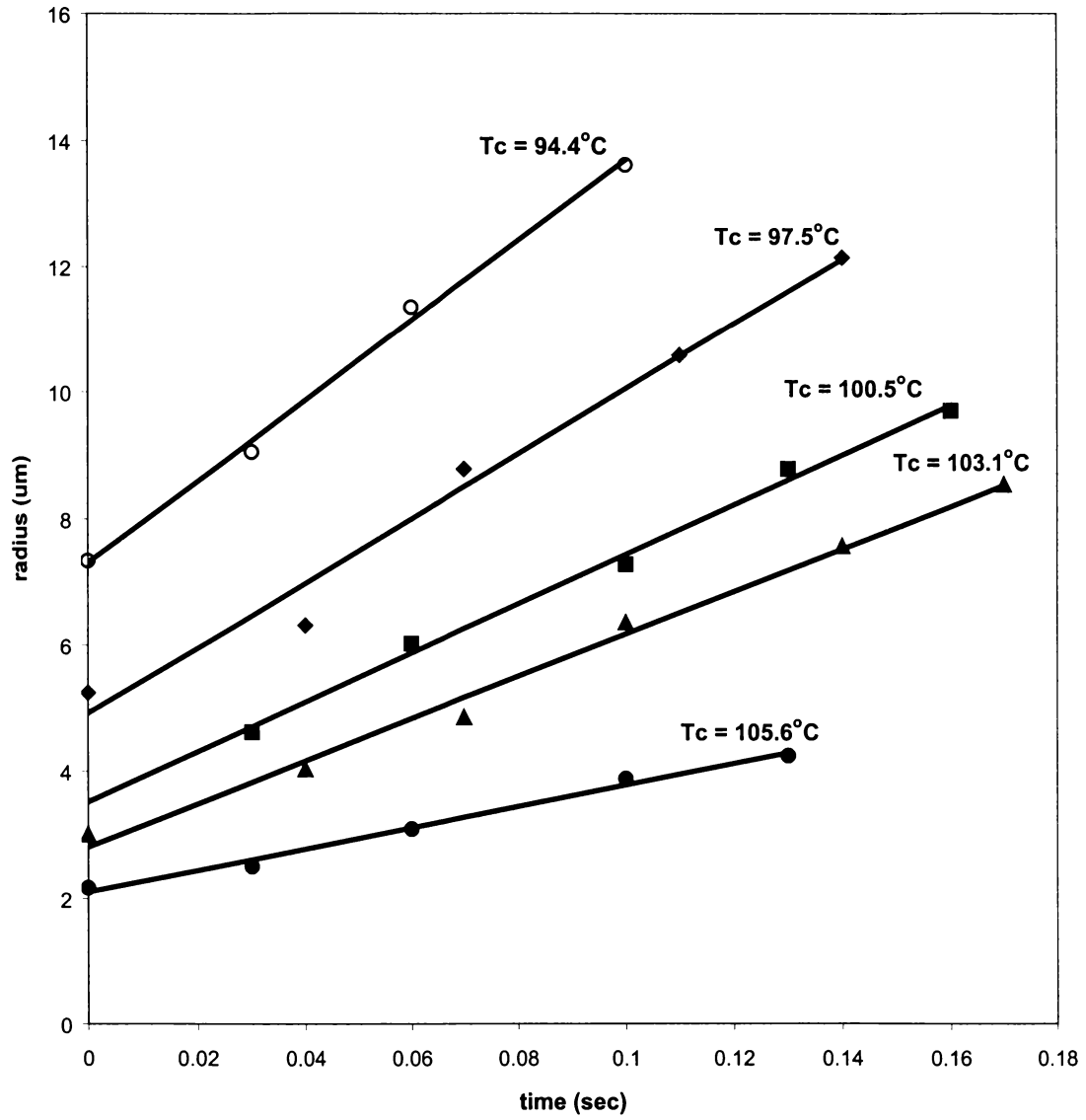


Figure 4.1. Radius as a function of crystallization time for the specified crystallization temperature,  $T_c$ .

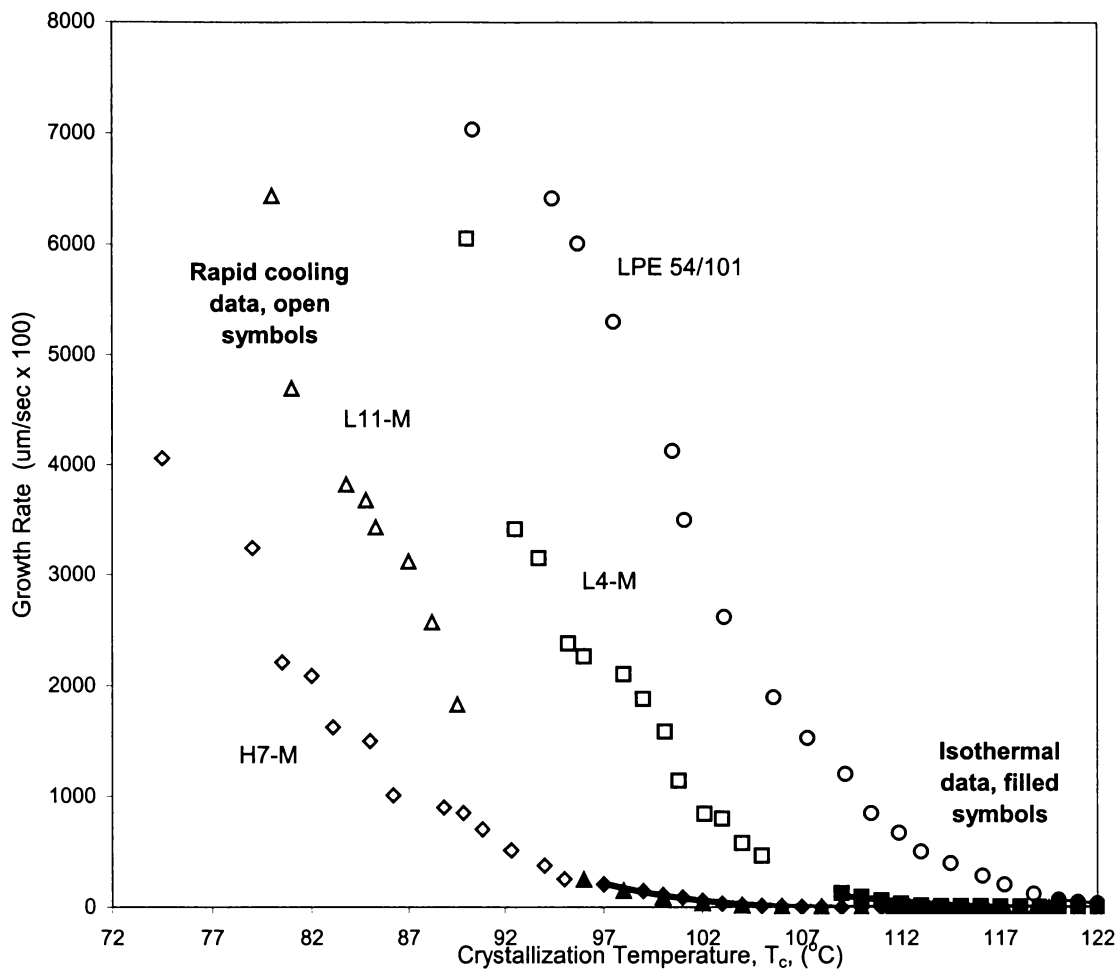


Figure 4.2. Growth rate for ethylene copolymers. a. Plot of growth rate ( $G$ ) versus crystallization temperature ( $T_c$ ) for ethylene copolymers. Open symbols represent data obtained by rapid cooling experiments and closed symbols represent data obtained through isothermal experiments.



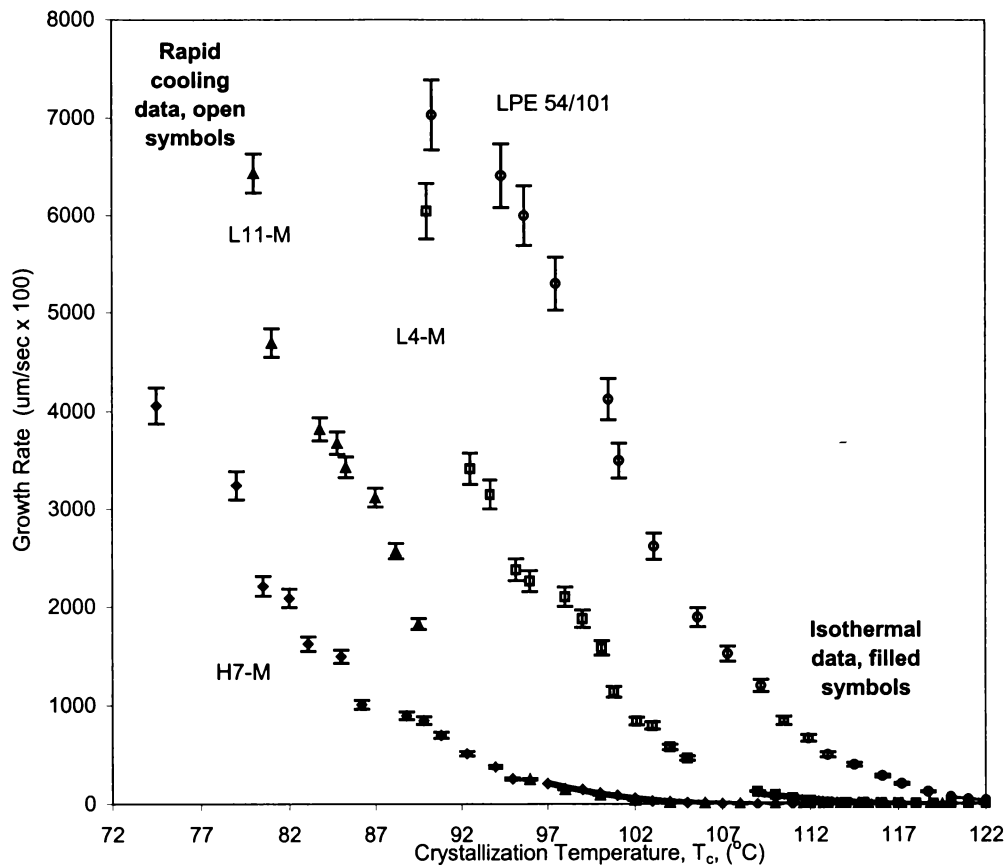


Figure 4.2. Continued. b. Error bars for the growth rate ( $G$ ) versus crystallization temperature ( $T_c$ ) for ethylene copolymers. Open symbols represent data obtained by rapid cooling experiments and closed symbols represent data obtained through isothermal experiments.

probably due to a greater influence of molecular weight than of copolymer content. This effect will be discussed later. The reduction in crystallization rate is due to a reduction in secondary nucleation rate as the copolymer content is increased.

In Figure 4.2.b the range of the error bars are given in terms of one standard deviation as a percent of the growth rate values. The error bar range is from 3.1% for the L11-M to 5.1% for LPE 54/101. H7-M contained error bars with 4.5% and L4-M with 4.7%. Percent error bar measurement was slightly higher for rapid cooling region for the same polymer by typically 0.3%.

#### 4.1.2 Measurement Dynamics

In the use of polarized optical microscopy there are inherent sources of error involved to measure the radius of the spherulite. In this study the measurements were taken across the diameter of the spherulite. However, as is apparent from Figure 4.3 there are fringes on the edges of the spherulites. Fringes are due to problems with focusing of the optical microscope. Fringes are not associated with the polymer morphology or crystallization. There is always a pair of fringes, a dark fringe and a light fringe. The light fringe doesn't show as well as the dark one. In this photo the light fringe can be seen outside the dark one. Problems associated with focusing is a challenge in a dynamic experiment in the case of non-isothermal crystallizations, which take only



Figure 4.3. Linear polyethylene LPE-54/101 at 122°C (Regime II), arrow pointing to the fringe of a spherulite.

0.1 to 0.2 seconds. Extreme care is taken to ensure that no part of the fringes is included in any of the diameter measurements. Taking the diameter and dividing it by two derive the radius. It is important to take measurements correctly and consistently each time and not to include any area of the fringes. This means that measurements were taken from the inside of the dark fringe on each side of the spherulite when measuring across for the diameter. This issue will be discussed in more detail in section 5.3.1.

## **4.2 Morphology**

The superstructures of the linear and copolymer polyethylene were studied using optical microscopy and are dependent on the crystallization temperature and molecular weight of the sample. The morphologies of the linear and copolymer polyethylene will be discussed further in section 5.5.

### **4.2.1 Low Molecular Weight Series**

The morphologies of the low molecular weight series are spherulitic as seen in Figures 4.4, 4.5, and 4.6 for samples L4-M and L11-M respectively for temperatures that correspond to the Regime II and Regime III regions. This compares to previous work by Hoffman et al. (1997) in which it was reported that copolymers heated to a quite high  $T_m$

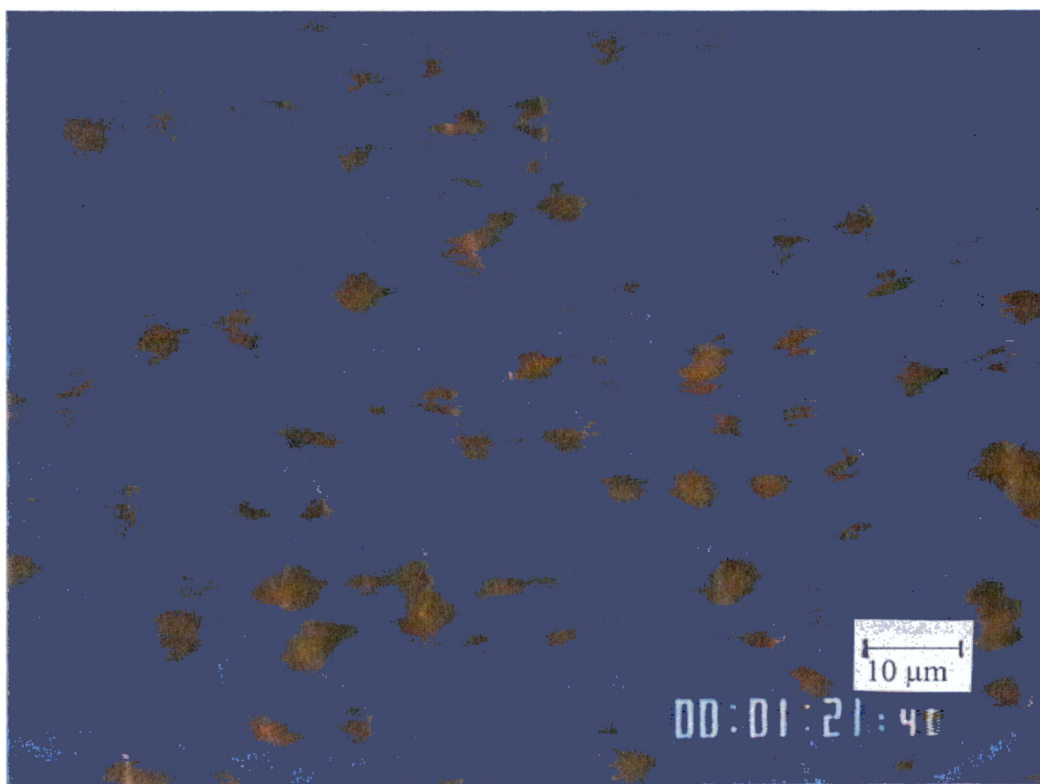


Figure 4.4. Morphology of L4-M at 92.5°C (Regime III).

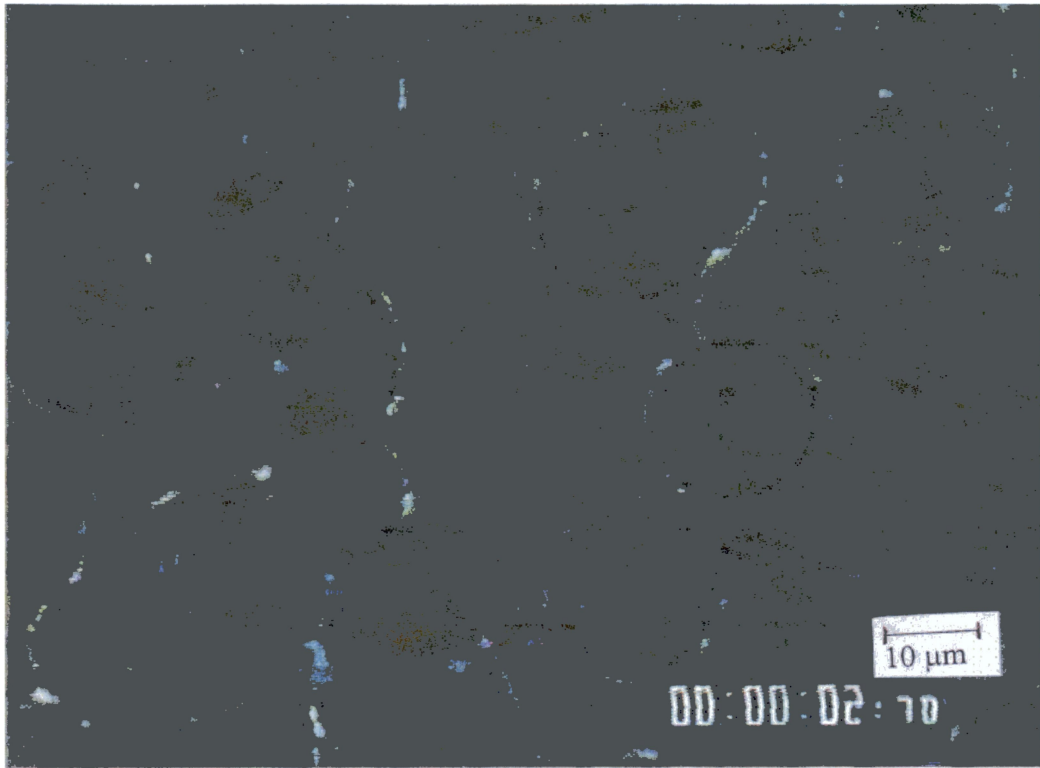


Figure 4.5. Morphology of L11-M at 83°C (Regime III).

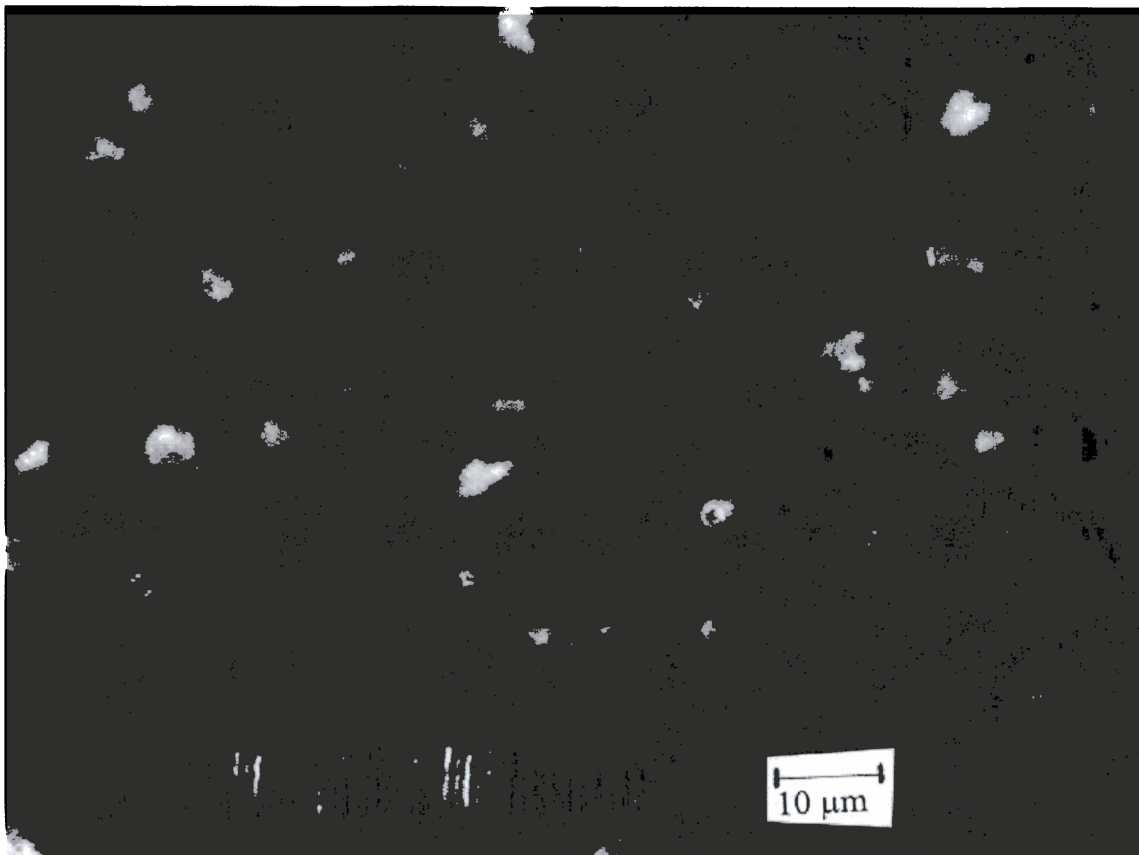


Figure 4.6. Morphology of L4-M at 117°C (Regime II).

(i.e. degraded) tended to exhibit only ringed spherulites rather than the non-banded type everywhere in Regime III.

The morphologies for the low molecular weight series of these polyethylenes for the Regime I and Regime II temperature regions previously investigated by Lambert (1991), Hoffman (1975), and Allen and Mandelkern (1987). Lambert reported that the temperature at which the axialitic structures develop correspond to both Regime I and Regime II (high temperature). Previous work by Hoffman on polyethylene fractions has shown that there are axialites formed in Regime I and spherulites in Regime II, although Allen and Mandelkern later showed that changes in morphology do not necessarily coincide with changes in growth regime. This investigation reports axialites in Regime I for the low molecular weight sample of L4-M, which is consistent with findings from both Lambert and Hoffman. The morphology of L11-M will be studied further in an ongoing investigation by Abu-Iqyas (2000).

#### 4.2.2 Intermediate Molecular Weight Series

Figures 4.7 and Figures 4.8 show that the structures of LPE 54/101 and H7-M are well-formed spherulites in the Regime III transition temperature range. Previous investigation by Lambert (1991) and Hoffman et al (1997) has shown that axialites in regime I, non-banded spherulites in main body of Regime II, coarse bands at lowest  $T_c$  in this regime. In this investigation spherulites are seen for Regime II for both LPE 54/101



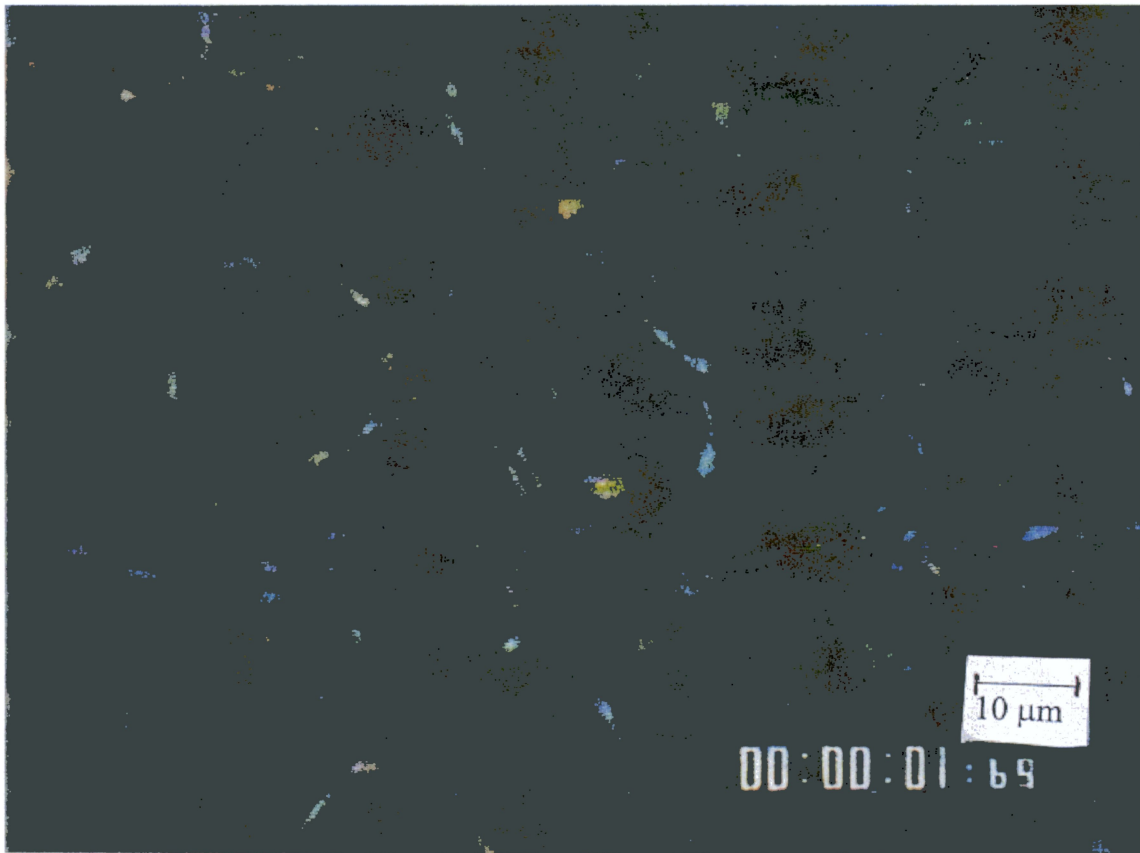


Figure 4.7. Morphology of LPE 54/101 at 97.5°C (Regime III).

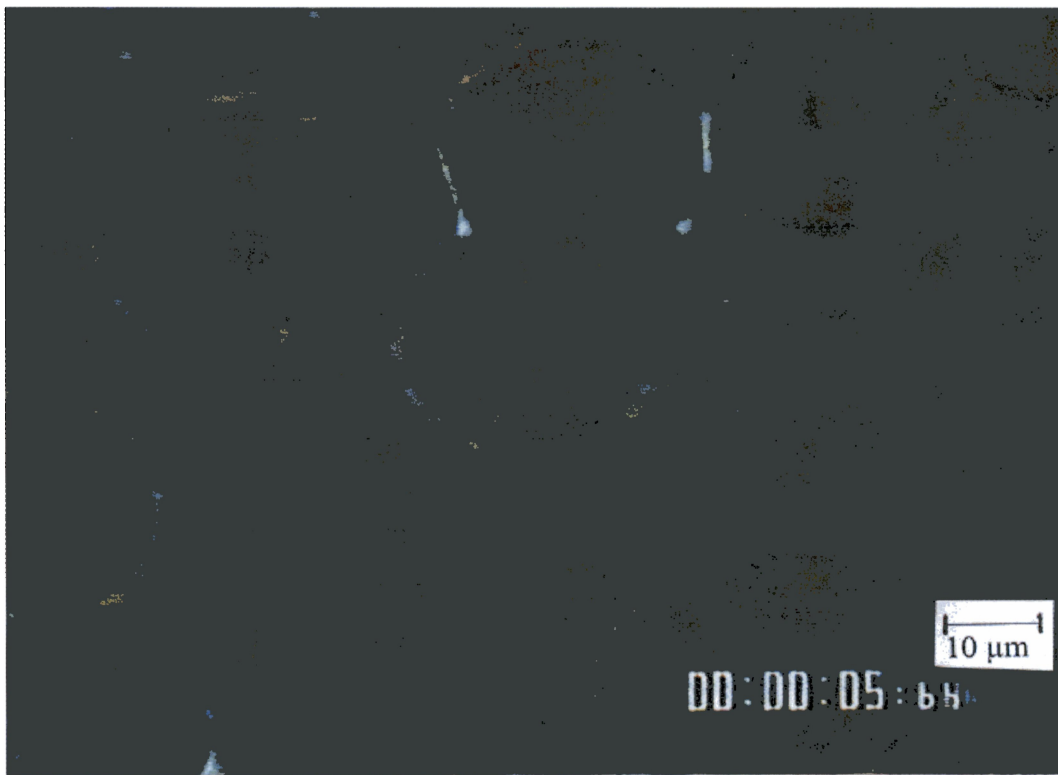


Figure 4.8. Morphology of H7-M at 87.5°C (Regime III).

(Figure 4.9) and H7-M, which is consistent with Lambert and Hoffman. However, as seen in Figure 4.10, the linear polymer LPE 54/101 has non-banded spherulites for Regime I. This may be consistent with Hoffman's findings if you consider LPE 54/101 a high-molecular weight polymer. By Hoffman's definition LPE 54/101 is on the borderline between being considered an intermediate molecular weight polymer and a high molecular weight polymer.

### **4.3 X-ray Analysis**

#### **4.3.1 Wide Angle X-ray Diffraction**

WAXD was carried out on the linear fraction and copolymer fractions to determine the effect of crystallization temperature on the crystallinity and structure of the polyethylene. Results for the crystallinity measurements of the linear fraction and the copolymers polyethylene are given in Table 4.1. Unit cell parameters are shown in Table 4.2. Figure 4.11 shows a representative WAXD for the polyethylene, which shows LPE 54/101 at varying crystallization temperatures,  $T_c$ .

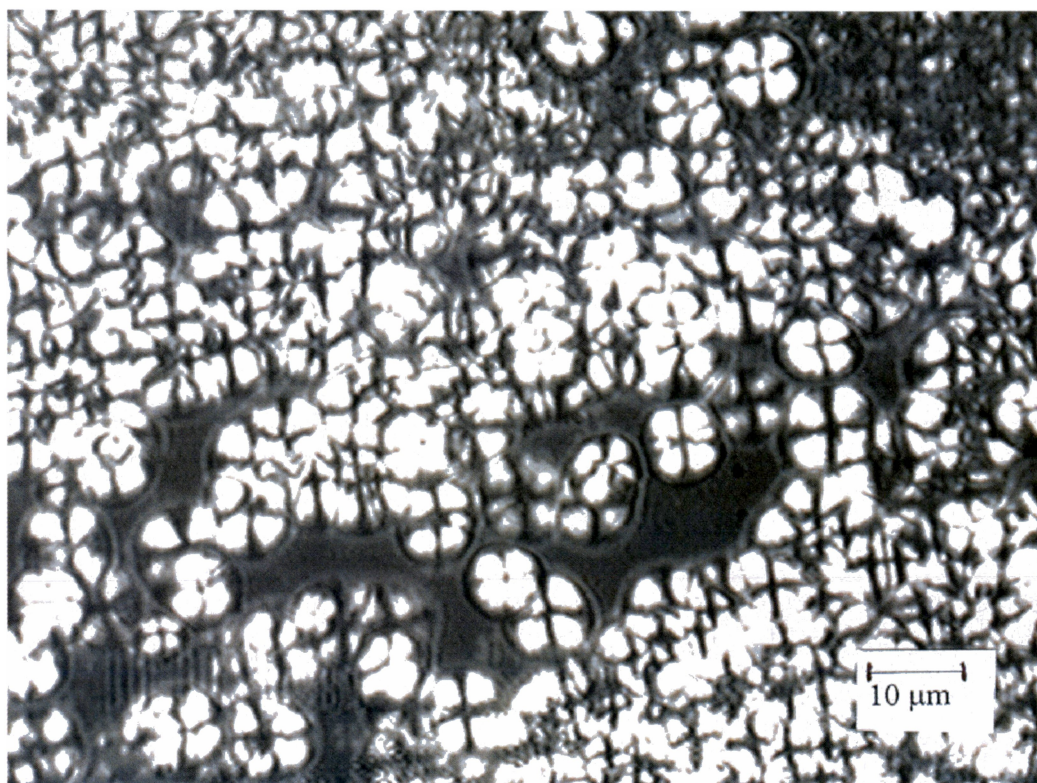


Figure 4.9. Morphology of LPE 54/101 at 122°C (Regime II).

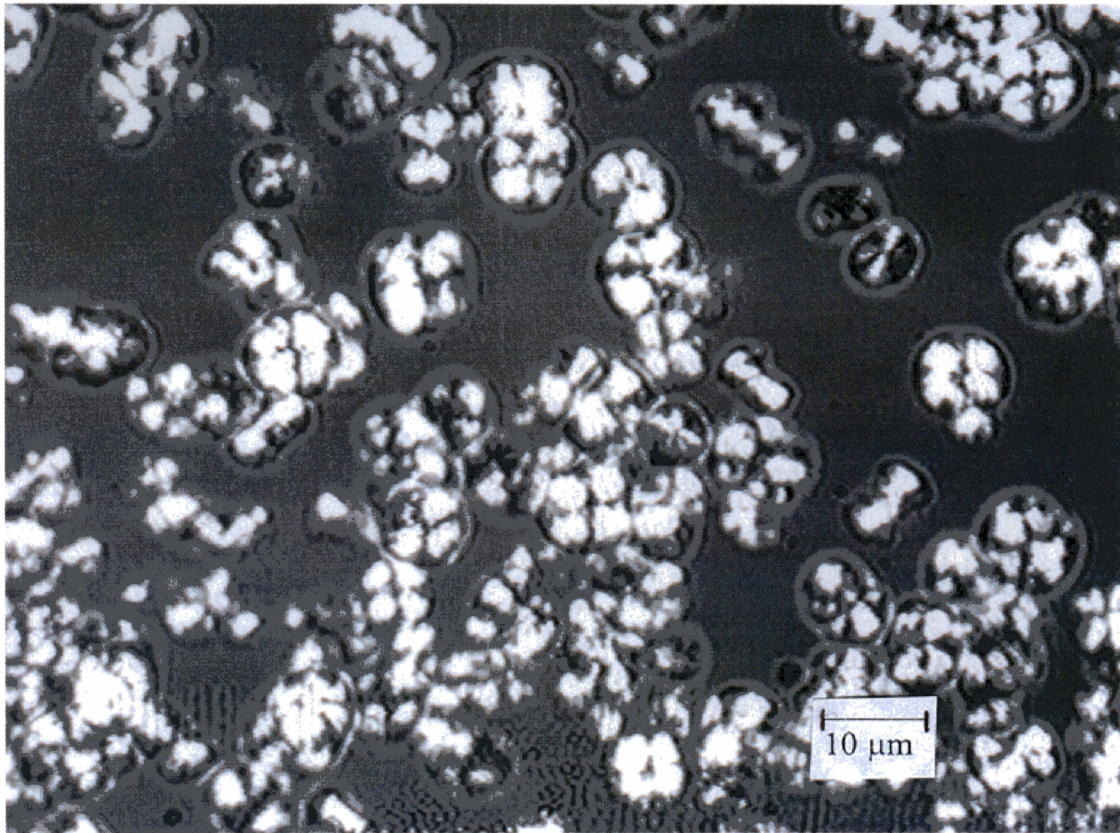


Figure 4.10. Morphology of LPE 54/101 at 127°C (Regime I).

Table 4.1: Summary of Percent Crystallinity Results by WAXD.

<b>Sample</b>	<b>T<sub>c</sub>(°C)</b>	<b>%X<sub>c</sub> (WAXD)</b>
LPE-54	90.0	51.2
	109.0	57.0
	116.0	60.4
L4-M	95.0	52.1
	104.0	53.9
	111.0	58.4
L11-M	81.0	45.8
	87.5	49.2
	89.0	50.6
H7-M	82.0	45.6
	89.5	48.8
	96.0	51.0

Table 4.2: Summary Of Unit Cell Parameters by WAXD.

Sample	T <sub>c</sub> (°C)	Hkl	d(A°)	hkl	d(A°)	hkl	d(A°)	a(A°)	b(A°)	c(A°)
LPE-54	90	110	4.13	200	3.72	011	2.29	7.45	4.97	2.58
	109		4.14		3.73		2.29	7.46	4.98	2.66
	116		4.15		3.74		2.29	7.47	4.99	2.58
L4-M	95	110	4.22	200	3.8	011	2.14	7.6	5.08	2.35
	104		4.23		3.81		2.31	7.62	5.08	2.6
	111		4.25		3.82		2.32	7.64	5.1	2.61
L11-M	81	110	4.15	200	3.76	011	2.29	7.52	4.98	2.57
	87.5		4.19		3.77		2.29	7.54	5.03	2.58
	89		4.2		3.8		2.28	7.6	5.04	2.58
H7-M	82	110	4.3	200	3.88	011	2.3	7.77	5.16	2.57
	89.5		4.23		3.82		2.3	7.64	5.07	2.57
	96		4.4		3.98		2.32	7.96	5.29	2.53

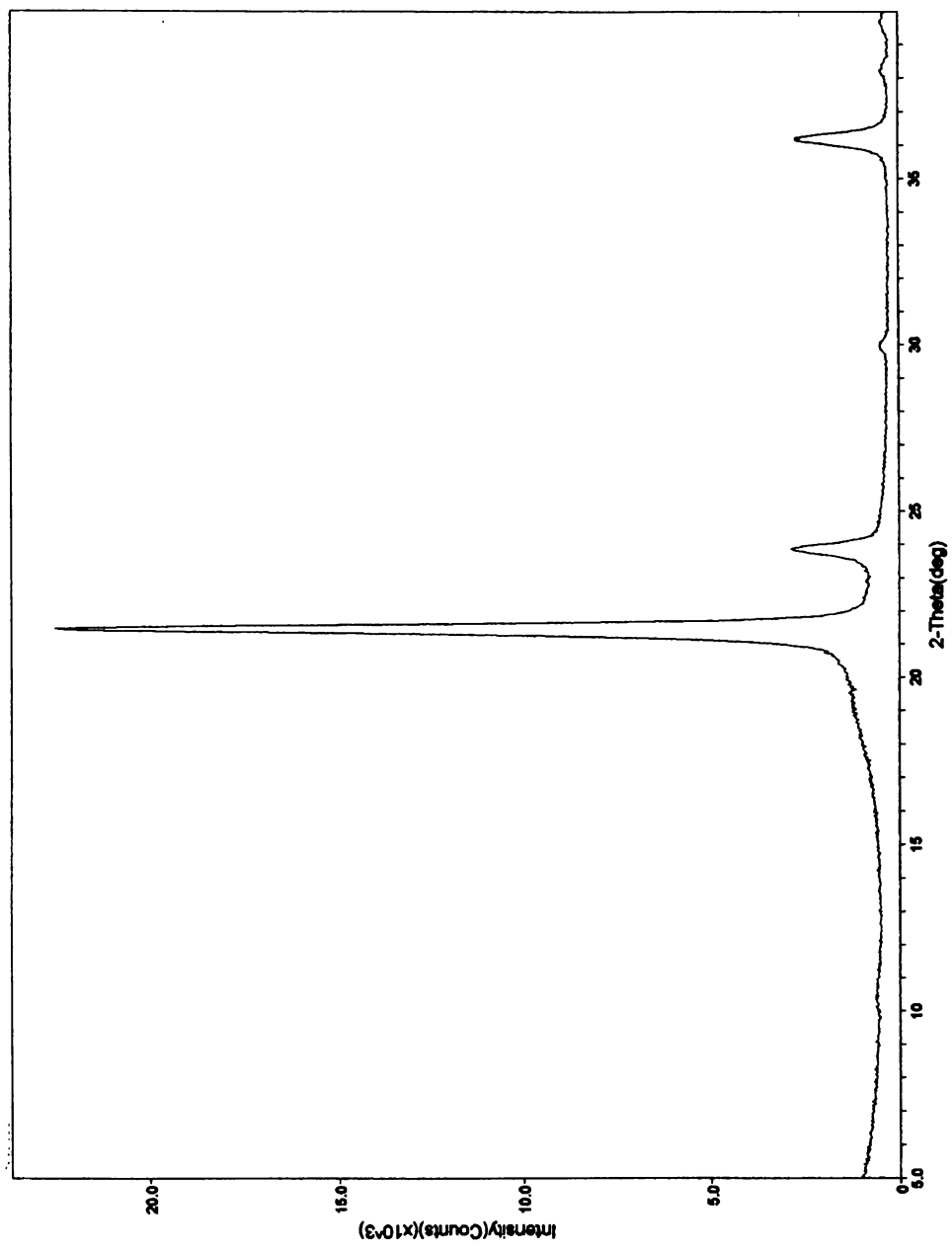


Figure 4.11. Wide angle X-ray diffraction of LPE 54/101 with  $T_c = 116^\circ\text{C}$ .



### 4.3.2 Small Angle X-ray Scattering

SAXS profile observed from 5-meter geometry, measured at room temperature, of the linear polyethylene LPE 54/101 is shown in Figure 4.12. The Lorentz corrected SAXS intensity profile (Figure 4.13). The one-dimensional correlation function for LPE 54/101 at  $T_c = 90.0^\circ\text{C}$  is shown in Figure 4.14. From section 2.9.2, the lamellae thickness or crystal thickness,  $d$ , is therefore simply the long period,  $L$ , multiplied by the fraction of the polymer, which is crystalline,  $w_c$ , as shown in equation 2.9.5. The taking of lamellar thickness from the maximum in the Lorentz corrected intensity assumes incorrectly that the lamellae are separated by the same amount of amorphous material, and that the crystallinity is constant in each long period. Therefore, the long period is measured from the one-dimensional correlation function. The long period is a weighted average obtained from point L in Figure 4.14 this is the point where the one-dimensional correlation function is at maximum using equation 2.9.8. The percent crystallinity was measured via WAXD (Table 4.1) and using equation 2.9.5 was used to measure the lamellar thickness (Table 4.3).

## 4.4 Melting Behavior of Ethylene Copolymers

Differential scanning calorimetry was performed on non-isothermally crystallized samples of the polyethylene copolymers as outlined in section 3.2. A summary of the DSC data is given in Table 4.4. Samples were crystallized using the Ding-Spruiell rapid

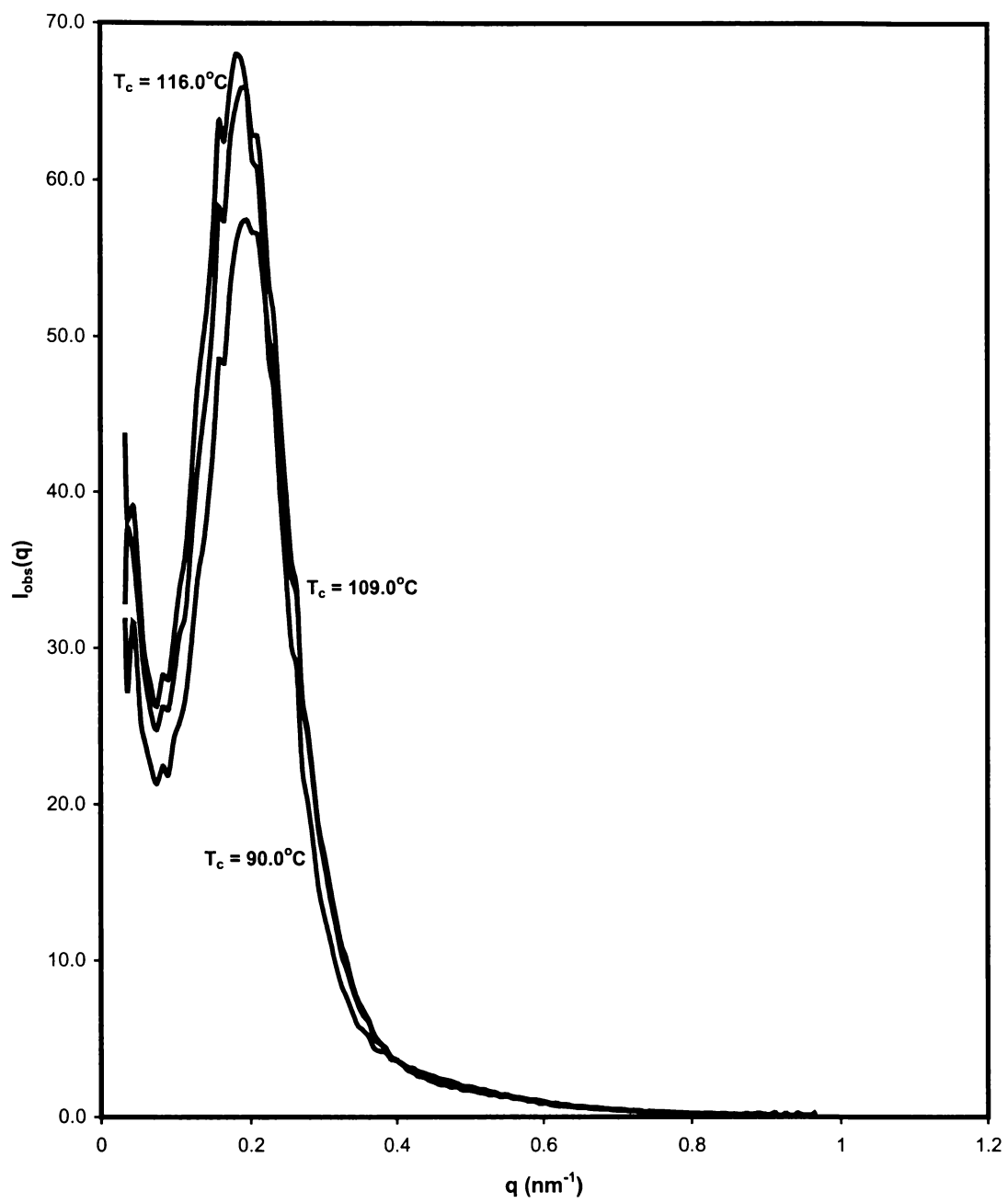


Figure 4.12. SAXS intensity profile for the LPE 54/101 at different  $T_c$ 's.

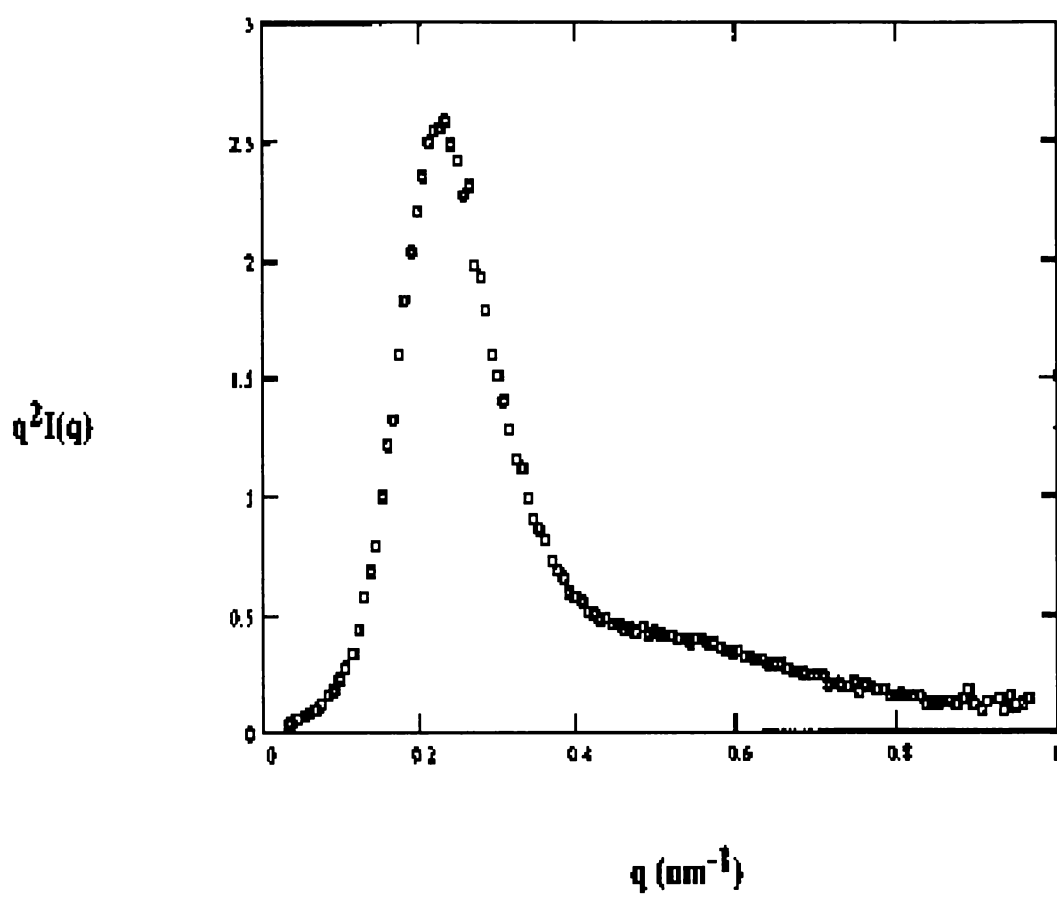


Figure 4.13 Lorentz corrected SAXS intensity profile for LPE 54/101 with  $T_c = 90.0^\circ\text{C}$ .

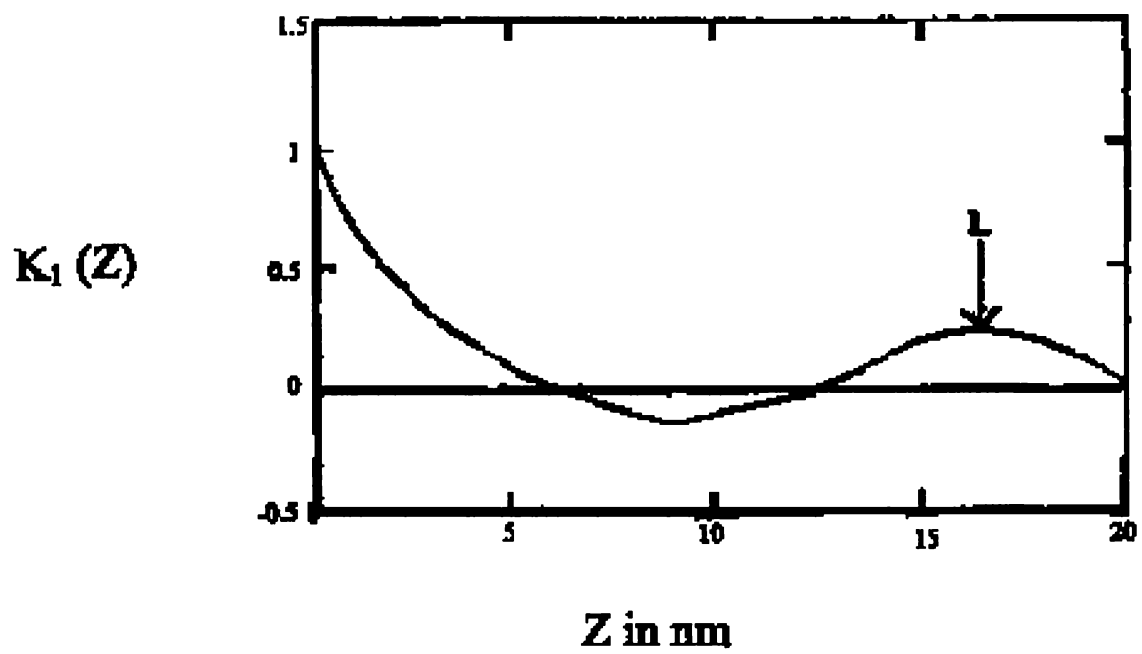


Figure 4.14. One-dimensional correlation function analysis of the data from LPE 54/101 at  $T_c = 90.0^\circ\text{C}$ .

Table 4.3. Corrected SAXS data for linear polyethylene from one-dimensional correlation function calculations.

$T_c$ (°C)	% $X_c$ (XRD)	$L$ (Å)	$l$ (Å)
90.0	51.2	258.9	132.6
109.0	57.0	264.5	150.8
116.0	60.4	276.8	167.2

Table 4.4: Summary of Percent Crystallinity Results by DSC.

Sample	$T_c$ (°C)	$T_m$ (°C) (Peak) <sup>a</sup>	$T_m$ (°C) (RTB) <sup>b</sup>	% $X_c$ (DSC)
LPE-54/101	90.0	131.2	135.3	51.2
	109.0	131.9	135.5	56.9
	116.0	133.3	136.1	60.2
L4-M	95.0	121.3	125.3	52.0
	104.0	121.5	125.0	52.9
	111.0	122.8	125.8	57.8
L11-M	81.0	109.1	113.0	45.8
	87.5	109.0	112.7	49.0
	89.0	108.9	112.9	50.3
H7-M	82.0	111.1	115.1	45.2
	89.5	110.5	114.2	49.0
	96.0	110.8	114.8	51.5

a)  $T_m$  was taken from the peak of the melting endotherm of the DSC profile.

b)  $T_m$  was taken from the return to baseline (RTB) of the endotherm to the baseline. This is the temperature value that is the intersection of a line from the tangent from the steepest part of the slope of the high temperature side of the endotherm with the other intersecting line being the tangent from the baseline after the melt has been completed.

cooling apparatus as determined by a thermocouple imbedded in the sample as well as by optical microscopy. The crystallization times are given on each curve. From the melting endotherms, information can be gained concerning the crystallization and melting behavior, and the structure of the polyethylene copolymer. This will be discussed in section 5.6.

All DSC sample experiments included baseline correction. The  $\Delta H_f$  was measured over a large temperature range, typically from 20°C to 125°C. The percent crystallinity was calculated from:

$$\%crystl. = \frac{\Delta H_f^{measurement}}{\Delta H_f^o} \quad (4.1)$$

where  $\Delta H_f^o$  is 272.6 J/g (Brandup, 1989) of 100% crystalline low-density polyethylene.

Measured percent crystallinity for each sample experiment is shown in Table 4.4.

The melting endotherms of the isothermally crystallized LMWS may be seen in Figure 4.15, 4.16, 4.17, and 4.18 for samples LPE 54/101, L4-M, L11-M, and H7-M respectively. Several important features can be seen from these results. At crystallization temperatures closer to the melt the melting temperature will increase as the crystallization is increased. However, in the rapid cooling region this effect is more difficult to see and is only observed for LPE 54/101 and L4-M. It should be kept in mind that the change occurs by a small amount. It can also be seen that as the crystallization

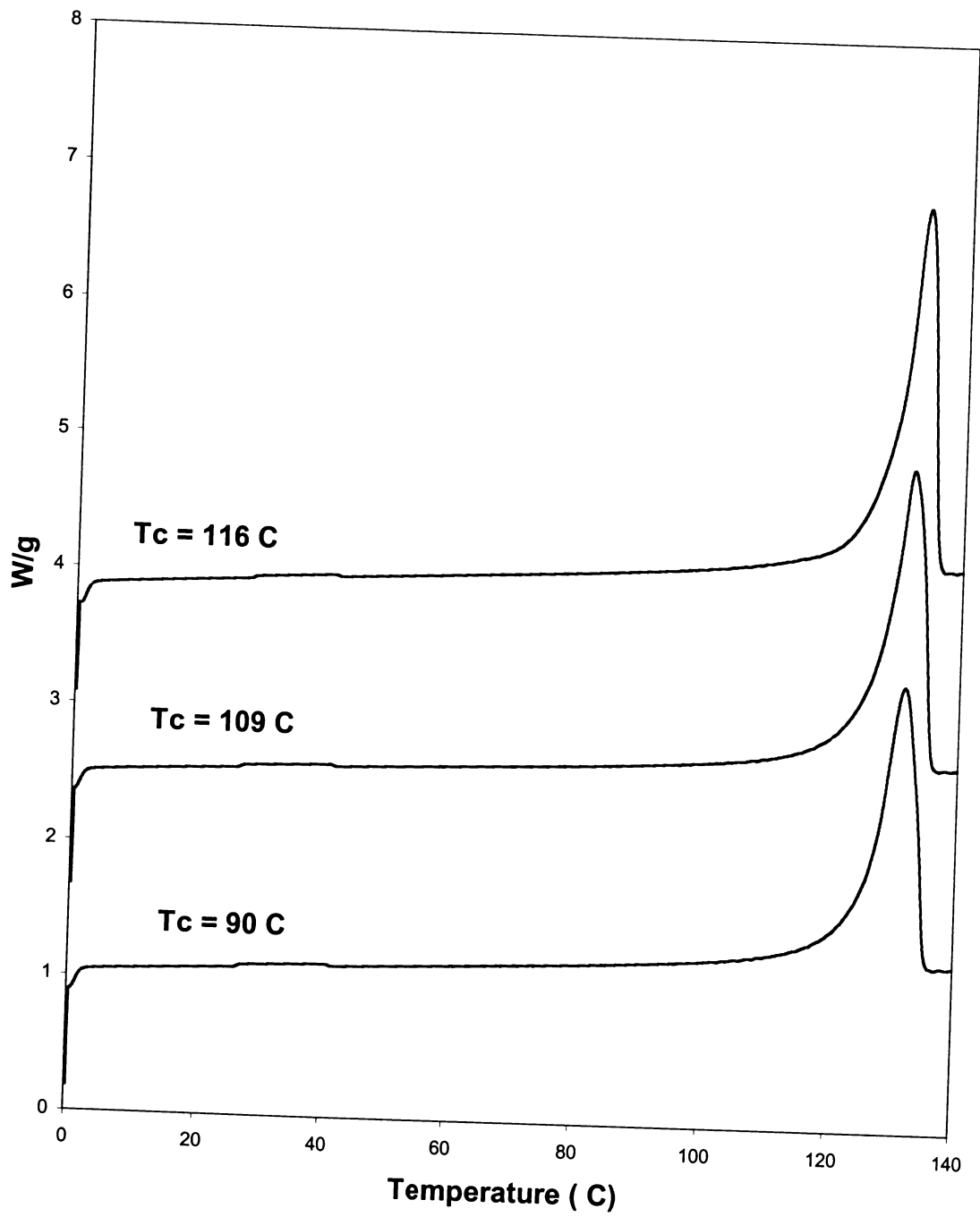


Figure 4.15. Melting behavior of LPE 54/101.



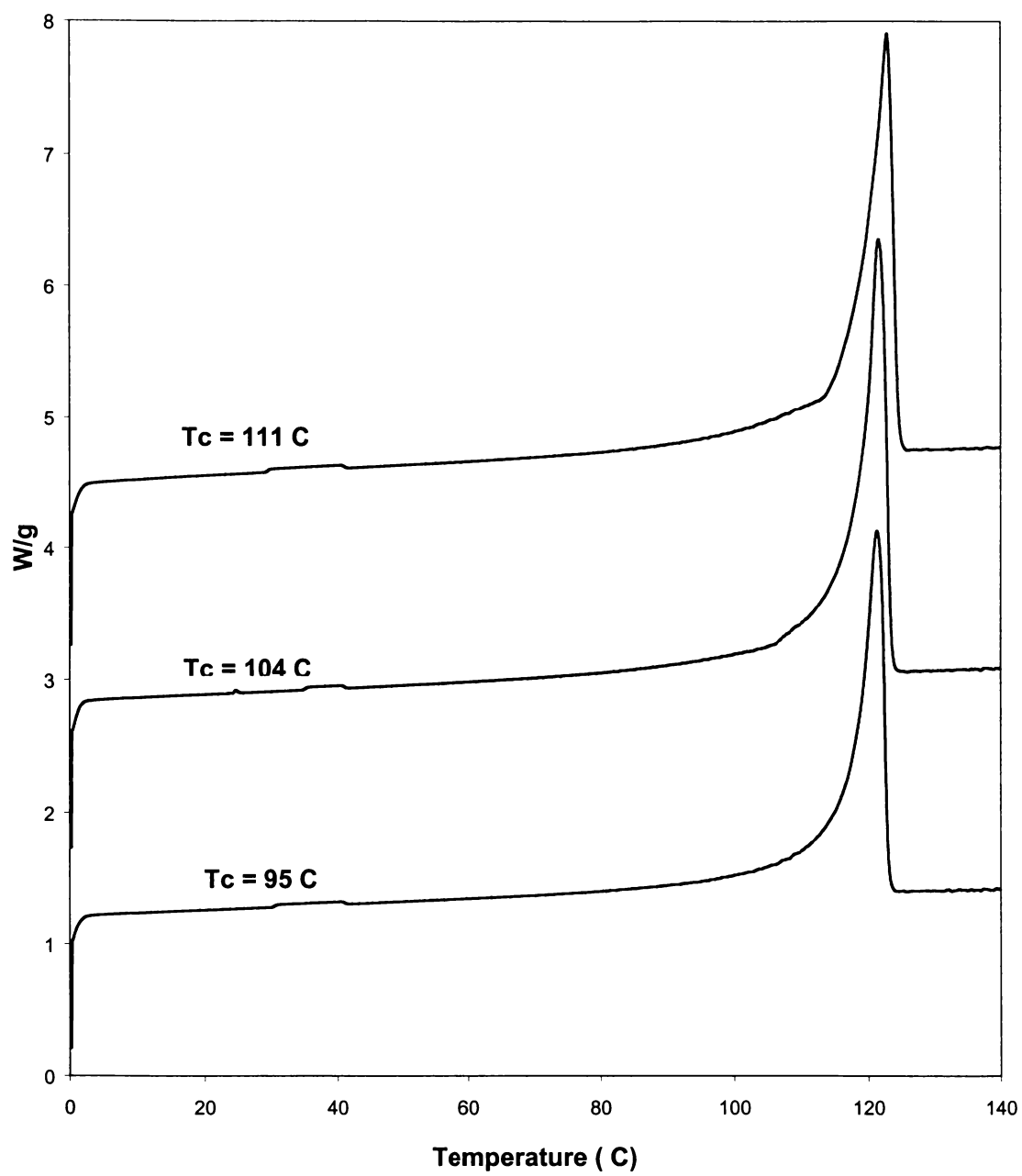


Figure 4.16. Melting behavior of L4-M.

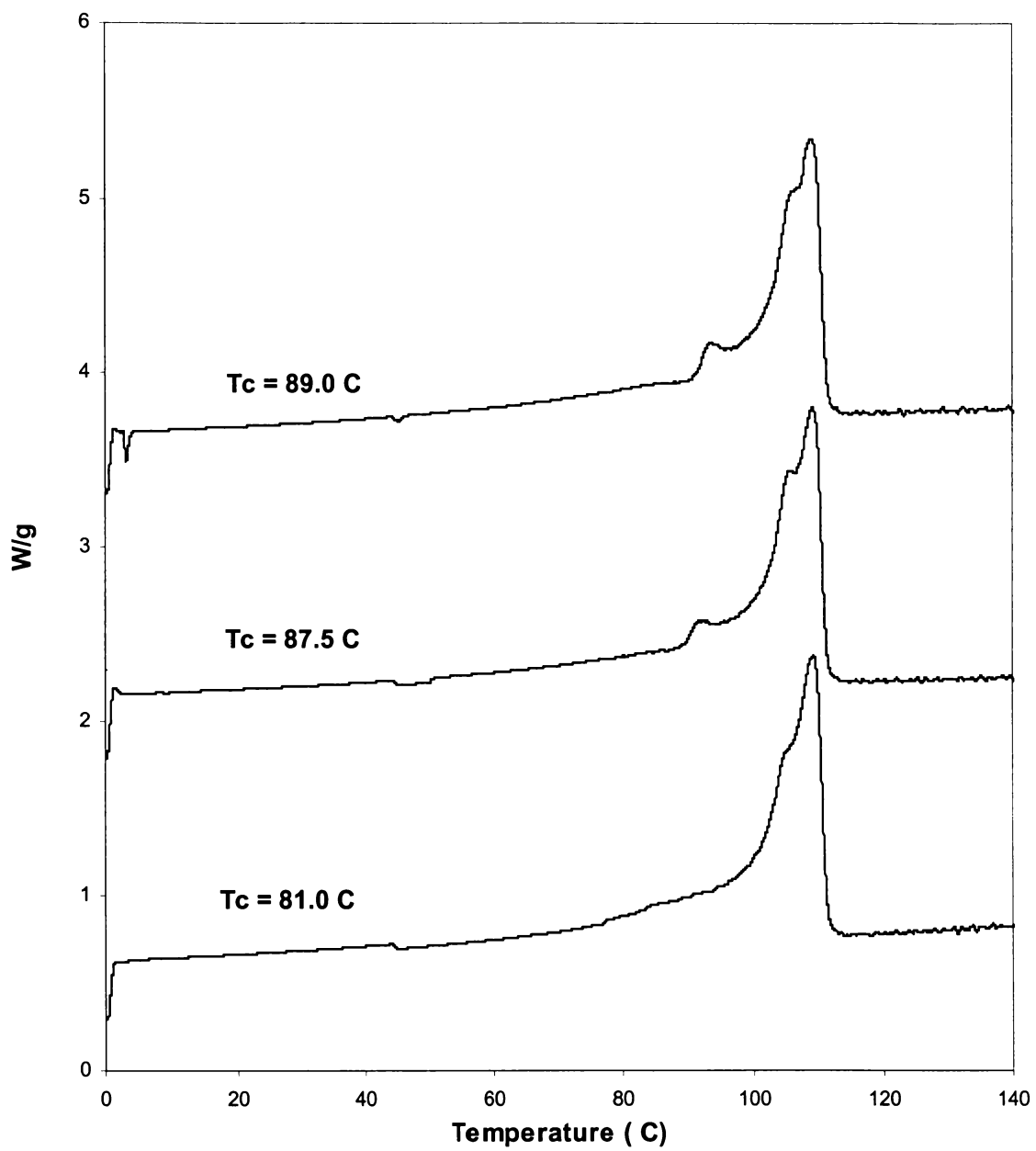


Figure 4.17. Melting behavior of L11-M.

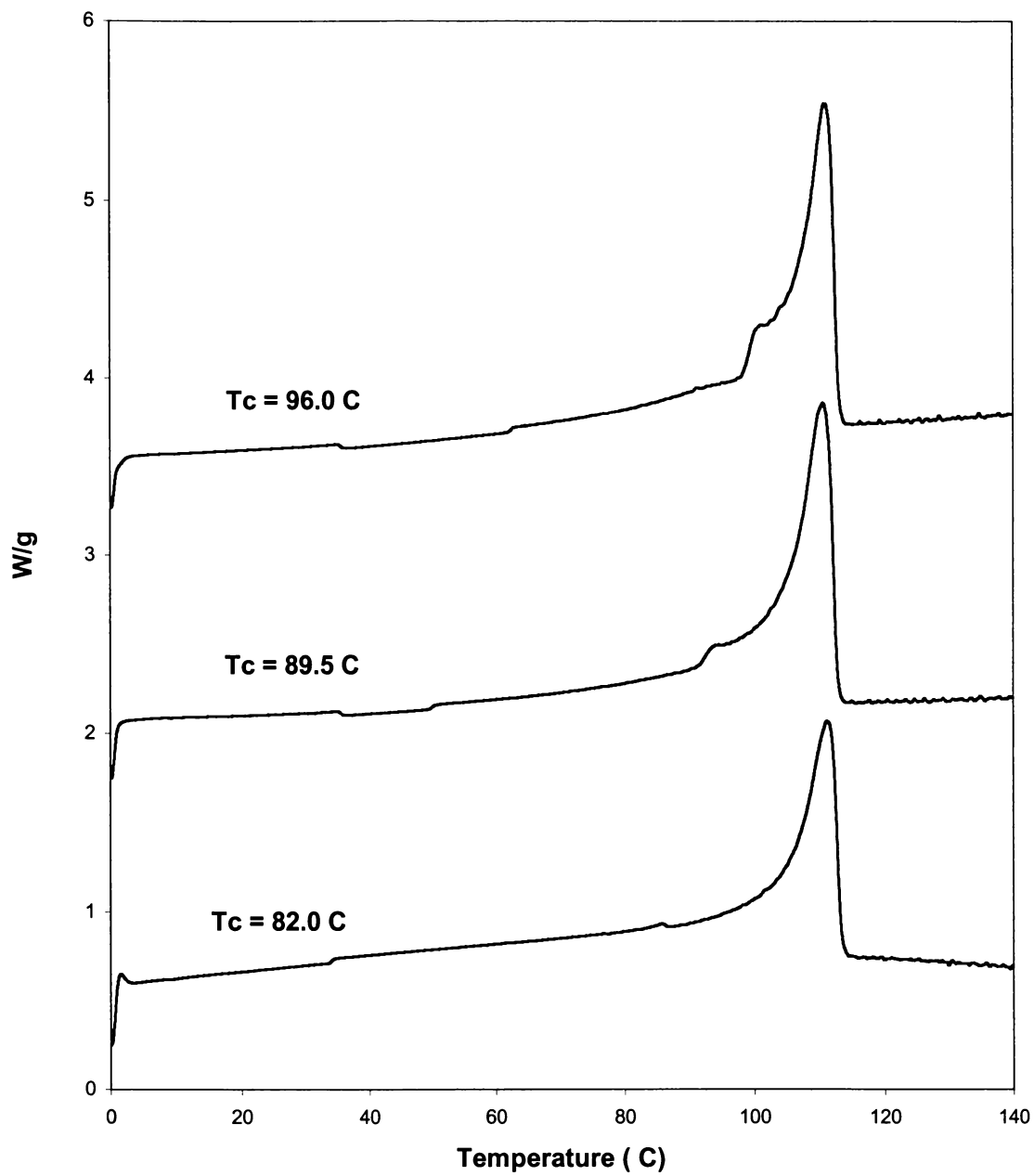


Figure 4.18. Melting behavior of H7-M.

temperature is increased, the relative heights and areas of the high temperature and low temperature peaks change in particular for L11-M and H7-M. The movement and appearance of shoulders or “humps” can be seen as the crystallization temperature is varied. These features in the melting endotherms will be discussed and related to the crystallization behavior and structure of the linear and copolymer polyethylene.

Using DSC to determine percent crystallinity contains an uncertainty in error. In particular with problems associated with baseline correction can alter the area used in the calculation of the heat of fusion. This is why it is extremely important to verify percent crystallinity by at least one alternate method such as WAXD.

#### **4.5 Equilibrium Melting Temperature ( $T_m^\circ$ )**

The melting temperatures are plotted as a function of the lamellar thickness  $l$  in Figure 4.19 for the linear polyethylene LPE 54/101 and the results compared with Kim (1996). The results of this study represented by filled symbols and the results of Kim’s study represented by open symbols. The melting temperature was taken as the peak temperature of DSC with a heating rate 10°C/min and was assumed to correspond to the average lamellar thickness.

The lamellar thickness was estimated from the one-dimensional correlation function analysis of the SAXS intensity profile. In the Thompson-Gibbs plots, an

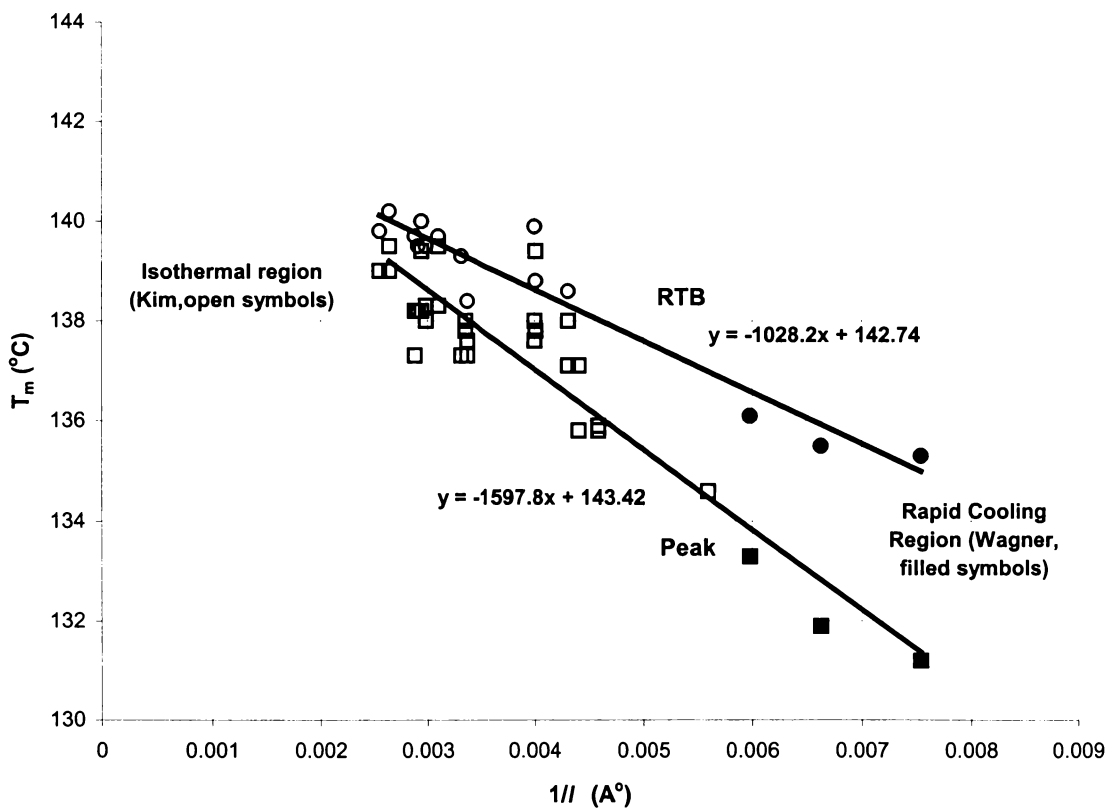


Figure 4.19. Melting temperature (°C) against reciprocal lamellar thickness (Å<sup>-1</sup>) for the linear polyethylene a comparison with Kim (1996).

intersection, at which the reciprocal lamellar thickness goes to zero, that is, infinite lamellar thickness, was determined to be the equilibrium melting temperature,  $T_m^\circ$ . From Figure 4.19,  $T_m^\circ = 143.4^\circ\text{C}$ , which compares to  $142.7^\circ\text{C}$  with previous work by Kim (1996) for melting temperature at peak maximum. This is a small but measurable temperature difference. When using return to baseline (RTB) values are used a  $T_m^\circ = 142.7^\circ\text{C}$  is obtained. Equation (2.8.2) forms the basis of the Thompson-Gibbs plot.

## CHAPTER 5. DISCUSSION

### 5.1 Wide Angle X-ray Diffraction of Polyethylene Copolymers

In typical polymeric systems, as the crystallization temperature of the system is increased, the resultant melting temperature also increases due to an increase in its lamellar thickness. Such a relationship follows equation 2.8.2. An increase in the lamellar thickness often corresponds to an increase in the crystallinity of the system. Therefore, it would be expected that an increase in crystallization temperature would result in an increase in the crystallinity of a typical polymeric system. This behavior can be explained from DSC studies and an understanding of the crystallization process of systems containing chain defects.

One confounding point in the use of WAXD to determine the crystallinity of the polyethylene copolymers is that scattering occurs not only from the crystals formed at the crystallization temperature, but also from those formed upon quenching from the crystallization temperature to room temperature. The crystals formed at the crystallization temperature are thicker; more perfect crystals, and should have a higher crystallinity than those formed upon quenching. This means that the crystallinity values in Tables 4.2 and 4.4 are on average of both sets of crystals and indicative of the average crystallinity of the system, and not necessarily of the crystals formed at the crystallization temperature. This is discussed in more detail in section 5.6. The relative crystallinity for any given polymer at its melt temperature is 0% and as the glass transition is approached

the relative crystallinity is 100%. What this means is that at 100% relative crystallinity the polymer can crystallize no further. The actual or measured crystallinity is dependent on the density of the polymer. Each polymer has its own characteristic density. This is compared to a polymer that is 100% crystalline and no measurable amorphous area as verified by WAXD. At or near the glass transition temperature a polymer can have 100% relative crystallinity meaning that it cannot crystallize any further but still contain amorphous areas, which gives it an actual crystallinity less than 100%.

## **5.2 Small Angle X-ray Scattering of Polyethylene Copolymers**

SAXS has been used to probe the structure of the ethylene copolymers and correlated with the growth kinetics to develop a better understanding of the crystallization process and structure of polyethylene. Table 4.3 gives the results for the long periods ( $L$ ) and lamellar thickness ( $l$ ) calculated from the one-dimensional correlation SAXS data for the linear polyethylene. Several possibilities exist to explain the effect of crystallization temperature on long period and lamellar thickness. The scattering monitored from the isothermally crystallized samples is the result of scattering from the crystals formed upon quenching and those formed isothermally. Therefore, the measured long period is some combination of these two long periods, this being especially true at higher crystallization temperatures.



The calculated long periods are only as accurate as the calculated crystallinity values. Care must be taken when measuring crystallinity and that is the reason for having two methods. WAXD is considered the most reliable method for measuring percent crystallinity. However, DSC was used as a backup method to verify the WAXD results. Both sets of data are summarized in Tables 4.2 and 4.4. It must be remembered that the crystallinity includes contributions from both the grown crystals at the crystallization temperature and the quenched crystals from cooling between the crystallization temperature and room temperature.

### **5.3 Rapid Cooling Crystallization of Polyethylene**

The variation of linear growth rate,  $G$ , with crystallization temperature,  $T_c$ , is shown in Figure 5.1 for several different materials, where the filled symbols represent points obtained in conventional isothermal crystallization experiments. Open symbols represent data points obtained in rapid cooling experiments, where the polymers generate their own pseudo-crystallization temperature. It can be clearly shown that as high supercoolings are approached the curves of all the copolymers are tending to merge into a single curve, regardless of the comonomer content or molecular weight. It has to be remembered that the equilibrium melting point is dependent on molecular weight and comonomer content and the data should be corrected for that variable using the supercooling, relative to the equilibrium melting point of each copolymer. In Figure 5.2 when the linear growth rate,  $G$ , data are plotted as a function of supercooling,  $\Delta T$ , the

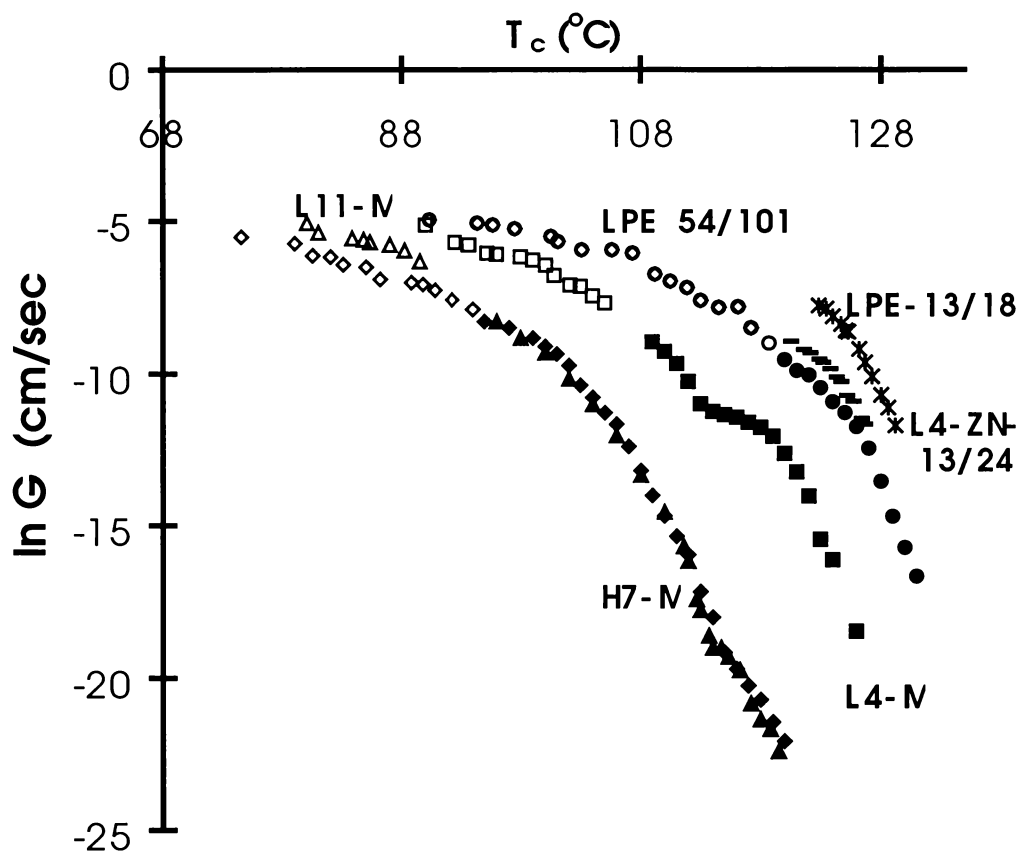


Figure 5.1. Logarithm of radial growth rate versus crystallization temperature for the polymers, as indicated.

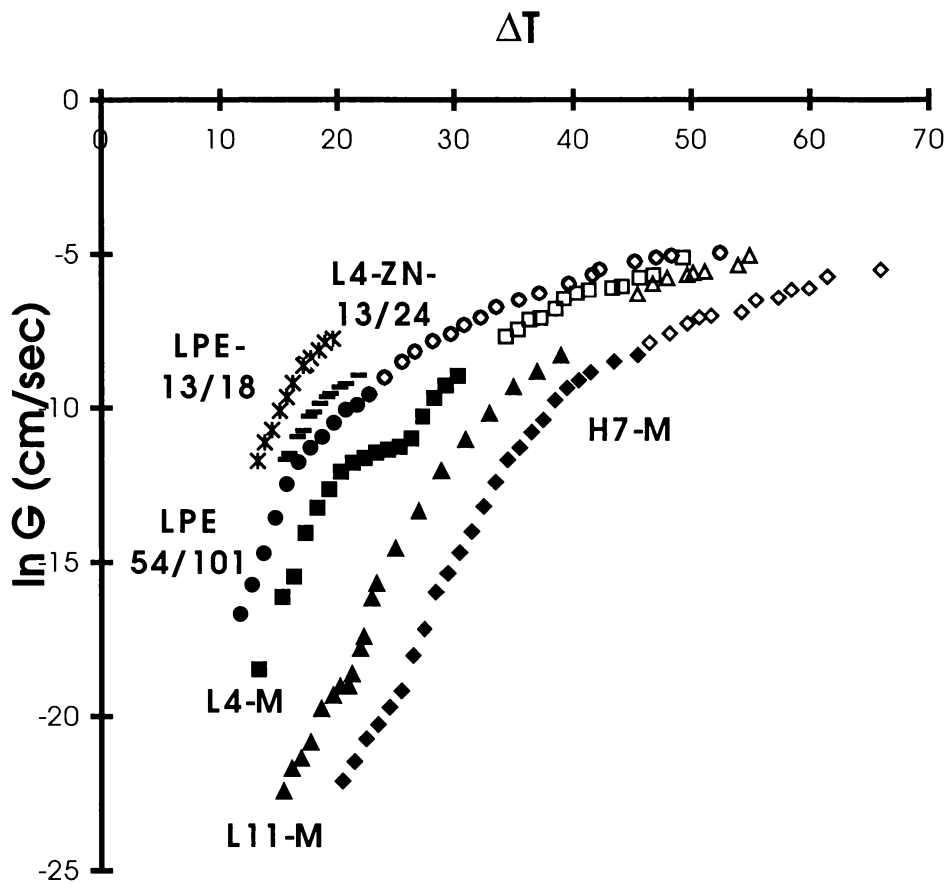


Figure 5.2. Logarithm of radial growth rate versus supercooling, using established equilibrium melting points of each individual copolymer.

$1/fT_c\Delta T = 6.3329$ . The different regimes can be identified and the crystallization behavior of the polymer can then be assessed. Such a plot is shown in Figure 5.3.

The crystallization regime plot of polyethylene copolymer is obtained from equation 2.7.1 and 2.7.2. The input values were  $U^* = 1500$  cal/mol and  $T_\infty = T_g - 30^\circ\text{C} = -85^\circ\text{C}$ . The glass transition,  $T_g$  used in this work for polyethylene is  $-55^\circ\text{C}$ . The equilibrium melting point,  $T_m^\circ$ , values used in this study were obtained from previous work by Kim (1996).

The rapid cooling experiments, as shown by the open symbols, continue on the same lines as the filled symbols. This tells us that there is no significant difference between an experiment carried out isothermally and one that is carried out dynamically in a rapid manner. As the experiments proceed to successively higher and higher cooling rates the slope for all the lines for polyethylene show evidence of alternative crystallization mechanisms. Alternative crystallization mechanisms are discussed in detail in section 5.4. This observation suggests that alternative mechanisms are at work here and will be discussed and evaluated in the following discussion sections.

### 5.3.1 Measurement Dynamics

In order to properly address possible sources of error a systematic method of measurement of the radius of the spherulite was maintained. For each crystallization temperature point on the secondary nucleation plot 4 to 5 spherulites were chosen from

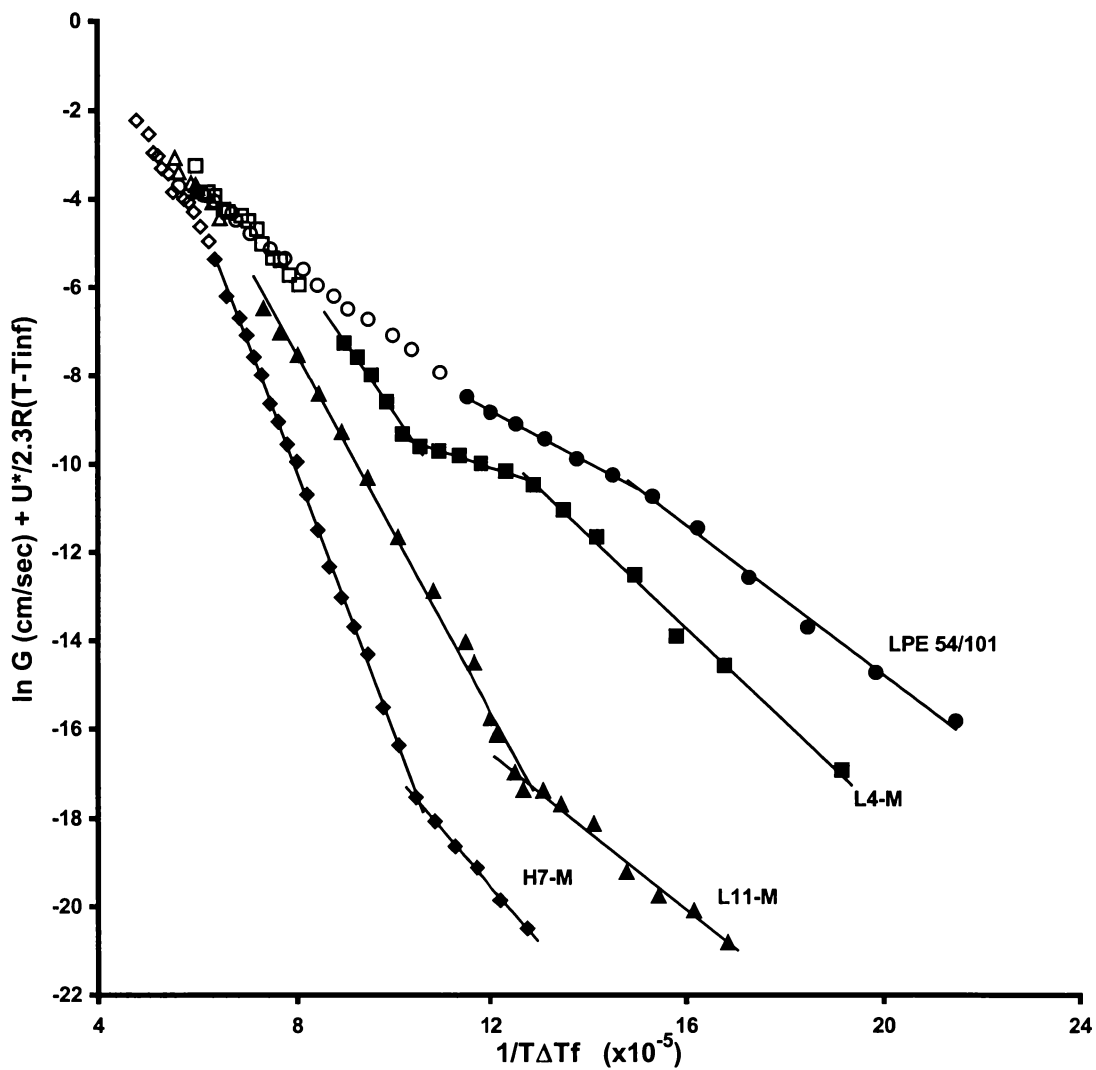


Figure 5.3. Secondary nucleation plot for the copolymers indicated (filled symbols are isothermal crystallizations; open symbols are pseudo-isothermal crystallizations obtained from rapid cooling experiments).

which to make measurement of the diameter or the radius of the spherulite. For each of these spherulites, however, the growth of the radius was measured at 5 to 7 time intervals until impingement between spherulites occurred. If a calculated growth rate value in ( $\mu\text{m}/\text{sec}$ ) was beyond two standard deviations from the average it was discarded. This happened in a few cases. Regime II of the linear polyethylene LPE 54/101 was chosen for this discussion as a representative region. This regime contains 6 crystallization temperature points on the secondary nucleation plot. A total of 147 different spherulite radius measurements were taken to come up with the slope of Regime II. If one takes into account that the regimes of some of the samples contain up to 12 to 15 crystallization temperature points it is entirely possible that 360 to 450 individual radius measurements were taken that ultimately factored into the slope of that regime on the secondary nucleation plot. An occasional random error would be averaged out.

However, if a systematic error were made every time in the measurement of the radius of the spherulite a determination would need to be made of the effect of that error. Such an error would include the outer fringes of the spherulite in every measurement of the radius. Such a fringe was shown previously in Figure 4.3. Figure 5.4 shows the results where two different sets of measurements were obtained. The first experiment no fringes were measured and the second experiment the outside of the fringes were measured each time. As can be seen the slope is 0.5863 when the fringes are not measured. In a worse case scenario the outside of the outer fringe was taken into the measurement every time the slope is 0.5883. The real slope of regime II is somewhere

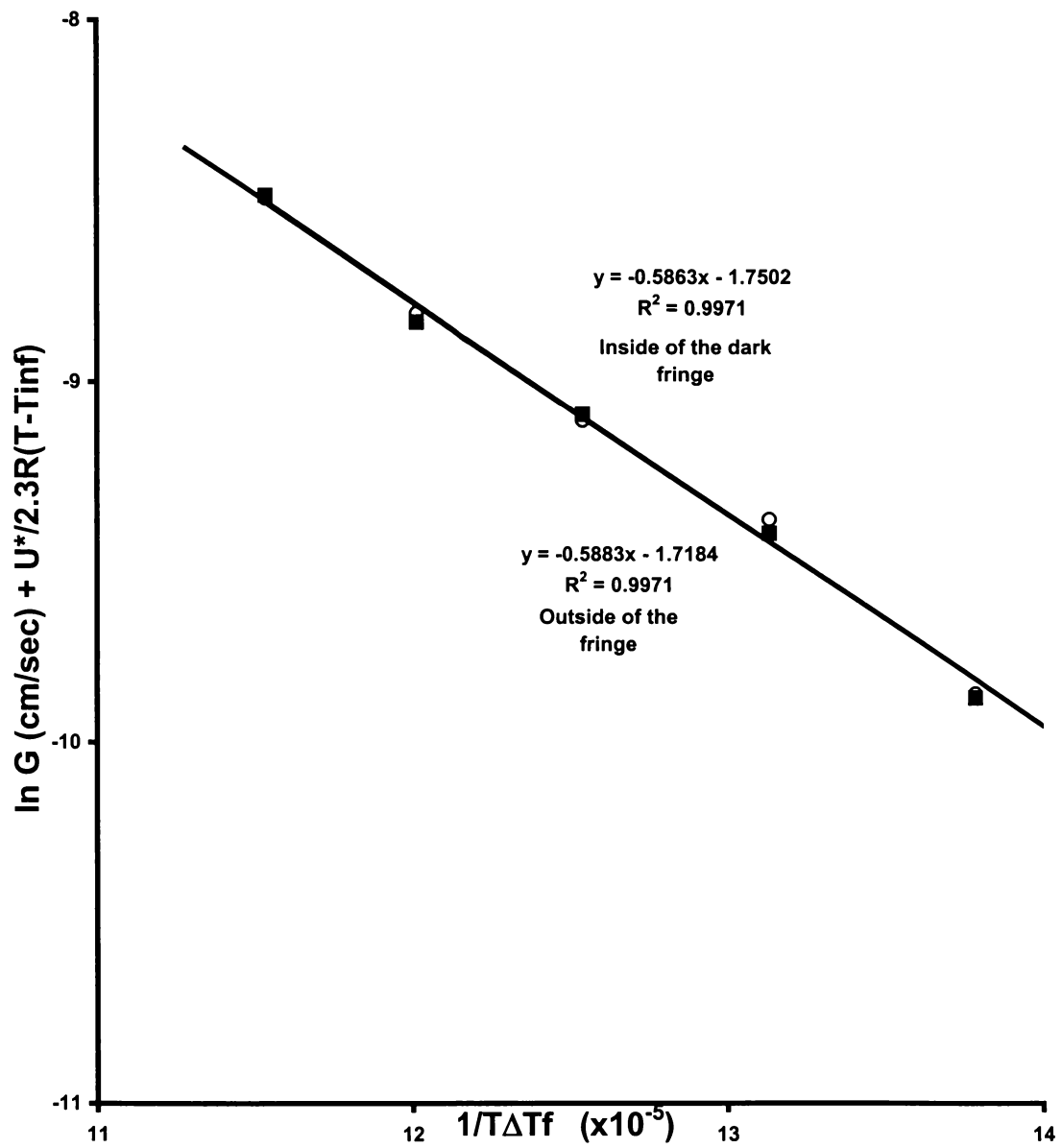


Figure 5.4. The linear polyethylene LPE 54/101 of only Regime II showing the effect of fringes in spherulite measurements.

between these two values. However, this difference of 0.3% is not considered to be significant and is well within the operational error of the experiment.

## **5.4 Alternative Mechanisms**

### 5.4.1 Molecular Weight Effect

#### 5.4.1.1 Chain Mobility

The effect of molecular weight on the crystallization rate can best be analyzed when branch content is fixed. When LPE-13/18 and LPE-54/101 are compared, in Figure 5.5 (only isothermal region is shown here), the crystallization rate of high molecular weight LPE-54/101 is lower than that of low molecular weight LPE-13/18. Using Figure 5.3 with Figure 5.5 at growth rate of  $7.03 \times 10^{-3}$  cm/sec, this is the lowest point on the plot for LPE 13/18, which corresponds with the highest point on the plot for LPE-54/101 the crystallization temperature decreases from 129.2°C (LPE-13/18) to 90.3°C (LPE-54/101). The difference between the growth rates at the same crystallization temperature between the low molecular weight LPE-13/18 and the high molecular weight LPE-54/101 is about a factor of 10. The reason may be due to chain mobility since the chain must have a conformational change to transform from the amorphous state to the crystalline phase. By disregarding the branch content or considering branched polymers like linear polymers the reptation theory can then be applied. According to de Gennes (1971), the



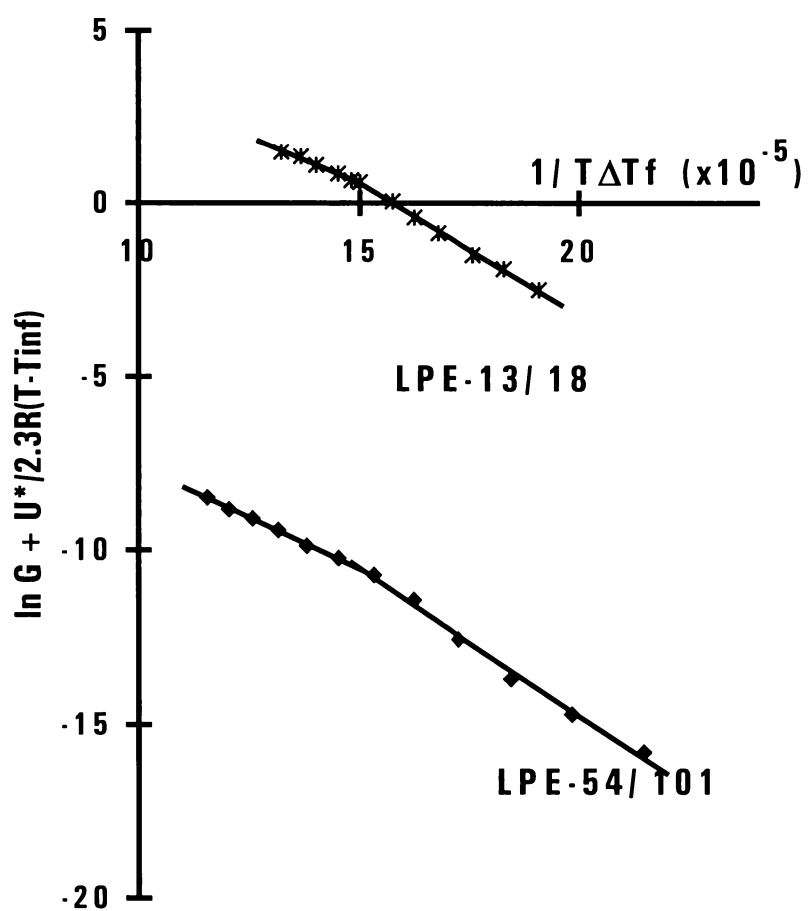


Figure 5.5. Secondary nucleation plots of linear growth rates showing the effect of molecular weight.

entangled polymers can rearrange their conformation through reptation process. The self-diffusion coefficient  $D$  of a single free chain  $P$  in a polymer melt where the polymers are entangled is dependent on the chain length or molecular weight as follows:

$$D \sim 1/M^2 \quad (5.2)$$

and the relaxation time required for complete renewal of the chain conformation:

$$\tau \sim M^3 \quad (5.3)$$

Also the long chain will have high friction coefficient  $\xi_r = n\xi_0$  on reptation causing the rate of crystallization to slow. Here  $\xi_0$  are the friction coefficients of the repeating unit,  $n$ . High molecular weight LPE-54/101 needs more time for conformational change and its long chain will cause higher friction coefficient. Therefore the crystallization rate is reduced with molecular weight.

Figure 5.3 shows that between H7-M and L11-M the higher molecular weight polyethylene H7-M have the lower growth rate. In this case even with a slightly higher branching value the higher molecular weight appears to have a greater effect on the reduction of growth rate. It is usually observed that an increase in branching leads to a reduction in the growth rate. There is additional discussion on the effect of branching on growth rate in section 5.4.2. Table 3.1 contains a summary of the molecular weight and branching characteristics of polyethylene in this study.

#### 5.4.1.2 Cellulation in Polymers

Spherulites are a direct consequence of molecular length. The behavior of branched polyethylene differs from the uniform growth of the linear polymer in coarsening and developing a corrugated growth front all the while slowing continuously towards an asymptotic steady state (Bassett, 1999). When there is sufficient separation between polyethylenes with high branching, spherulites begin to cellulate. This effect increases with higher branch content. The phenomenon of cellulation is one in which molecules rejected at the growth interface accumulate there, affect the growth kinetics and then give the resulting solid a texture in which rejected species are concentrated between cells. It is well known for binary metallic alloys and has been proposed to exist also for crystalline polymers in general (Keith, 1963). Only recently, however, has it been unambiguously observed for an undoped polymer (Janimak, 1999; Abo el Maaty and Hosier, 1998; Abo el Maaty and Bassett, 1998). It is an unusual phenomenon, which may be superimposed on regular spherulitic growth if appropriate conditions are met. The required conditions are that rejected species of polyethylenes with high branching are of a kind able to slow the growth rate significantly, most likely by lowering the local equilibrium temperature and with it the isothermal supercooling, and that their concentration is sufficiently high.

## 5.4.2 Branch Effect

### 5.4.2.1 Friction Coefficient

At constant crystallization temperature or supercooling, the highly branched polymer chains have lower rates of crystallization. The branch effect on the reptation rate ( $\overline{r_{rept}}$ ) is not well known theoretically. Relying on experience (Hoffman, 1979), branching may cause an extra friction force during a polymer chain movement due to the junction point and bulky side group. Side chains also possess their own frictional force. If we assume that the independent side chains contribute in a linear manner, the total friction force  $f(n, n_i, n_j, n_k, T)$  for  $T \gg T_g$  can be expressed as follows:

$$\zeta_i(n, n_i, n_j, n_k, T) = n \cdot \zeta_o(T) + \sum_i n_i \zeta_i(T) + \sum_j n_j \zeta_j(T) + \sum_k n_k \zeta_k(T) \quad (5.4)$$

where  $n$ ,  $n_i$ , and  $n_j$ , and  $n_k$  are the number of repeating unit of the main chain, the number of the branch with length  $i$ , the branching point and the branch end. For this study, linear polyethylene would have an  $n$  repeating unit of 4,500. And  $\zeta_o$ ,  $\zeta_i$ , and  $\zeta_j$  and  $\zeta_k$  are the corresponding friction coefficients. When we consider that the reeling-in rate contributes to crystal growth, the rate of crystallization should decrease with increasing branch content as in the following manner (Hoffman, 1979):

$$\overline{r_{rept}} (\sim 1/t_{1/2}) \sim \overline{f_c} / \zeta_i(n, T) \quad (5.5)$$

$$\bar{f}_c = (1/l_g^*)a_0b_0(\delta l)\left(\frac{\Delta H_f \Delta T}{T_m^0}\right) \quad (5.6)$$

where  $\bar{f}_c$  is the mean force drawing the polymer chain onto the substrate that is proportional to  $\Delta G$  (See Figure 4.2). Also as branch length increases, the rate of crystallization will decrease. As branch length increases further to 10% of the length (Doi, 1980) of the polymer main chain, the reptation process becomes impossible causing no crystallization. Using reptation theory developed for explaining viscoelastic behavior of star shaped polymers (Doi, 1980; Pearson, 1984) we can reach the same expectation that there is no reptation process for a polymer chain with long branching.

Crystallization temperature for a given crystallization rate shifts to lower temperature with the increasing copolymer content. This behavior can be rationalized using the relationship 5.5 and equation 5.6. For the highly branched polymer chain to be crystallized, the mean force,  $\bar{f}_c$ , associated with crystallization should overcome the total friction coefficient. Therefore, the low crystallization temperature (i.e., high supercooling) is necessary for highly branched chain to be crystallized as long as the crystallization temperature is above the glass transition temperature.

In Figure 5.3 the highly branched L4-M which has a lower regime I-II transition temperature of  $T_{I-II} = 119.5^\circ\text{C}$  compared to the linear LPE 54/101 which has a higher regime I-II transition temperature of  $T_{I-II} = 125.6^\circ\text{C}$ . Figure 5.6 emphasizes the effect of

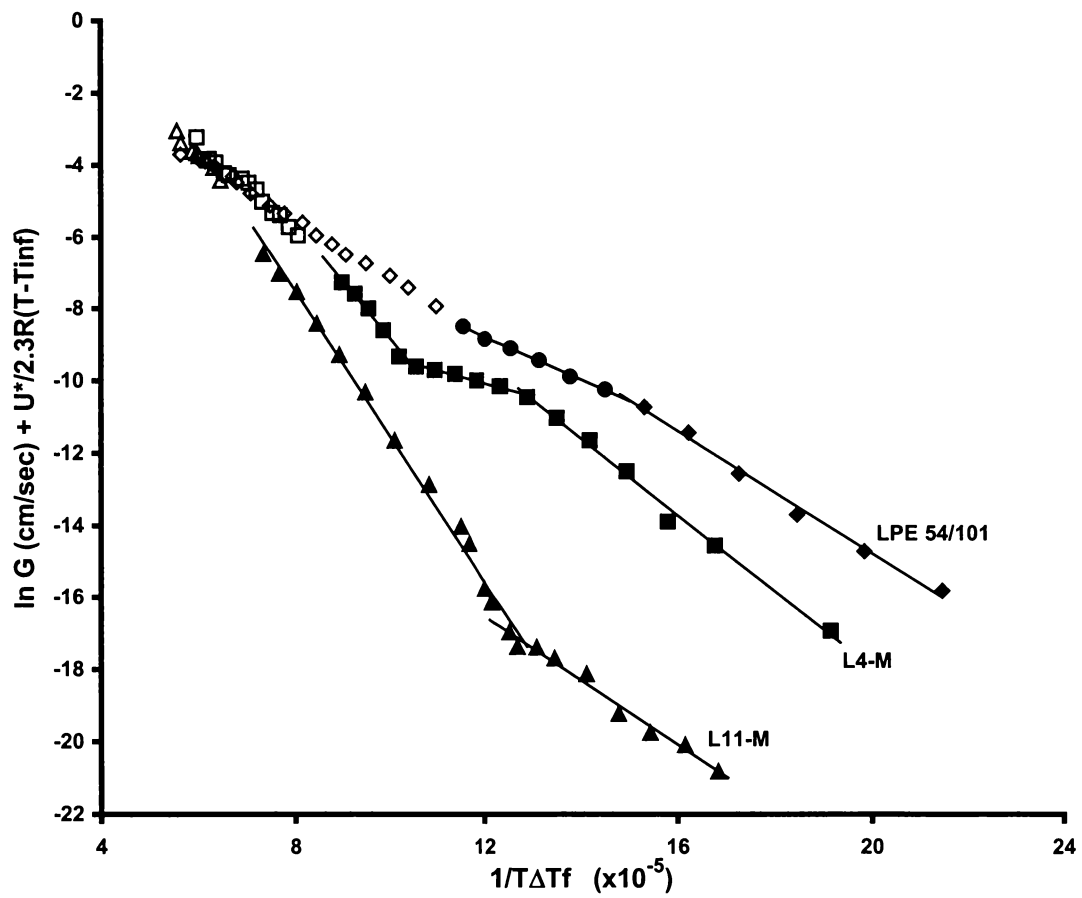


Figure 5.6. Secondary nucleation plots of linear growth rates showing the effect of increasing branching.

increasing branching among the linear polyethylene LPE-54/101, L4-M, to L11-M. A summary of the transition temperature regimes of polyethylene in this study is shown in Table 5.1. The transition temperature is the point of intersection between the regimes. The intersections of the specific regimes indicated in enclosed parenthesis ( ). Table 3.1 contains a summary of the branching characteristics of polyethylene in this study.

This regime transition behavior of the branched polymer chain as a function of supercooling can be understood as the same way with the molecular weight effect using equation (5.4) ~ (5.6). Based on equation (5.4) and (5.5) the reeling-in rate  $\bar{r}_{rept}$  for high branched chain must be slow or zero due to the large total friction coefficient,  $\zeta_t (n, n_i, n_j, n_k, T)$ . For a single polymer chain to reptate to the substrate, it is required for  $\bar{f}_c$  to be larger than friction coefficient. Remember  $\bar{f}_c$  is the mean force drawing the polymer chain onto the substrate and proportional to the supercooling. Therefore, high supercooling is necessary condition for high-branched polymer chain to overcome the total friction coefficient (based on equation (5.6)). The regime I-II transition temperature takes place at lower crystallization temperature and higher supercooling than the linear polymer. As an example, the highly branched L4-M has lower crystallization temperature,  $T_{I-II} = 119.5^\circ\text{C}$  and  $\Delta T_{I-II} = 19.9^\circ\text{C}$ , than those,  $T_{I-II} = 125.6^\circ\text{C}$  and lower supercooling  $\Delta T_{I-II} = 17.1^\circ\text{C}$ , of the linear polyethylene, LPE 54/101.

Of course, as temperature decreases, the friction may be increased. Therefore, the reeling-in-rate depends on the relative contribution of  $\zeta_t (n, n_i, n_j, n_k, T)$  and  $\bar{f}_c$ . Below a

Table 5.1. Regime Transition Temperatures for Polyethylene and Copolymers.

Sample	Regime Transition Temperature, $T_c$ (°C)	Regime Transition Temperature, $\Delta T$ (°C)	Growth Rate (cm/sec)
LP-ZN-13/18 (I-II)	125.3	17.1	1.75E-04
LPE-54/101 (I-II)	125.6	17.1	9.46E-06
LP-ZN-13/24 (I-II)	124.2	18.1	4.47E-05
L4-M (I-II)	119.5	19.8	5.45E-06
LPE-54/101 (II-III)	120.8	21.9	5.45x10-5
L4 (II-III)	113.5	25.9	1.52E-05
L11-M (II-III)	114.2	20.7	4.28E-09
H7-M (II-III)	115.1	25.3	5.00E-09

- a) The linear growth data was taken from the work of Hoffman et al (1975). Ziegler-Natta (ZN) catalyzed linear polyethylene.
- b) The linear growth data was taken from the work of Lambert (1994). Ziegler-Natta (ZN) catalyzed polyethylene-octene copolymer with 4.22 branches/1000 CH<sub>2</sub>.

Note: ( ) indicates the intersection of the two specified regimes. The temperature and growth rate at this transition point is shown in the table.



certain temperature but above a glass transition temperature, if the contribution of  $\zeta_i$  ( $n_i, n_j, n_k, T$ ) becomes much larger than  $\overline{f_c}$ , then there is no reeling-in process.

#### 5.4.2.2 Copolymer Equation

The introduction of co-units at random positions of a chain generally leads to a downward shift of the temperature ranges of crystallization and melting accompanied by a decrease of the crystallinity. The effect is qualitative as expected, comparable to the melting point depression in low molecular weight compounds resulting from the addition of a noncrystallizable solute to the melt. It should be noted that crystallizable solutes such as Cu, Al, and Pb-Sn reduce the melting point. If samples with different co-unit are available, data are commonly evaluated by employing Flory's copolymer equation (Flory, 1953), usually in its simplest form, which relates the melting point depression to the heat of melting and the content of co-units only (Balbontin, 1992). However, as one surveys through the literature, one rarely finds agreement between Flory's theoretical prediction and measured data. In the majority of cases shifts are much larger than expected.

With an increase in the content of noncrystallizable units (ie. octene units) Hauser (1998) observed, as expected, a shift of the melting points to lower temperatures and similar shifts of the growth rates versus temperature curves. However, both Hauser (1998) and Heck (1999) found unexpectedly no effect at all of the co-unit content on the crystal thickness of polypropylene copolymers. Heck found temperature dependence for

all samples. Heck demonstrated that crystal thickness is not determined by the supercooling below the respective melting point of a copolymer, but depends on the absolute temperature chosen for the crystallization. The thickness of all samples show a common temperature dependence, being inversely proportional to the supercooling below the equilibrium melting point of perfect syndiotactic polypropylene. Crystal thickness and growth rates are, according to the observations, independent properties (Hauser, 1998).

This is contrary to what has been reported by Kim (1996) with polyethylene copolymers and Hugel (1999) with syndiotactic polypropylene. Kim found a dependence of lamellae thickness variant with octane copolymer content among the low molecular weight and high molecular weight content polyethylene. Lamellar thickness would decrease as the copolymer content increased. Slightly higher lamellar thickness was seen for the high molecular weight as compared to the low molecular weight linear polyethylene. As can be observed in Figure 4.19 the results in this study correlated well with Kim for the linear polyethylene LPE 54/101.

An interesting point at the end of Heck's (1999) paper is that he does state that thickening is always suppressed if co-units are included in the chains and that this held for the polyethylene copolymer samples in his investigation. The co-units cannot be transported through the crystallites and therefore their presence suppresses a long-range longitudinal diffusion and therefore crystal thickening. Again, this is consistent with

accepted knowledge of copolymers, however this is inconsistent with the claim at the beginning of Heck's paper.

#### 5.4.3 Growth and Nucleation Rate

Crystallization rates have been measured for the linear polyethylene and copolymers and have been summarized in Figure 5.3 as a secondary nucleation plot. The copolymers merge with linear polyethylene in the low crystallization temperature range of regime III. The copolymer L4-M merges at  $T_c$  of 107.3°C, L11-M merges at  $T_c$  of 100.5°C, and H7-M merges at  $T_c$  of 90.3°C of the linear polyethylene. The point of intersection of the copolymers with the linear polyethylene varies with branch content and molecular weight. Organ (1996) and Bassett (1996) speculated on the crystallization of long chain pure n-alkanes in their work that showed evidence of rate minima at the once folded form of the long chain  $C_{294}H_{590}$  in which spherulites are formed. In particular, if one inspects Figure 5.1 and Figure 5.2 one indeed finds evidence of rate minima in the region of Regime II. While the actual growth rate is not decreasing, the absolute value of the slope of the line in Regime II is reduced to a smaller absolute value. In other words, the growth rate while still increasing at lower crystallization temperatures in Regime II decreases by a slower amount as compared to Regime I. In Regime III there is an increase in the rate at which the growth rate increases such that there is a significant increase in the absolute value in the slope of the Regime III for L11-M and H7-M as seen in Figure 5.3. The appearance of Regime III and Regime II for the crystallization rate has

the characteristic “self-poisoning” effect (Ungar, 1988). Whereby the growth front is repeatedly blocked by the deposition of transient folded-chain conformations.

Organ (1996) reported maxima and minima in a plot of the overall crystallization rate versus crystallization temperature of the n-alkanes  $C_{246}H_{494}$  and  $C_{198}H_{398}$ . It was evident from non-isothermal experiments that the anomaly was present at least in the crystal-growth rate, if not in both the growth and the nucleation. The sharp upturn in crystallization rate below the temperature of the minimum coincides with the onset of once-folded crystallization. Higgs and Ungar (1994) reported using a simple  $C_{246}H_{494}$  model, with a stem consisting of either one (chain-folded) or two (chain-extended) crystallizing segments. The essential condition for growth to proceed was that all of the folded over chain be removed at the particular location to allow a chain at the crystal surface to extend. In the case of the rate minimum, the hindrance to growth, i.e. self-poisoning, is the extreme manifestation of Sadler’s kinetic ‘entropy barrier’, considered to be dominant in polymer crystal growth.

Ungar (1993) said that the present limited morphological evidence supports the trend that was previously established for PEO fractions for self-poisoning to be associated with circular crystal habits. If retarded step propagation, leading to curved crystal faces, is caused by self-poisoning, then it is not difficult to extrapolate to the situation envisaged in the vicinity of the growth-rate minimum where surface obstruction to growth become exceptionally prominent. In the extreme case, step propagation is virtually halted and growth ceases to be a nucleation-controlled process, leading to a high

degree of surface roughness. A very high degree of kinetic surface roughening has indeed been observed in the simulation of the growth of alkane crystals near the growth rate minimum.

It is important to point out the fundamental difference between the present kinetic roughening caused by self-poisoning and the equilibrium surface roughening, invoked by Sadler in his roughness-pinning theory of crystal growth (Sadler, 1983). However, both types of roughening can lead to curved-faced, ultimately circular, crystals.

#### 5.4.4 Spinodal Transformation/Intermediate Phase Approach

It is possible that what is seen in the rapid cooling region is not effect of Regime III behavior but the introduction of a metastable phase or unstable phase as a result of very rapid quenching (Gunton, 1983; Ezquerra, 1995). The second unstable phase behaves such that the growth rate of the polymers begins to level off and merge at lower crystallization temperatures. This acts to retard the overall spherulitic growth rate. Keller et al. (1994) described the role of metastable phases, specifically the mobile hexagonal phase in polyethylene which can arise in preference to the orthorhombic phase in the phase regime where the later is the stable regime, and the recognition of “thickening growth” as a primary growth process, as opposed to the traditionally considered secondary process of thickening. The scheme relies on considerations of crystal size as a thermodynamic variable, namely on the melting point depression, which

is different for different polymorphs. Keller found that under rapid quenching conditions phase stabilities could invert with size. That is a phase, which is metastable for infinite size, can become the stable phase when the crystal is sufficiently small. When applied to crystal growth, it follows that a crystal can appear and grow in a phase that is different from that in its state of ultimate stability, maintaining this in a metastable form when it may or may not transform into the intermediate initial state. This is a form with high-chain mobility capable of “thickening growth” which in turn ceases or slows down upon transformation, when and if such occurs, thus “locking in” a finite lamellar thickness.

There are certain transformations where there is no barrier to nucleation. One of these is the spinodal mode of transformation. Consider the phase diagram with a miscibility gap as shown in Figure 5.7a. If an alloy with composition  $X_0$  is solution treated at a high temperature  $T_1$  and then quenched to a lower temperature  $T_2$  the composition will initially be the same everywhere and its free energy will be  $G_0$  on the  $G$  curve in Figure 5.7b. However, the alloy will be immediately being unstable because small fluctuations in composition that produce A-rich and B-rich regions will cause the total free energy to decrease. Therefore, “up-hill” diffusion takes place as shown in Figure 5.8 until the equilibrium compositions  $X_1$  and  $X_2$  are reached.

The above process can occur for any alloy composition where the free energy curve has a negative curvature, i.e.

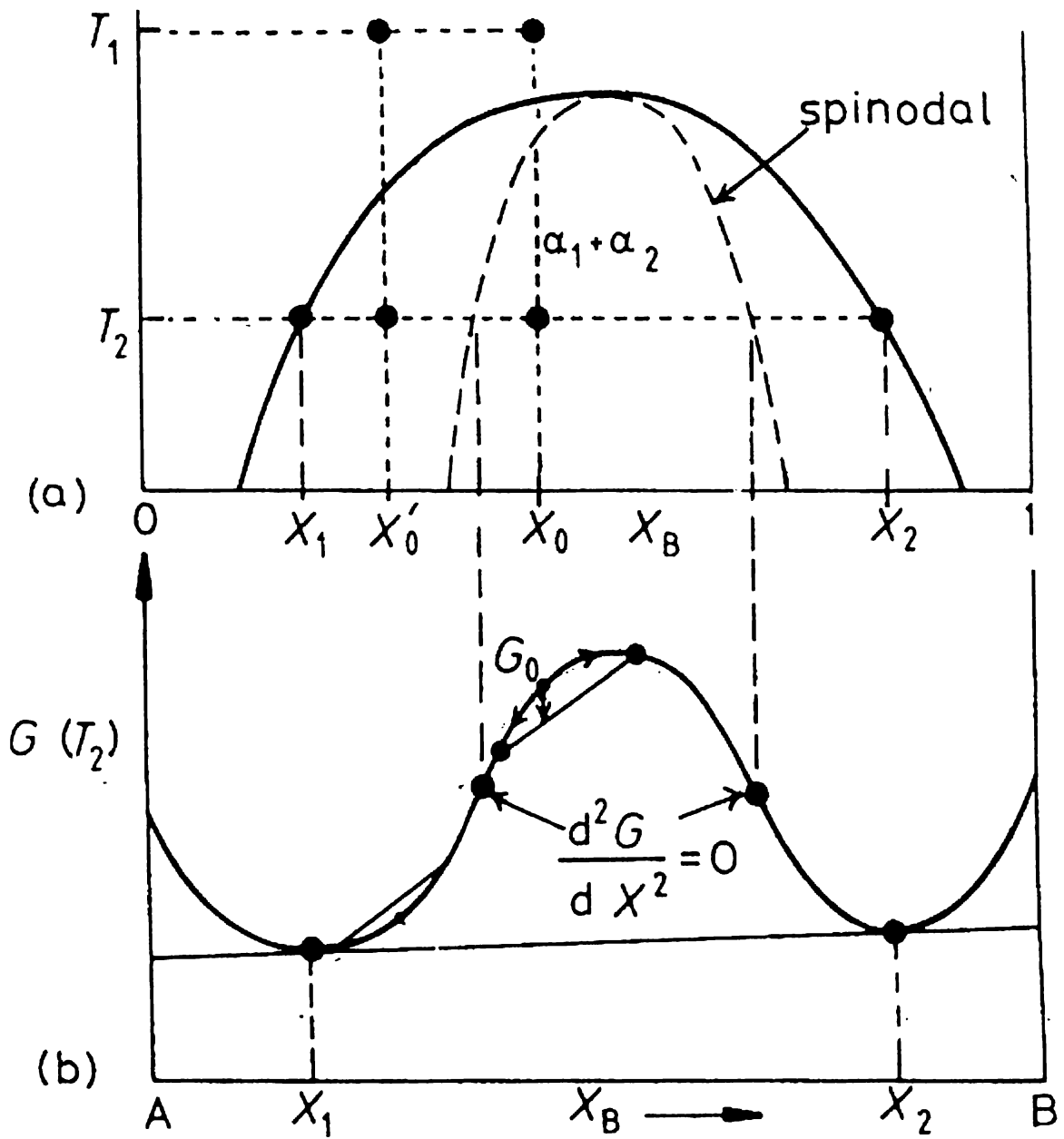


Figure 5.7. Alloy compositions between the spinodal points (Olmsted, 1998).

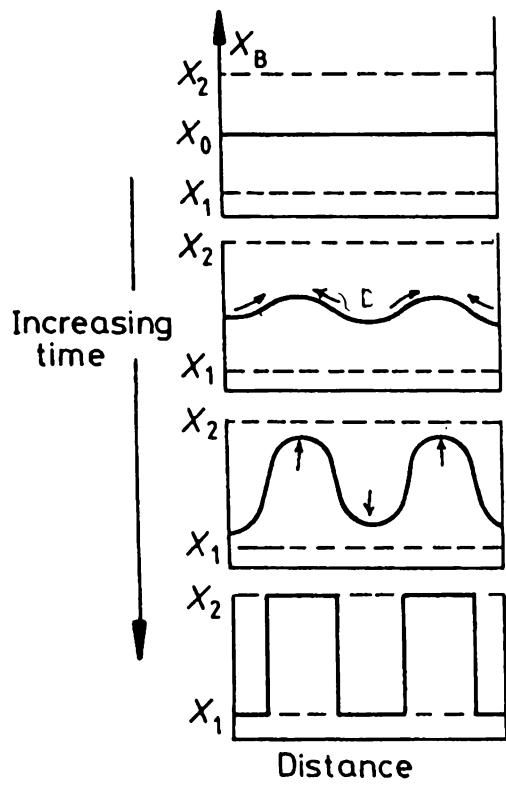


Figure 5.8. Schematic composition profiles (Olmsted, 1998).



$$\frac{d^2G}{dX^2} < 0 \quad (5.7)$$

Therefore the alloy composition must lie between the two points of inflection on the free energy curve. The locus of points on the phase diagram, Figure 5.7a is known as the spinodal.

Alloy compositions between the spinodal points are unstable and can decompose into two coherent phases  $\alpha_1$  and  $\alpha_2$  without overcoming an activation energy barrier. Alloy compositions between the coherent miscibility gaps and the spinodal are metastable and can decompose only after nucleation of the other phase (Olmsted, 1998).

If the alloy lies outside the spinodal, small variations in composition lead to an increase in free energy and the alloy is therefore metastable. The free energy of the system can only be decreased in this case if nuclei are formed with a composition very different from the matrix. Therefore, outside the spinodal the transformation must proceed by a process of nucleation and growth.

Inaba et al. (1988) studied spinodal decomposition and crystallization using a polypropylene and ethylene-propylene random copolymer. The solid texture consisted of dual morphological units, first being the modulated network structure resulting from spinodal decomposition and its coarsening processes in the isothermal demixing of the mixture in the molten liquid state. In the second unit the spherulite structure resulting

from crystallization by subsequent cooling of the demixing liquid. It was found that controlling the time and temperature of the mixture in the molten liquid state controls the modulated structure, and the size of the spherulite is controlled by crystallization conditions. The diffusion-limited crystallization was found to lock in further growth of the modulated structure in the molten liquid and hence conserve the structure memory in the liquid. The criterion for the diffusion-limited crystallization is clearly manifested in the linear versus nonlinear growth of spherulite size with time.

Nucleation and growth occurs if the unmixing is induced near the binodal, where the system is still stable with regard to small concentration fluctuations. Further away from the binodal this restricted “metastability” gets lost and spinodal decomposition sets in. Transition from one to the other growth regime occurs in the range of the “spinodal”. It might appear at first that the spinodal marks a sharp transition between two growth regimes but this is not true. Activation barriers for the nucleation are continuously lowered when approaching the spinodal and thus may lose their effectiveness already prior to the final arrival. As a consequence, the transition from the nucleation and growth regime to the region of spinodal decompositions is actually diffuse and there is no way to employ it for an accurate determination of the spinodal (Oliver, private communication; Brooks, private communication).

In the ‘classical’ picture of polymer melt crystallization we expect, and indeed observe, Bragg peaks in WAXD after an induction period  $\tau_i$ . SAXS accompanies the WAXD, corresponding to interleaved crystal lamellae and amorphous regions (Strobl,

1996). No SAXS is expected during  $\tau_i$ . However, recent experiments (Olmsted, 1996) have reported SAXS peaks during the induction period and before the emergence of Bragg peaks. Initially, SAXS peak intensity grows exponentially while its position remains constant, the behavior predicted by Cahn-Hilliard (CH) theory for spinodal decomposition – the spontaneous growth of fluctuations indicative of thermodynamic instability (Gunton, 1983). Later the peak moves to smaller angles, stopping suddenly when Bragg peaks emerge. By fitting to CH theory, an extrapolated spinodal temperature,  $T_s$ , (Figure 2.10),  $T_s < T_m$  can be obtained.

A plausible explanation for the observation of spinodal dynamics in polymer melts is the presence of a metastable liquid-liquid (LL) phase coexistence curve (or ‘binodal’) buried deep inside the equilibrium liquid-crystal coexistence region as shown in Figure 2.10. Quenching sufficiently below the equilibrium melting point  $T_m^\circ$ , we may cross the spinodal associated with the buried LL binodal at temperature  $T_s < T_m^\circ$ .

It is believed that in a melt the chain conformation alone cannot drive a phase transition. However, conformation is coupled to density. Chains with the ‘correct’ helical conformation typically pack more densely than those with more or less random conformations. In other words, phase separation occurs between a denser phase with a large fraction of helical conformations and a less dense phase with a large fraction of random conformations. Moreover, the energy barriers between different rotational isomeric states (RIS) are density-dependent (Pratt, 1978). Conformational-density coupling can induce a LL phase transition. A phenomenological free energy which

incorporates these effects is a function of the following order parameters: the average mass density  $\bar{\rho}$ ; the coefficients  $\{\rho_q\}$  in the Fourier expansion of the crystal density in terms of the appropriate stars of reciprocal lattice vectors  $\{q\}$  which essentially the intensities of Bragg peaks (Landau, 1980); and the occupancies  $\{\eta_i\}$  of various RIS and therefore chain conformation.

This concept has been suggested to account for the behavior of LPE 54/101 and L4-M as observed in Figure 5.3. LPE 54/101 and L4-M in the secondary nucleation plot appear to merge as the slope of the growth rate in Regime III appears to level off. Spinodal transformation has implications for my work and is presented here as a hypothesis, a possible explanation yet to be proven. Additional work would further clarify the role of spinodal transformation in the quenching and crystallization of polyethylene. Spinodal transformation is a conformational process not a chemical process.

#### 5.4.5 Surface Free Energy of Copolymers

In the isothermal regions (filled points) of Figure 5.3 the slopes of the lines increase as the comonomer content increases. It was reported in an earlier paper by Wagner (1999), that in regime theory this could result from two possible changes. The first change is an increase in the fold surface free energy,  $\sigma_e$  that appears in the numerator of the term used for the slope,  $K_g$ . Crowding of the rejected side branches in the

interfacial regions probably causes this. Second point is there may be reduction in the latent heat of fusion, which appears in the denominator of the  $K_g$  term for the slope of line in the secondary nucleation plot. This would be from the incorporation of hexyl branches in the crystal. The equilibrium melting point of the copolymers will decrease if a substantial incorporation of defects exists. If this is the case then the equilibrium melting points of the copolymers may progressively decrease as the crystallization temperature decreases. If this turns out to be the case, then the estimates of effective supercooling used in Figures 5.2 and 5.3 will be high. This could be responsible for the decreasing slope found at very high supercoolings (open symbols). Furthermore, if large amounts of hexyl branches are incorporated in the crystals, rather than being excluded, and then the crystal will expand increasing the unit cell lattice parameters, thus lowering the latent heat of fusion. If at the same time the crowding in the interfacial regions reduces causing a reduction of the fold surface free energy. All of these effects would result in a decrease in the slope. These effects would be occurring simultaneously. Additionally, it should be noted that expansion of the crystal lattice, through incorporation of defects, would reduce the surface free energy by allowing more surface area per emerging chain in the fold surfaces.

Tables 4.1 and 4.4 show the percent crystallinity decreasing for all of the polyethylene samples as  $T_c$  decreases across the rapid cooling temperature range studied. Percent crystallinity was calculated using heat of fusion data obtained by DSC using equation 4.1. This would indicate that heat of fusion decreases as  $T_c$  decreases for this temperature range. Upon inspection of Table 4.2 the unit cell parameters for the linear

polyethylene remain essentially unchanged over the rapid cooling temperature region. However, moving down the table to higher comonomer content and higher molecular weight the unit cell lattice parameters appear to decrease by greater amounts as  $T_c$  decreases over the temperature region. This would indicate that more hexyl branches are being excluded and the fold surface free energy,  $\sigma_e$  is going to increase by a greater amount moving down the table or down the secondary nucleation plot in Figure 5.3. The slope of the copolymers is going to increase by a faster amount which helps to explain why the curves not only intersect the slope of the linear polymer, but actually each has at least 2 or more crystallization temperature points with growth rates that are faster than the linear polymer. Intuitively this stands to reason as the crystallization rate becomes so fast at the lower  $T_c$ 's or higher supercoolings ( $\Delta T$ ) that the hexyl branches of the copolymers do not have time to fold back into the crystal by the time crystallization is completed at these temperatures.

## **5.5 Morphology of Polyethylene Copolymers**

Morphologies of the linear and copolymer polyethylene have been studied using optical microscopy data obtained during crystallization. In section 4.3, the superstructures of the polyethylene copolymers were shown to be dependent upon crystallization temperature and molecular weight. Hoffman et al. (Hoffman, 1997) have shown a variation in morphology with molecular weight. They report axialitic morphologies for molecular weights less than 18,000. For molecular weights ranging

from 18,000 to approximately 120,000 spherulitic morphologies were formed in Regime II and axialitic morphologies formed in Regime I. For molecular weights greater than 120,000 Hoffman reported the growth of irregular spherulitic structures. Allen and Mandelkern (1987) have shown that the change from spherulitic to non-spherulitic morphologies does not coincide with the regime I-II transition. Lambert (1991) had reported similar behavior in his work, as axialitic morphologies have been observed for the low molecular weight series, spherulitic and axialitic morphologies for the intermediate molecular weight series, and irregular spherulites for the high molecular weight series. Regime III behavior in this work is consistent with work reported by Hoffman et al (1997) for the entire molecular weight range studied here.

There was a difference between the work of Hoffman and this work for the linear polyethylene in the intermediate molecular weight range. Another possible explanation for the spherulitic behavior seen in Regime I for the linear polyethylene is that the structures formed are not dependent on the regime in which the growth occurs, but rather on the degree of supercooling (crystallization temperature), branch content, as well as the molecular weight, this being in agreement with the work of Allen and Mandelkern and Benson (1978). Changes in growth behavior are due to changes in the relative rates of secondary nucleation and lateral spreading which are affected by microstructure. Therefore, changes in morphology should not be automatically be linked to changes in growth behavior.

## 5.6 Thermal Analysis of Polyethylene Copolymers

The melting behavior of the polyethylene copolymers illustrated in Figure 4.15 through 4.18 is complex. An understanding of the crystallization behavior and microstructure of these polyethylenes is helpful in understanding their melting behaviors.

Figures 4.17 and 4.18 contain two distinct melting peaks. These two peaks are formed as a result of the crystallization process. The polyethylene copolymers were heated to just above their melting points before being crystallized at their non-isothermal indicated temperatures. The higher temperature peak is formed by material, which is able to crystallize at the crystallization temperature. In the rapid cooling process once the material crystallizes at the indicated temperature it is allowed to cool down to room temperature. The lower peak consists of material, which crystallizes upon further quenching to room temperature, this being primarily material of high copolymer content. The minimum, which exists between the two peaks, corresponds to the temperature of crystallization.

Material in the high temperature-melting peak consists primarily of copolymer free segments of the chain. This is true since only copolymer free segments are able to nucleate in the crystal, as copolymers cannot fit into the crystal. A low sequence length would not be favorable to nucleation whereas a high sequence length between hexyl groups on the polyethylene chain would be favorable to nucleation. Thus the low temperature peak consists primarily of copolymer material. The melting temperature of



the high temperature peak increases with increasing crystallization temperature. The relative peak areas of the high and low temperature peaks changes with crystallization temperature. As the crystallization temperature is increased, the area of the high temperature peak decreases and that of the low temperature peak increases. This is due to the fact that only copolymer free chain lengths, which are able to form a stable nucleus and crystallize at the crystallization temperature. As the crystallization temperature increases, less material is able to crystallize because nucleation is unable to occur. This being true, then the material will crystallize upon cooling, meaning that the area below the surface of the polymer material will crystallize upon cooling, meaning that the area under the low temperature melting peak will increase with increasing crystallization temperature.

So-called shoulders or “humps” may be seen in both the high and low temperature peaks. This is due to the distribution of copolymers along the molecules. The difference between the crystallinity distributions explains the appearance and movement of shoulders in the DSC traces of the polyethylene copolymers. It can be seen that L11-M and H7-M samples with the highest copolymer contents have very pronounced shoulders in their melting traces. It is known that the lowest copolymer material crystallizes first, while the highest copolymer material crystallizes upon quenching. This means that copolymer chains will crystallize together in some stacks, resulting in a distribution of thickness and crystallinity. Samples of the highest copolymer content will have wider crystallinity and thickness distributions, and therefore more distinct shoulders in their melting behavior. These same samples also exhibit broader melting ranges as the onset

of melting begins at lower temperatures for the higher copolymer content samples of broad crystallinity and thickness distribution.

The shoulders show limited movement with increasing crystallization temperature. Material, which crystallizes in the shoulder area, has limited thickening ability and can crystallize over a limited crystallization temperature range, thus shifting the shoulder to higher temperatures. The intensity of the peak becomes smaller as less material is able to crystallize at the crystallization temperature, and eventually the shoulder disappears from the high temperature peak. The disappearance of the high temperature shoulder coincides with an increase in the low temperature peak area, and in some cases, the formation of low temperature shoulders. The total peak area shows a small increase as the crystallization temperature is increased.

## **5.7 Equilibrium Melting Temperature**

A reliable and reasonable method for the estimation of the equilibrium melting point is to rely on the classical observation that melting temperature is a linear function of crystal thickness known as the Thompson-Gibbs equation. The most important step is to determine the lamellar thickness precisely in addition to the melting temperature. The ORNL 10m-SAXS with high-resolution power was used with a correlation function of one. The SAXS intensity was measured at room temperature. The SAXS intensity profile results from an average of all the crystal thickness present.

A typical Thompson-Gibbs plot is shown in Figure 4.19 for the linear polyethylene LPE 54/101. With the additional data obtained in this study in the rapid cooling region the equilibrium melting temperature came out to be 143.4°C. This compares very nicely with the equilibrium melting temperature by Kim (1996) of 142.7°C. The observed melting temperatures of the linear polyethylene decreased linearly as the number average lamellar thickness decreased, as shown in the plot of observed melting temperature against reciprocal number-average lamellar thickness. The plot shows that the lamellar thickness was a factor in controlling the melting temperature. Kim (2000) and subsequent follow up work by Abu-Iqyas, S. (2000) shows the a plot of the polyethylene copolymer samples that the apparent thickening coefficient decreased with branch content in the system, which demonstrates that branches prevented lamellae from becoming thick. At a fixed lamellar thickness, the melting temperatures of low-branched samples were always higher than those of highly branched samples. This may be due to the incorporation of defects in the crystallization phase. The values of the equilibrium melting point from these plots are listed in Table 3.1.

## **5.8 Andrews Analysis of Polyethylene**

The Andrews equation shows the logarithm of the growth rate to decrease linearly with an increase in the defect content (Andrews, 1971). Figure 5.9 shows that the analysis of Andrews et al. applies to linear polyethylene and copolymers. Linear growth rates are taken only in Regime III. The shape of the data is similar to that for SAXS data

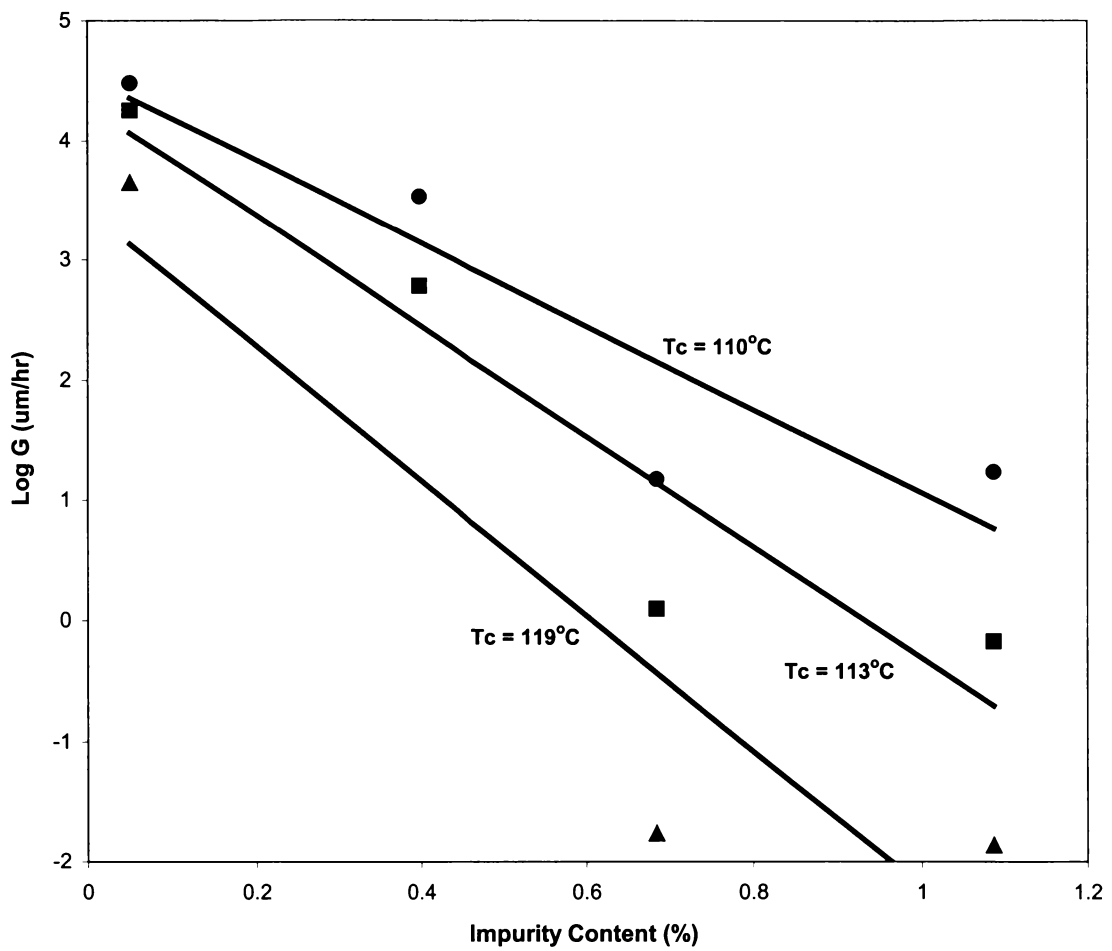


Figure 5.9. Log of growth rate verse impurity content of the linear and ethylene copolymers.

plotted as lamellar thickness versus defect content (Lambert, 1991). Straight-line fits have been applied over a limited range of defect contents. From Figure 5.9, it can be seen that as the crystallization temperature is increased, the slope of the line increases. Since the slope of the line is (negative number)  $-(N-1)$ , where  $N$  is the number of crystallizable units in sequence required to form the nucleus, the size of the critical nucleus increases with increasing temperature. This being the case, then at higher crystallization temperatures the rate of nucleation would be expected to decrease. The reduction in secondary nucleation is due to the fact that fewer chain lengths between defects are able to participate in the nucleation step since at higher temperatures a longer chain length is required to form the nucleus.

Andrews et al. concluded that a three-stem nucleus was present in cis-polyisoprene. As pointed out by Phillips and Lambert (1990) this may also be the situation in natural rubber, or any high molecular weight polymer, where the chains are long enough to be above the entanglement limit, thus serving as virtual crosslinks. Upon the determination of the lamellar thickness of the polyethylene and with a further understanding of the growth process, the size of the nucleus has been recalculated.

From the slopes from Figure 5.9 which are tabulated in Table 5.2 and range from 346 to 561, the values corresponding to methylene units assuming an all trans configuration. The ranges of the slopes can vary significantly if only two points are used for each of the plots and depending on which two points are used. The maximum range is given in the table as the percent that the average value could vary therefore introducing

Table 5.2. Nucleus Shape Characteristics Calculated From Andrews' Analysis for LPE 54/101.

Temperature (°C)	Slope <sup>a</sup>	Nucleus Length (Å°)	Lamellar Thickness (Å°)	# of stems <sup>d</sup>
110.0	346.0 ± 24%	437.3	150.2 <sup>b</sup>	2.9
113.0	460.0 ± 29%	581.4	226.8 <sup>c</sup>	2.2
119.0	561.0 ± 36%	709.1	298.2 <sup>c</sup>	2.1

a) From slopes of the lines in Figure 5.8.

b) Lamellar thickness from Table 4.3.

c) Lamellar thickness from Kim (1996).

d) Calculated assuming a 30° tilt angle.

significant experimental error. This suggests that the confidence of the fit is not high. These percent error values are derived from the plot for that temperature assume that the point deleted is a point that has the further most deviation from the slope of that line. Nucleus size increases with increasing crystallization temperature as expected. This means that nucleation rate decreases at higher crystallization temperatures since fewer chains will be able to participate in the nucleation step. This suggests that nucleation becomes selective at higher crystallization temperatures.

However, if the extreme case is performed in which only the two rightmost points for each of 110°C, 113°C, and 119°C in Figure 5.9 is used the margin of error increases by a substantial amount. If this is done then the slope,  $-(N-1)$ , becomes 15.4, -67.6, and -24.5 for each of 110°C, 113°C, and 119°C. Note the positive value of 15.4. All of these results would make the calculation of the nucleus length by the Andrews plot impossible. The Andrews plot may not be valid for high polymer content. There is large margin of error involved with using the Andrews plot.

Assuming a one-stem nucleus for all temperatures on the plot in Figure 5.9 the values of 173.4 Å, 261.4 Å, and 344.3 Å for nucleus length are obtained for 110°C, 113°C, and 119°C. Using the margin of error shown in Table 5.2 for 110°C, 113°C, and 119°C the lower limit of the nucleus length values are 263.0 Å, 326.6 Å, and 359.0 Å. Upon comparison at 119°C the values of 344.3 Å and 359.0 Å are very close. This is why it is important to have at least three, preferably four or more values for each

temperature plotted. Clearly, however, additional work can be done in this area to further clarify the experimentally obtained nucleus length values.

The number of stems has been calculated as the nucleus length divided by the stem length assuming a 30° tilt angle (Voigt-Martin and Mandelkern, 1989). It is possible that the tilt angle changes as a function of crystallization temperature. The number of stems ranges from 2.1 to 2.9 and is consistent with results obtained by Lambert (1991). These values suggest that the nucleus consists of multiple stems. At low crystallization temperatures, three-stem nucleation takes place, followed by limited spreading of the molecule. When the nucleation mechanism changes so that a two stem or a one-stem nucleus is laid down, spreading can occur to a greater extent. This suggests that at higher crystallization temperatures the rate of spreading increases, in addition to the decrease in nucleation with increasing crystallization temperature.

Although the three-stem nucleus is in conflict with the single stem model of Hoffman et al., it is not in conflict with regime analysis. Regime transitions depend only on the relative rates of secondary nucleation and lateral spreading, and not on the detailed model of chain attachment. However, it is very important to consider the effect of the three-stem nucleus on secondary nucleation theory, and its consequences on subsequent kinetic equations.

Considering the critical nucleus to consist of three stems, the free energy of formation of the nucleus will be changed to account for an increase in the fold surface



energy due to the two folds in the nucleus. The free energy of formation of the nucleus then becomes:

$$\Delta\Phi = 2bl\sigma + 4ab\sigma_e - 2abl\Delta f \quad (5.7)$$

This varies from single stem nucleation by the  $4ab\sigma_e$  term. Development of regime theory can then begin by developing an equation for the flux  $S$  over the barrier of nucleation.

Once nucleation has occurred, spreading of the molecule along the growth face can occur in several different ways depending upon the shape and size of the chain in the nucleus.

Assuming a nucleus shape as shown in Figure 5.10a, growth of the chain can occur in one direction. The resulting flux equation will be:

$$S(l) = \frac{N_o A_o (A - B)}{(A - B + B_1)} \quad (5.8)$$

and will depend upon the size of the nucleus. The values of  $A_o$  and  $B_1$  are dependent upon the size of the nucleus and are given as:

Single stem nucleus:

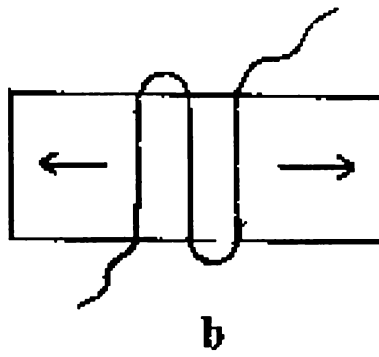
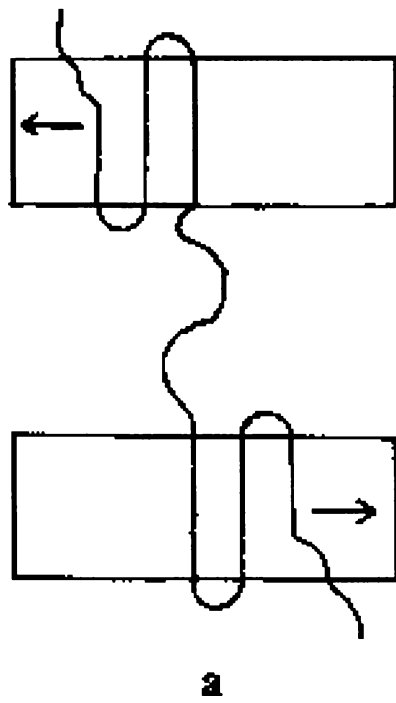


Figure 5.10. Possible nucleation and growth mechanisms.

$$A_o = \beta \exp\left(\frac{-2bl\sigma + abl\Delta f}{KT}\right)$$

$$B_1 = \beta \exp\left(\frac{-(1-\psi)abl\Delta f}{KT}\right)$$

Three stem nucleus:

$$A_o = \beta \exp\left(\frac{-2bl\sigma - 4ab\sigma_e + \theta\phi abl\Delta f}{KT}\right)$$

$$B_1 = \beta \exp\left(\frac{\theta(1-\phi)abl\Delta f}{KT}\right)$$

In both approaches:

$$A = \beta \exp\left(\frac{-2ab\sigma_e + \phi abl\Delta f}{KT}\right)$$

$$B = \beta \exp\left(\frac{-(1-\phi)abl\Delta f}{KT}\right)$$

$\theta$  can take a value of two or three depending upon whether the nucleus has two half stems or three full stems. A single stem nucleus as depicted in Figure 5.10a will result in

the flux given in the theory of Lauritzen and Hoffman. Obviously the same flux will result for a polymer chain, which nucleates at its chain end and spreads in one direction. Figure 5.10b if spreading occurs in both directions along the growth face.

The fluxes presented above can be integrated so that a growth equation can be derived. Such equations do not lend themselves to simple integration so that general solutions can be obtained and included in growth equations. It is obvious that the calculation of the flux, lamellar thickness, and ultimately the linear growth rate equations will depend upon the shape and size of the nucleus.

It is possible for the nucleus to conform to a variety of shapes and sizes, so that a stable nucleus can be formed. The size and shape of the nucleus will depend on a number of factors that include the defect content and the crystallization conditions. The presence of defects disrupts crystallization because this must be excluded from the crystal. However, they make it possible for multiple stem nuclei to form because of constraints placed on chains. The structure of polyethylene copolymers will depend largely upon the nucleation process, this being particularly true since the crystallization process of polyethylene copolymers is a nucleation driven process.

## 5.9 Secondary Nuclei and Surface Spreading

Hoffman and Miller (1988) have demonstrated the use of secondary nucleation theory and experimental results to estimate the rate of deposition of secondary nuclei,  $i$ , and the rate of surface spreading,  $g$ , found in regime theory. These parameters can only be estimated at the regime transition temperature. The equations used in this study are too detailed to list here but have been dealt with thoroughly by Hoffman and Miller (1975) and had been used previously by Lambert and Phillips (1994). The results obtained are presented in Table 5.3. The data are separated into two groups each consisting of the regime I-II transition and the regime II-III transition. The most striking result of the regime I-II transition tabulated data is the remarkably constant value of the rate of surface spreading. Of course there is the expected reduction between LPE-13/18 and LPE-54/101 expected because of the increase in molecular weight and presumably a result of a decrease in the rate of reptation. L4-M and L4-ZN copolymers have approximately the same rate of surface spreading, close to the value of LPE-54/101.

The regime transition temperature occurs at whatever temperature is necessary for the rate of secondary nucleation to equal the rate of surface spreading, when expressed in equivalent units of course. Using data obtained from the Andrews plot, lamellar thickness, and number of stems an attempt was made to make comparisons of the  $i$  and  $g$  data for the regime (II-III) transitions in Table 5.3. For LPE 54/101, the linear polyethylene, the lamellar thickness and number of stems at 119°C from Table 5.2 was used in the calculations.  $2.98 \times 10^{-8}$  cm times  $4.15 \times 10^{-8}$  cm, the layer thickness,  $b_o$ ,

Table 5.3. Regime Transition Analysis

Sample	Transition Temperature (°C)	Growth Rate (cm/sec)	$i^a$ ( $10^6/cm \cdot s$ )	$g^a$ ( $10^{-5}cm/s$ )
LPE-ZN-13/18(I-II)	125.3	$1.75 \times 10^{-4}$	458	5.2
LPE-54/101(I-II)	125.6	$9.46 \times 10^{-6}$	831	3.13
LPE-4-ZN (I-II)	124.2	$4.47 \times 10^{-5}$	13.7	4.73
L4-M(I-II)	119.5	$5.45 \times 10^{-6}$	199	4.34
LPE-54/101(II-III)	120.8	$5.45 \times 10^{-5}$	2005	4.21
L4-M(II-III)	113.5	$1.52 \times 10^{-5}$	809	8.29
L11-M(II-III)	114.2	$5.00 \times 10^{-9}$	$1.59 \times 10^{-4}$	4.56
H7-M(II-III)	115.1	$4.28 \times 10^{-9}$	$6.61 \times 10^{-4}$	8.04

a) These values were calculated using a program original developed by Lambert (1991).

(Hoffman, 1997) times 2.1 (number of stems at 119°C) times  $2005 \times 10^6$  /cm·sec (Table 5.3) gives an area value for  $i$  of  $5.211 \times 10^{-6}$  cm/sec. Using the Andrews Analysis and lamellar values from Kim (1996) area calculations were done for all polyethylene samples for the II-III transition and are shown in Table 5.4. By comparison from Table 5.3 the  $g$  value at the regime II-III transition for LPE 54/101 at 120.8°C is  $4.21 \times 10^{-5}$  cm/sec. These values are reasonably close comparison. Reasonably close values were also obtained for L4-M. For example,  $i$  for L4-M was  $1.67 \times 10^{-6}$  cm/sec compared to  $g$  value of  $8.29 \times 10^{-5}$  cm/sec. However, as seen in Table 5.4 when the same approach is used for L11-M, and H7-M the  $i$  values calculate out substantially lower than the  $g$  values. Hoffman's regime transition analysis was originally set up for only linear polyethylene at the regime I-II transition. Clearly in future work, additional considerations need to be taken into account for the copolymers for the regime II-III transitions.

## 5.10 Summary

There is a known molecular weight effect and branching effect on the growth rate of ethylene copolymers. Mobility and friction coefficients will slow down the growth rate in particular at low supercooling temperatures. High molecular weight and long chain polyethylenes go through a reduction in growth rate at a mid crystallization temperature region before accelerating at the higher supercooling temperatures. This in particular appears hold true for the H7-M ethylene copolymer in this study. Spinodal transformation offers insight into the nucleation mechanism of the linear polyethylene,

Table 5.4. Regime Analysis for II-III Transitions with Area Calculations

Sample	Transition Temperature (°C)	Growth Rate (cm/sec)	$f^c$ ( $10^{-6}$ cm/s) (area)	$g$ ( $10^{-5}$ cm/s)
LPE-54/101 (II-III)	120.8	$5.45 \times 10^{-5}$	5.21	4.21
L4-M (II-III)	113.5	$1.52 \times 10^{-5}$	1.67	8.29
L11-M (II-III)	114.2	$5.00 \times 10^{-9}$	$3.04 \times 10^{-5}$	4.56
H7-M (II-III)	115.1	$4.28 \times 10^{-9}$	$1.26 \times 10^{-4}$	8.04

c) Area calculation performed as described in section 5.9.



LPE 54/101 and the ethylene copolymer L4-M. The effect of surface free energy on the copolymers H7-M and L11-M is such that at the very high supercooling the nucleation begins to surpass that of the linear polyethylene. The reduction of unit cell parameters versus decreasing temperature as well as the increase of slope of the secondary nucleation plot offers support to the surface free energy effect. The change in lamellar thickness at higher supercoolings for the linear polyethylene not only provides insight into the equilibrium melting temperature but with the calculation of the number of stems this allows us to experimentally verify the behavior of secondary nucleation growth rate and the lateral spreading rate.

## CHAPTER 6. CONCLUSIONS

### 6.1 Conventional Crystallization Process

Branching decreases the rate of crystallization in the branched polyethylene due to a reduction in the rate of secondary nucleation. The growth behavior of branched polyethylene is dependent upon the branch content and molecular weight of the polyethylene. Growth occurs in all three regimes I, II, and III, with the regime I-II transition decreasing from 125.6°C to 119.5°C with increasing branch content for the LPE 54/101 and L4-M polyethylene. The reduction in the regime I-II transition temperature is due primarily to a decrease in the rate of secondary nucleation. The increase in the molecular weight results in the reduction of the mobility of the polyethylene meaning that the rate of reptation is reduced for the LPE 54/101 and H7-M polyethylene. The reduction in mobility and rate of reptation of the LPE 54/101 and H7-M is present in the Regime I and II and the isothermal temperature regions of this study.

### 6.2 Rapid Cooling Crystallization

What has been found at the very high crystallization rates at the highest supercooling regions or at lowest crystallization temperature is that the growth rates of the copolymers not only merge but also pass that of the linear polyethylene at the lowest crystallization temperatures. In addition, surface free energy plays a very important role

in the way the copolymers behave. It was found in this study that the hexyl branches and long chains of the higher molecular weight polymers might actually contribute to a faster spherulitic growth rate once you get past a high enough supercooling or low enough crystallization temperature. What WAXD has been able to show is that the size of the unit cell decreases for the copolymers indicating the hexyl branches are excluded. This increases the available surface free energy so that the crystallization growth rate actually surpassed that of the linear polyethylene. However, some caution needs to be exercised when interpreting WAXD unit cell parameters because these changes are small amounts.

A zero defect polyethylene has the faster nucleation rate which it does in Regimes I, II, and the higher temperatures of Regime III. However by pushing the cooling rate faster with the Ding-Spruiell rapid cooling apparatus for all the copolymers studied these defects and higher molecular weight polymers actually have growth rates that increase past that of the linear polyethylene.

The Ding-Spruiell rapid cooling apparatus was designed to simulate processing conditions and indeed in this study 3600°C per minute and greater cooling rates was obtained. What this means for process and injection molding conditions is that the copolymers take on a much different behavior and evidence indicates that copolymers may actually be favored in situations where very fast crystallizations conditions are required.

### 6.3 Spinodal Transformation or Alternative Intermediate States

The spinodal mode of transformation is an intermediate state that involves a two-step ordering process. There may be a helical not completely crystalline phase with random packing. A second phase would be comparably unstable to a primary phase in the melt. Miscibility gaps in the phase diagram occur where the change in free energy is at a minimum. If a polymer is quenched between the miscibility gaps and the spinodal then nucleation will take place first then followed by spinodal transformation. This process helps to explain the leveling off of the growth rate curves for the L4-M copolymer and the linear polyethylene at the lower crystallization temperatures.

It is also possible that spinodal transformation may consist of chains mostly with trans bonding and random melt phases. The recognition of “thickening growth” as a primary growth process can also arise as opposed to the traditionally considered secondary process of thickening. This scheme relies on considerations of crystal size as a thermodynamic variable, namely on the melting point depression, which is different for different polymorphs. Further evidence suggests an intermediate phase such that different mechanisms were effective during phase separation such as “nucleation and growth”. Further investigations could ultimately lead to describing “nucleation and growth” as the separation through surface nucleation or surface roughening.

## CHAPTER 7. FUTURE WORK

### 7.1 Rapid Cooling Effects

Additional rapid cooling work will further clarify the behavior of the polyethylene copolymers at the very high crystallization rates. A high-speed camera for faster data acquisition and the incorporation of the use of liquid nitrogen to obtain faster crystallization rates to push the past the current limits of this rapid cooling study. It is also important that additional WAXD unit cell work be performed to obtain additional unit cell parameters at additional crystallization temperatures throughout the rapid cooling region. Small angle light scattering experiments (SALS) would clarify spinodal transformation at the rapid cooling temperatures. The appearance of a peak which grows in intensity, initially at a fixed position and then shifts to lower scattering angles would be indicative of a spinodal transformation. Furthermore, combining multi-axial stretching with rapid cooling would provide additional details into the crystallization behavior, morphology, and physical/mechanical properties of the branched polyethylene. This could be useful in determining possible applications for branched polyethylene.

### 7.2 Lamellar Detail

Further SAXS work is required for all the copolymers in the rapid cooling region, as well as representative temperatures in the isothermal region. Also, this would be

helpful for reevaluation of the equilibrium melting points of polyethylene. This in addition to the Andrews plot would further clarify multiple stem nuclei among copolymers in the rapid cooling region.

The lamellar structures of the branched polyethylene may also be studied using transmission and scanning electron microscopy. In addition, electron microscopy may be used to analyze the growth tips of the branched polyethylene in order to determine if branching has any effect on the growth face of polyethylene.

### **7.3 Mechanical Properties**

The structure of a polymer greatly influences its physical/mechanical properties. It would be of interest to study the effect of branch content, branch size, and molecular weight on the physical/mechanical properties of the branched polyethylene. Such studies would be useful in determining possible applications for branched polyethylene.

### **7.4 Pressure Effects**

In polymer processing, pressure is a very important variable. It would be of interest to study the influence of pressure using rapid cooling experiment on the crystallization behavior, morphology, and physical/mechanical properties of the branched polyethylene. This could be useful in determining possible applications for branched polyethylene.

## **REFERENCES**

- Abo el Maaty, M.I., Hosier, I.L., and Bassett, D.C., *Macromolecules*, 31, 153 (1998).
- Abo el Maaty, M.I., Bassett, D.C., Olley, R.H., and Jaaskelainen, P., *Macromolecules*, 31, 7800 (1998).
- Abu-Iqyas, S. and Phillips, P.J., anticipated paper submission in 2000.
- Alamo, R.G., Fatou, J.G. and Guzman, J., *Polymer*, 23, 6480 (1982).
- Allen, R.C. and Mandelkern, L., *Macromolecules*, 5, 147 (1972).
- Allen, R.C. and Mandelkern, L., *Polymer Bulletin*, 17, 473 (1987).
- Alexander, S. and McTague, J., *Phys. Rev. Lett.*, 41, 702 (1978).
- Alexander, L.E., Stack, G.M., "X-Ray Diffraction Methods in Polymer Science", R.E. Kreiger Publishing Co., Fl., (1979).
- Al-Raheil, I.A. and Al-Share, M., *J. Appl. Polym. Sci.*, 72, 1125 (1999).
- Andrews, E.H., Owen, P.J., and Singh, A., *Proc. R. Soc. A*, 324, 79 (1971).
- Armistead, K. and Goldbeck-Wood, G., *Adv. Polym. Sci.*, 100, 219 (1992).
- Avrami, M., *J. Chem. Phys.*, 9, 177 (1941).
- Balbontin, G., Dainelli, D., Galimberti, M., and Paganetto, G., *Makromel. Chem.* 193, 693 (1992).
- Balta Calleja, F.J. and Vonk, C.G., "X-ray Scattering of Synthetic Polymers", Elsevier, Amsterdam (1989).
- Barham, P.J., Jarvis, D.A. and Keller, A., *J. Polym. Sci., Polym. Phys. Ed.*, 20, 1733 (1982).
- Bassett, D.C., *Polymer*, 17, 460 (1976).
- Bassett, D.C., *CRC Crit Rev Solid State Phys Mater Sci*, 12, 1297 (1984).
- Bassett, D.C. and Vaughan, A.S., *Polymer*, 27, 1472 (1986).
- Bassett, D.C., Olley, R.H., Sutton, S.J., and Vaughan, A.S., *Macromolecules*, 29, 1852 (1996).
- Bassett, D.C., *Polymer Journal*, 31(9), 759 (1999).



- Benson, R.S., Ph.D. Dissertation, Florida State University (1978).
- Blundell, D.J., *Polymer*, 19, 1258 (1978).
- Brandrup, J. and Immergut, E.H., "Polymer Handbook, 3<sup>rd</sup> Ed., Wiley, New York (1989).
- Brooks Jr., C., private communication.
- Bunn, C.W., *Trans. Faraday Soc.*, 35, 482 (1939).
- Cahn, J.W., *Trans. Metall. Soc. AIME*, 242, 166 (1968).
- Caze C., Devaux E., Crespy A., and Cavrot, J.P., *Polymer*, 38, 497 (1997).
- Chuah, K.P., Gan, S.N., and Chee K.K., *Polymer*, 40, 253 (1998).
- Cook, H.E., *Acta Metall.*, 18, 297 (1970).
- Crist, B., *J. Polym. Sci., Polym. Phys.*, 11, 463, 635 (1973).
- Debye, P., *Annalen der Physik*, 46, 809 (1915).
- Debye, P. and Bueche, A.M., *J. App. Phys.*, 20, 518 (1949).
- Debye, P., Anderson, H.R., and Bumgardner, H., *J. Appl. Phys.*, 28, 679 (1957).
- de Gennes, P.G., *J. Chem. Phys.*, 55, 572 (1971).
- Dettenmaier, M, Fischer, E.W., and Stamm, M, *Colloid Polymer Sci.*, 258, 343 (1980).
- Ding, Z. and Spruiell, J.E., *J. Polym. Sci., B, Poly. Phys., Ed.*, 34, 2783 (1996).
- Ding, Zhuomin, "The Study of the Kinetics of Crystallization of Polymers During Rapid Cooling and Computer Modeling of the Melt Spinning Process.", Ph.D. Dissertation, University of Tennessee. (1996).
- Doi, M. and Kuzuu, N.Y., *J. Polym. Lett.* 18, 775 (1980).
- Eder, M., and Wlochowicz, A., *Polymer*, 24, 1593 (1983).
- Estes, G.M., Cooper, S.L., and Tobolosky, A.V., *J. Macromol. Sci., Rev. Macromol Chem*, 4, 313 (1970).
- Ezquerro, T.A., Roslaniec, Z., Lopez-Cabarcos, E., and Balta-Calleja, F.J., *Macromolecules*, 28, 4516 (1995).

- Fakirov, S., Fakirov, C., Fischer, E.W., Stamm, M., and Apostolov, A.A., *Colloid Polym Sci*, 271, 811 (1993).
- Fischer, E.W., Sterzel, H.J. and Wegner, G., *Kolloid Z.Z. Polym.*, 251, 980 (1973).
- Flory, P.J., *J. Chem. Phys.* 17, 223 (1949).
- Flory, P.J., "Principles of Polymer Chemistry", Cornell University Press (1953).
- Flory, P.J., *Trans. Faraday Soc.*, 51, 848 (1955).
- Flory, P.J., *J. Am. Chem. Soc.*, 84, 2857 (1962).
- Flory, P.J. and Vrij, A., *J. Am. Chem. Soc.*, 85, 3548 (1963).
- Flory, P.J., "Statistical Mechanics of Chain Molecules", Oxford University Press, New York (1989).
- Frenkel, J., "The Kinetic Theory of Liquids", Oxford (1946).
- Geil, P.H., "Polymer Single Crystals", Interscience, New York (1963).
- Goldbeck-Wood, G., *Polymer*, 33(4), 778 (1992).
- Goldbeck-Wood, G., "Science and Technology of Crystal Growth", (edited by J.P. van der Eerden and O.S.L. Bruinsma), Kluwer, Dordrecht, 313 (1995).
- Gunton, J.D., San Miguel, M., and Sahni, P.S., "Phase Transitions and Critical Phenomena", (edited by C. Domb and M.S. Green), Academic, New York, Vol. 8, (1983).
- Gupta, V.K., Satish, S., Bhardwaj, I.S., *Macromol. Chem. Phys.*, C34(3), 439 (1994).
- Guttman, C.M. and DiMarzio, E.A., *J. Appl. Phys.*, 54, 5541 (1983).
- Hauser, G., Schmidtke, J., and Strobel, G., *Macromolecules*, 31, 6250 (1998).
- Hearle, J.W.S., "Polymers and Their Properties." Vol. 1, John Wiley and Sons, New York (1982).
- Heck, B., Hugel, T., Lijima, M., Sadiku, E., and Strobel, G., *New Journal of Physics*, 1, 17.1 (1999).
- Hendricks, R.W., *J. Appl. Cryst.*, 11, 15 (1978).

- Higgs, P.G. and Ungar, G.J. *J. Chem. Phys. Edn.*, 23, 1533 (1985).
- Hillert, M., *Acta Metall.*, 9, 525 (1961).
- Hoel, Y, Moteki, Y., and Shackleton, J.S., *J. Polymer Sci.: Part B: Polymer Physics*, 36, 1293 (1998).
- Hoffman, J.D. and Lauritzen, J.I., *J. Res. NBS*, A65, 297 (1961).
- Hoffman, J.D. and Weeks, J.J., *J. Chem. Phys.*, 37, 1723 (1962).
- Hoffman, J.D. Frolen, L.J., Ross, G.S., Lauritzen J.I., *Res. Nat. Bur. Stand., Sect. A* 79A, 671 (1975).
- Hoffman, J.D., Davis, G.T., Lauritzen, Jr., J.I., "Treatise on Solid State Chemistry", N.B. Hannay, Ed., Vol. 3, Plenum Press, New York, (1976).
- Hoffman, J.D., Guttman, C.M. and DiMarzio, E.A., *Disc. Faraday Soc.*, 68, 198 (1979).
- Hoffman, J.D, *Polymer*, 23, 656 (1982).
- Hoffman, J.D., *Polymer*, 24, 3 (1983).
- Hoffman, J.D. and Miller, R.L., *Macromolecules*, 21, 3038 (1988).
- Hoffman, J.D. and Miller, R.L., *Polymer*, 38(13), 3151 (1997).
- Holden, G., Legge, N., Quirk, R., and Schroeder, H.E., Eds., "Thermoplastic Elastomers", Hanser, Munich (1996).
- Horton, A.D., *Trip*, 2(5), May, 158 (1994).
- Hosemann, R., and Bagachi, S.N., "Direct Analysis of Diffraction by Matter," North Holland, Amsterdam (1962).
- Hugel, T., Strobl, G., Thomann, R., *Acta Polymerica*, In Press (1999).
- Hsieh, Y.L., and Ju, J., *J. Appl. Polym. Sci.*, 53, 1599 (1968).
- Imai, M., Kaji, K., Kanaya, T. and Sakai, Y., *Phys. Rev. B*, 52, 12696 (1995).
- Inaba, N., Yamada, T., Suzuki, S., and Hashimoto, T., *Macromolecules*, 21, 407 (1988).
- Janimak, J.J., and Bassett, D.C., *Polymer*, 40, 459 (1999).

- Kawasaki, K., "Phase Transitions and Critical Phenomena", C. Domb and M.S. Green, Ed., Vol. 5a, Academic, New York (1976).
- Keller, A., *Phil. Mag.*, 2, 1171 (1957).
- Keller, A., Hikosaka, M., Rasogi, S., Toda, A., Barham, P.J., and Goldbeck-Wood, G., *J. Materials Science*, 29, 2579 (1994).
- Keith, H.D. and Padden, F.J., *J. Appl. Phys.*, 34, 2409 (1963).
- Keith, H.D. and Padden, F.J., Jr., *J. Polym Sci, Polym Phys Ed.*, 25, 2371 (1987).
- Keith, H.D., Padden, F.J., Jr., Lotz, B. and Wittmann, J.C. *Macromolecules*, 22, 2230 (1989).
- Kim, Man-Ho, "The Melting Behavior and Structure of Ethylene Copolymers from Metallocene Catalysts", Ph.D. Dissertation, University of Tennessee. (1996).
- Kim, M.H., Phillips, P.J., and Lin, J.S., *J. Polym. Sci., B, Polym. Phys.*, 38, 154 (2000).
- Kim, Y.C., Kim, C.Y., and Kim, S.C., *Polym. Eng. Sci.*, 31, 1009 (1991).
- Kratky, O., Pilz, I., and Schmitz, P.J., *J. Colloid and Interface Sci.*, 21, 24 (1966).
- Langer, J.S., Bar-on, M., and Miller, H.D., *Phys. Rev.*, A11, 1417 (1975).
- Lambert, Scott, "The Effects of Chain Microstructure on Crystallization in Polyethylene", Ph.D. Dissertation, University of Tennessee. (1991).
- Lambert, S.W. and Phillips, P.J., *Macromolecules*, 27, 3537 (1994).
- Landau, L.D. and Lifschitz, E.M., "Statistical Physics", 3<sup>rd</sup> Ed., Part 1, Pergamon, Oxford (1980).
- Lauritzen, J.I. and Hoffman, J.D., *J. Res. Nat. Bur. St.*, A64, 73, (1960).
- Lazcano, S., Fatou, J.G., Marco, C. and Bello, A., *Polymer*, 29, 2076 (1988).
- Lopez, L.C. and Wilkes, G., *Polymer*, 30, 882 (1989).
- Mandelkern, L., "Comprehensive Polymer Science", Vol. 2, Pergamon Press, Oxford, (1989).
- Martinez, S., Barham, P.J. and Keller, A., *J. Poly. Sci., Polym. Phys. Ed.*, 22, 1085 (1984).

- McLean, R.S. and Sauer, B.B., *J. Polym. Sci.: Part B: Polym. Phys.*, 37, 859 (1999).
- Miller, R.L.(Ed.), "Flow-induced Crystallization in Polymer Systems", Gordon and Breach, New York (1979).
- Monasse, B. and Haudin, J.M., *Colloid Polym. Sci.*, 263, 822 (1985).
- Morra, B.S. and Stein, R.S., *J. Polym. Sci. Polym. Phys. Ed.*, 20, 2243 (1982).
- Odian, G., "Principles of Polymerization", 3<sup>rd</sup> ed., Wiley, Chapter 8 (1991).
- Oliver, B., private communication.
- Olmsted, P.D., Poon, W.C.K., McLeish, T.C.B., Terrill, N.J., and Ryan, A.J., *Phys. Rev. Letters*, 81(2), 373 (1998).
- Organ, S.J. and Keller, A., *J. Mater Sci*, 20, 1571 (1985).
- Organ, S.J., Keller, A., Hikosaka, M., and Ungar, G., *Polymer*, 37(12), 2517 (1996).
- Ozawa, T., *Polymer*, 12, 150 (1971).
- Pratt, L.R., Hsu, C.S., and Chandler, D., *J. Chem. Phys.*, 68, 4202 (1978).
- Pearson, D.S. and Helfand, E., *Macromolecules*, 17, 888 (1984).
- Phillips, P.J. *Polymer Prepr. (Am. Chem. Soc. Div. Polym. Chem.)* 20, 438 (1979).
- Phillips, P.J. and Lambert, W.S., *Macromolecules*, 23, 2075 (1990).
- Phillips, P.J. and Vatansever, N., *Macromolecules*, 20, 2138 (1987).
- Phillips, P.J., *Rep. Prog. Phys.*, 53, 549 (1990).
- Rabek, J.F., "Experimental Methods in Polymer Chemistry", John Wiley and Sons, New York (1980).
- Ruland, W., *Acta Cryst.*, 14, 1180 (1961).
- Sadler, D.M., *Polymer*, 24, 1401 (1983).
- Sadler, D.M. and Gilmer, G.H., *Phys. Rev. Lett.*, 56, 2708 (1986).
- Sanchez, I. and Eby, R.K., *J Res. Natl. Bur. Stand., Sect. A*, 77, 353 (1973).

- Sanchez, I. and Eby, R.K., *Macromolecules*, 8, 638 (1975).
- Schultz, J.M., "Diffraction for Materials Scientists", Prentice-Hall, Inc., New Jersey (1982).
- Schwank, D., *Modern Plast. Inter.*, August, 40 (1993).
- Sinn, H. and Kaminsky, W., *Adv. Organomet. Chem.*, 18, 99 (1980).
- Spruiell, J.E., private communication.
- Stribeck, N., Sapoundjieva, D., Denchev, Z., Apostolov, A.A., Zachmann, H.G., Stamm, M. and Fakirov, S., *Macromolecules*, 30, 1329 (1997).
- Strobl, G., "The Physics of Polymers", Springer, Berlin (1996).
- Suhm, J., Maier, R.D., Kressler, J., and Mulhaupt, R., *Acta Polymer*, 49, 80 (1998).
- Uedono, A., Kawano, T., Tanigawa, S., Ban, M., Kyoto, M. and Uozumi, T., *J. Polym. Sci.: Part B: Polymer Physics*, 35, 1601 (1997).
- Ungar, G., in "Interpretation of Fundamental Polymer Science and Technology", (Eds. P.J. Lemstra and I.A. Klientjens), Vol. 2, Elsevier, London, (1988).
- Ungar, G. in "Polymer Crystallization" (ed. M. Dosiere), NATO ASI Series, Kluwer, Dordrecht (1993).
- Van Krevelen, D.W., "Properties of Polymers", Chapter 4, Elsevier Scientific Co., New York (1976).
- Verma, R., Marand, H., and Hsiao, B., *Macromolecules*, 29, 7767 (1996).
- Voigt-Martin, I.G. and Mandelkern, J., *Polym Sci., Polym. Phys. Ed.*, 27, 967 (1989).
- Wagner, J.E., Abu-Iqyas, S., Monar, K. and Phillips, P.J., Proc. ANTEC 98, Society of Plastics Engineers (1998).
- Wagner, J.E., Abu-Iqyas, S., Monar, K., and Phillips, P.J., *Polymer*, 40, 4717 (1999).
- Wagner, J.E., Phillips, P.J. Unpublished data, (2000).
- Wignall, G.D., Lin, J.S., and Spooner S., *J. Appl. Cryst.*, 23, 241 (1990).
- Wood, A., *Chemical Week*, July, 18, 42 (1992).